DENND5A-related developmental and epileptic encephalopathy driven by loss of symmetric cell division of apical neural progenitors

Emily Banks

Integrated Program in Neuroscience

Montreal Neurological Institute

McGill University, Montreal

September 2023

A thesis submitted to McGill University in partial fulfillment of the requirements of the degree of Doctor of Philosophy in Neuroscience

Table of Contents

1.1 Abstract

Developmental and epileptic encephalopathies (DEEs) are a heterogenous group of epilepsies in which altered brain development leads to developmental delay and seizures, with the epileptic activity further negatively impacting neurodevelopment. Identifying the underlying cause of DEEs is essential for progress toward precision therapies. Here we describe a group of individuals with biallelic variants in DENND5A and determine that variant type is correlated with disease severity. We demonstrate that DENND5A interacts with MUPP1 and PALS1, components of the Crumbs apical polarity complex, which is required for both neural progenitor cell identity and the ability of these stem cells to divide symmetrically. Induced pluripotent stem cells lacking DENND5A fail to undergo symmetric cell division during neural induction and have an inherent propensity to differentiate into neurons, and transgenic DENND5A mice, with phenotypes like the human syndrome, have an increased number of neurons in the adult subventricular zone. Disruption of symmetric cell division following loss of DENND5A results from misalignment of the mitotic spindle in apical neural progenitors. A subset of DENND5A is localized to centrosomes, which define the spindle poles during mitosis. Cells lacking DENND5A orient away from the proliferative apical domain surrounding the ventricles, biasing daughter cells towards a more fate-committed state and ultimately shortening the period of neurogenesis. This study provides a mechanism behind DENND5A-related DEE that may be generalizable to other developmental conditions and provides variant-specific clinical information for physicians and families. [1]

1.2 Résumé

Les encéphalopathies développementales et épileptiques (EDE) constituent un groupe hétérogène d'épilepsies dans lequel une altération du développement cérébral peut entraîner un retard de développement et des convulsions – l'activité épileptique ayant un impact négatif supplémentaire sur le développement neurologique[1]. L'identification de la cause sous-jacente de la EDE est essentielle pour développer une thérapie personnalisée. Nous décrivons ici un groupe d'individus avec des variants biallélіques dans DENND5A et déterminer que le type de variant est corrélé à la gravité de la maladie. Nous démontrons que la protéine DENND5A interagit physiquement avec les protéines MUPP1 et PALS1, composantes du complexe de polarité apicale de Crumbs, qui est nécessaire à la fois à l'identité des cellules progénitrices neurales et à leur capacité à se diviser symétriquement. Les cellules souches pluripotentes induites dépourvues de DENND5A ne parviennent pas à subir une division cellulaire symétrique pendant l'induction neuronale et ont une propension inhérente à se différencier en neurones. De même, les souris transgéniques DENND5A, dont les phénotypes correspondent au syndrome humain, présentent un nombre accru de neurones dans la zone sous-ventriculaire adulte proliférative. La perturbation de la division cellulaire symétrique suite à la perte de DENND5A résulte d'un mauvais alignement du fuseau mitotique chez les progéniteurs neuraux apicaux. Un sous-ensemble de DENND5A est localisé dans les centrosomes, qui définissent les pôles du fuseau pendant la mitose. Les cellules dépourvues de DENND5A s'éloignent du domaine apical prolifératif entourant les ventricules, orientant les cellules filles vers un état plus engagé dans leur destin et raccourcissant finalement la période de neurogenèse. Cette étude fournit un mécanisme derrière le EDE lié à DENND5A qui peut également être généralisable à d'autres conditions de développement et fournit des informations cliniques spécifiques aux variantes pour les médecins et les familles.

1.3 Acknowledgments

I would first like to thank my supervisor, Dr. Peter McPherson, for taking me on as a PhD student and supporting me academically, professionally, financially, and personally throughout the years. I vividly remember a note you left on my desk saying you received an email about another patient that ended with “Let’s write this paper!”. What followed took much, much longer than either of us had thought for several reasons – coordinating a study between 15 (!) countries, during a pandemic, while recovering from two consecutive concussions is no easy feat. We have done important work together, and sometimes I’m amazed at how we managed to blend clinical, cell biological, and biochemical data together into one coherent story. I’ve always been fascinated about how the “bigger picture” is affected by microscopic changes in biology, and I’m grateful you gave me the opportunity to study just that during my time here.

I would also like to thank my thesis committee, Dr. Heidi McBride and Dr. Ziv Gan-Or, for their valuable feedback and for challenging me intellectually over the years. Heidi, you have always asked me difficult biological questions that stuck with me long after my committee meetings and ultimately strengthened the quality of my research. Ziv, you have been an essential part of my training here and have consistently provided invaluable input regarding genetic analysis and interpretations. My project would not have been possible without both of you.

Additionally, and perhaps most importantly, I would like to thank the families we’ve been in contact with. Their genuine interest and expressions of gratitude for what I was doing, even though they knew it would not help their children directly, gave me the motivation to continue whenever my progress “hit a wall” (which was very often). I am also extremely grateful for all the clinicians and geneticists that provided data, feedback, and guidance.

Finally, a huge thank-you is in order to my parents Linda and David, husband Vinc, and labmates Armin, Riham and Adriana, who encouraged me to continue whenever I wanted to give up (again, which was very often). Suleima, Fumika and Phil – our get togethers are what kept me sane! And lastly, to my dog Shadow, who was the best and fluffiest coworker while I worked from home.

1.4 List of Figures and Tables

1.5 List of Abbreviations

aa	Amino Acid
ACMG	American College of Medical Genetics and Genomics
AJ	Adherens Junction
aPKC	Atypical Protein Kinase C
ASD	Autism Spectrum Disorder
BSA	Bovine Serum Albumin
Crb	Crumbs (complex)
CSF	Cerebrospinal Fluid
CT	Computed Tomography
DEE	Developmental and Epileptic Encephalopathy
DENN	Differentially Expressed in Normal and Neoplastic cells
DIV	Days *in vitro*
ECM	Extracellular Matrix
FGF	Fibroblast Growth-Factor
GABA	Gamma-Aminobutyric Acid
GFAP	Glial Fibrillary Acidic Protein
GFP	Green Fluorescent Protein
GST	Glutathione S-transferase
IGF1	Insulin-like Growth Factor 1
IHC	Immunohistochemistry
iPSC	Induced Pluripotent Stem Cell
IPTG	Isopropyl β- d-1-thiogalactopyranoside
KD	Knockdown
KI	knock-in
KO	Knockout
M	Mean
Max	Maximum
MDCK	Madin-Darby Canine Kidney
Med	Median
Min	Minimum
MRI	Magnetic Resonance Imaging
MUPP1	Multi-PDZ Protein 1
NEC	Neuroepithelial Cell
NPC	Neural Progenitor Cell
OFC	Occipitofrontal Circumferance
PALS1	Protein Associated with Lin7 1
PATJ	Pals1-Associated Tight Junction Protein
PBS	Phosphate-buffered saline
PLAT	Polycystin-1, Lipoxygenase, Alpha-Toxin
PLO	Poly-L-Ornithine
RAB6IP1	Rab6-Interacting Protein 1
RT-qPCR	Real Time Quantitative Polymerase Chain Reaction
RUN	RPIP8 [RaP2 interacting protein 8], UNC-14 and NESCA [new molecule containing SH3 at the carboxyl-terminus]
SD	Standard Deviation
SDS-PAGE	Sodium Dodecyl Sulfate–Polyacrylamide Gel Electrophoresis
SEM	Standard Error of the Mean
Shh	Sonic Hedgehog
SVZ	Subventricular Zone
TJ	Tight Junction
VZ	Ventricular Zone
WT	Wild-Type

1.6 Preface

This thesis is written in the traditional monograph style. All quoted text is presented in AMA citation format and taken verbatim from a manuscript in pre-print, currently under review, that was written by the first author of the manuscript and author of this thesis. The only modifications made to quoted passages are figure/table numbers and citation superscript numbers to create a coherent list within the thesis. When the wording of quoted passages are slightly altered for clarity in the context of the thesis, the changed wording is surrounded by brackets. When quoted passages skip a portion of text within the manuscript, the skipped text is substituted with "…".

1.7 References

1. Banks E, Francis V, Lin S-J, Kharfallah F, Fonov V, et al. Loss of symmetric cell division of apical neural progenitors drives *DENND5A*-related developmental and epileptic encephalopathy. *medRxiv*. 2023-01-01 00:00:00 2023;doi:https://doi.org/10.1101/2022.08.23.22278845

2 Chapter 1: Introduction

2.1 Developmental and Epileptic Encephalopathy

Developmental and epileptic encephalopathies (DEEs) are a heterogenous group of epilepsies in which developmental delay is caused by both seizures and the underlying cause of the epilepsy. DEE is a relatively new term implemented in 2017 to highlight a key difference between DEE and epileptic encephalopathy: epileptic encephalopathy reflects how seizures adversely affect development, whereas DEE provides additional information indicating that developmental delay is also a direct result of the underlying pathology[1]. Disentangling which aspect plays a greater role in the clinical presentation of a child's DEE can be challenging, but it is crucial to implement the most effective treatment paradigm as early as possible to mitigate adverse developmental effects. DEEs are generally difficult to treat and a poor prognosis typically accompanies a diagnosis, but antiseizure medication can improve developmental outcomes by reducing the frequency of these damaging events. Seizures typically appear during infancy or early childhood and prevent the acquisition of developmental skills or result in developmental regression[2].

Although DEE can be caused by a combination of gene variants and/or environmental factors such as congenital infections[3,4], progress in understanding the underlying causes of DEE has been made primarily through studying monogenic cases. Disruptions in a wide variety of genes including those related to ion channels[5-13], neurotransmitter regulators[14], proton pumps[15], endocytosis[16,17], adapter proteins[18], GTPases[19], guanine nucleotide exchange factors[20], GTPase-activating proteins[21], tubulin[22], chromatin remodeling[23], metabolism[24-26], biosynthesis[27], and transcriptional activators[28], among others, have all been identified as causative factors. The sheer

scope of biological molecules and processes implicated in DEE underscores the challenges clinicians face when deciding the best course of treatment. Indeed, some common antiseizure medications can worsen seizures if an etiology is not prudently sought[29]. Generally, DEEs in which abnormal neuronal activity are the primary pathology have a better chance at successful pharmacological intervention, and DEEs accompanied by structural brain development pathology are associated with poorer developmental outcomes.

2.1.1 Electrophysiological pathology

Most DEEs with a genetic etiology involve pathogenic variants in genes, either inherited or arising *de novo*, encoding proteins directly involved with electrical transmission between neurons in the brain. Although DEE is often characterized by drug resistant seizures, some antiseizure medication can address the underlying cause of seizures and reduce their frequency and intensity. The most common and best studied monogenic cause of DEE is Dravet syndrome, in which mutations in the gene *SCN1A*, encoding a sodium channel subunit, often result in reduced sodium currents in GABAergic inhibitory interneurons and thus cause neuronal hyperexcitability and thus seizures[30]. A study examining the proteomic profiles of wild-type (WT) mice and a mouse model of Dravet syndrome prior to seizure onset, however, found that Dravet syndrome mice showed reduced protein expression in the guanine nucleotide exchange factor RASGRF1 and the Ca^{2+}/calmodulin-dependent serine/threonine protein kinase CAMK2A, and upregulated expression of the signaling receptor VEGFR2 which promotes cell proliferation, survival and migration[31,32]. This suggests that altered intracellular protein dynamics inherent to individuals with *SCN1A* mutations contribute to altered development and the baseline developmental delay is exacerbated by the epilepsy, thus fulfilling the diagnostic criteria for a DEE. Children with Dravet's syndrome tend to respond best to a pharmacological cocktail of clobazam or valproic acid with

stiripentol[29]. These medications are thought to function by enhancing both the export of intracellular excitatory glutamate and the import of extracellular inhibitory gamma-aminobutyric acid (GABA) [33], blocking voltage-gated sodium channels and inhibiting GABA degradation[34], and prolonging the time that a GABA receptor is open[34], respectively, effectively counterbalancing the hyperexcitability that is caused by *SCN1A* mutations.

Another example of DEE with genetic ion channel-related pathology includes pathogenic variants in fibroblast growth-factor (FGF) homologous factor (*FHF1*), encoding a protein that binds to the C-terminus of a voltage-gated sodium channel subunit to regulate its inactivation[10,35]. FHF1 was recently found to also interact with FGF receptors directly, triggering signaling cascades important for cell survival during development [36]. Thus, the pre-existing impacts of aberrant FGF signaling during neural development compound with those of sodium channel regulation and result in DEE when a child has pathogenic variants in *FHF1*.

2.1.2 Structural brain pathology

When DEE etiology involves impaired brain development resulting in structural abnormalities, there is no longer an opportunity to intervene by the time gross abnormalities in brain morphology are detected. The goal of treatment is currently to reduce the burden of seizures to improve patient quality of life and safety[2]. Rather than altered neuronal excitability alone, seizures likely also occur due to aberrant connections between neurons because they are not in their appropriate numbers or positions. Children with a structural DEE etiology may therefore not respond as readily to antiseizure medications. However, the development of precision therapies for DEEs with a structural component is a new and exciting area of research with the overall goal of minimizing developmental delays in children whose genetic cause of DEE is identified. A study evaluating an mRNA silencing therapy administered to mice with dominant negative *DNM1*

variants, which are known to cause DEE and can result in brain abnormalities such as ventriculomegaly and reduced cerebral cortex volume[17], found that a single dose administered to newborn mice significantly reduced seizure frequency, improved growth rate and motor abilities, and prolonged survival[37]. Understanding the functional effects of individual variants, then, could reveal avenues for drug discovery and gene therapy that may improve developmental outcomes when administered as early as possible.

2.2 Cell polarity during development

The establishment and maintenance of cell polarity is crucial throughout all stages of development. Polarization can be observed both at the cellular level, through differential distributions of proteins and organelles, as well as on the tissue level, where cell types and properties vary according to their position in the tissue. Polarization occurs along two major axes, apico-basal and planar, and is initiated by signaling events from molecules in the extracellular matrix (ECM) [38-41]. On the tissue level, apical cell membranes orient themselves toward a central fluid-filled lumen[42]; in early cortical development, this manifests as polarized neuroepithelial cells (NECs) that secrete and respond to cerebrospinal fluid (CSF) dynamics from their apical membranes in the developing lateral ventricles[43,44]. The basement (basal) membrane of the neuroepithelium contacts the pial surface and is the site of neurogenesis[45,46]. Cells also develop intrinsic planar cell polarity characteristics, in which proteins and cellular features directionally orient themselves along an orthogonal axis within the same apico-basal plane, creating organization within a tissue[47]. A graphical summary of these cell polarization concepts using ependymal cells as an example, the cells that line the mature brain's ventricles, is illustrated in **Figure 1.1**. Ependymal cells have motile cilia protruding from the apical membrane, which have basal bodies oriented in a uniform direction to properly direct CSF flow[48]. Although the two forms

of polarity during development are inextricably linked, the work done in this thesis relates primarily to apico-basal polarity and planar cell polarity will not be discussed further.

Tight junctions (TJs) and adherens junctions (AJs) are cell adhesion protein complexes that both define the apical plasma membrane as well as connect adjacent cells within a tissue. TJs, the most apical cell-cell junctions that establish apicobasal polarity, provide a physical barrier that regulates the paracellular passage of water, ions, and solutes and are critical for the establishment of apical polarity[49]. TJs are required throughout the vasculature and choroid plexuses of the brain to maintain the integrity of the blood-brain and blood-CSF barriers, respectively[50,51]. TJ proteins are involved in the initial establishment of apicobasal polarization[52-55] and AJs, slightly basal to TJs, control the size of the apical domain by preventing apical determinants from diffusing basolaterally[56].

In the context of cortical development, NECs, the stem cells of the nervous system, form a physical platform for the remainder of neural development to occur upon. The morphology of NECs is such that an apical process containing a primary cilium protrudes into the developing ventricle to uptake extracellular signaling molecules promoting stem cell proliferation and survival[57,58], a basal process radiates outward and contacts the pial surface, and a cell body containing the nucleus between the two that undergoes rapid apically-directed migration before mitosis[59]. This cytoarchitecture allows for newborn neurons during neurogenesis to migrate basally along the processes into their locations in the cortical plate. Although NECs initially develop TJs to establish apico-basal polarity, they lose their TJs in favor of AJs prior to the onset of neurogenesis[60-62].

NECs primarily undergo symmetric divisions to increase the number of identical neural stem cells, but prior to radial glial differentiation some divisions are also asymmetric and

neurogenic, where one daughter cell self-renews to remain a neuroepithelial cell but the other is a newborn neuron or basal progenitor[63]. Transient changes in signaling molecules trigger this switch from symmetric to asymmetric division[64] while NECs gradually change their gene expression profiles and transform into radial glial cells[65], the primary neural progenitor cell type. Radial glia retain the characteristic cytoarchitecture that provides a track for newborn neurons to migrate along, and this architecture depends upon AJ integrity; disrupting AJs results in the retraction of radial glial process, thus impairing neuronal migration and leading to problems with cell proliferation and cortical lamination[66-68]. The proportion of symmetric versus asymmetric cell divisions increasingly favors asymmetric divisions as development continues until the pool of progenitors is depleted. Finally, the radial glial cells that remain at the apical surface once neurogenesis is complete transform into postmitotic apico-basally polarized ependymal cells that line the lateral ventricles[69], some radial glial-like neural stem cells remain dormant in the subventricular zone (SVZ) to respond to potential future injuries[70,71], and the remaining progenitors terminally differentiate into various glial or neuronal subtypes[72].

2.2.1 The Crumbs complex

"Proteins comprising the apical membrane-defining Crumbs (Crb) complex in NECs include CRB2, MUPP1 (Multi-PDZ Protein 1, also known as MPDZ) or PATJ (Pals1-Associated Tight Junction Protein), and PALS1 [(Protein Associated With Lin7 1)] and have been extensively studied in their roles in cell polarization and tissue development[73,74]." [75] The Crumbs (Crb) complex centers around a transmembrane CRB protein, with its short cytoplasmic C-terminal tail containing an ERLI-COO- motif tightly bound to PALS1[76]. PALS1 is composed of two N-terminal L27 domains followed by a PDZ domain, an SH3 domain, and a noncatalytic guanylate kinase domain[77]. While the PDZ domain alone is sufficient to bind the cytoplasmic CRB tail, binding is

greatly enhanced with the PDZ-SH3-GUK domains present in tandem[76]. Through the most N-terminal L27 domain of PALS1, either PATJ or MUPP1 bind via their L27 domain[78]. PATJ and MUPP1 are made up of an N-terminal L27 domain followed by up to 10 and 13 PDZ domains, respectively, depending on RNA splicing[73]. Both are scaffolding proteins that are known to stabilize tight junctions through direct interactions with the core TJ transmembrane protein Claudin1[79] and indirect interactions via ZO-3 with another TJ transmembrane protein Occludin[80,81].

Most research on the Crb complex focuses on the version of the complex containing PATJ rather than MUPP1, and the only study directly comparing the function of the two highly similar proteins concludes that PATJ is essential but MUPP1 is dispensable for establishing and maintaining tight junctions (TJs) [81]. *Ex vivo* studies, however, reveal significant deficits in ependymal[82,83] and choroid plexus epithelial cells[84] upon loss of MUPP1, including a complete loss of PALS1 expression in ependymal cells of *MUPP1* KO mice[83]. Although ependymal cells do not have TJs[85] or stem cell properties[86], they derive from TJ-containing NECs that gradually transition into radial glial cells that rely on abundant AJ protein expression to maintain their progenitor identity and ability to divide symmetrically[60,87-89]. Indeed, MUPP1 may differ from PATJ in that it preferentially stabilizes AJs over TJs[81], which may suggest a radial glial-specific function for this complex during neural development. [75]

Figure 1.2 depicts the MUPP1-containing Crb complex. AJ proteins include junctional adhesion molecules (JAMs) and nectins, both of which bind MUPP1 with a greater affinity than PATJ. Conversely, MUPP1 binds TJ proteins with lower affinity than PATJ[81]. Additionally, nectin expression is highest in radial glial cells during development[90]. The lack of TJs and abundance of

AJs after the transition from NECs to radial glia, combined with the increased ability for MUPP1 to bind AJ proteins and decreased ability to bind TJ proteins, may suggest a radial glial-dominant function for the MUPP1-containing Crb complex during development.

2.2.2 Establishment of apical polarity

The establishment of apical cell polarity depends on many co-occurring cellular events and protein-protein interactions. Several excellent reviews have been published regarding this process, which is also dependent upon antagonistic interactions with basolateral protein complexes[73,91,92]; however, this thesis will only discuss apical protein interactions. Put as simply as possible, PAR3 associates with phosphatidylinositol (3,4,5)-trisphosphate (PIP_3)-enriched plasma membranes and is bound by PTEN[93,94], which catalyzes the conversion of PIP_3 to phosphatidylinositol 4,5-bisphosphate (PIP_2) [95]. Par3-PTEN accumulate at the plasma membrane, resulting in an expanded PIP_2- and PAR3-enriched domain[94,96]. A dimer containing PAR6 and atypical protein kinase C (aPKC) are recruited to the PAR3-enriched membrane and interacts with PAR3, forming another key apical polarity protein complex: PAR3-PAR6-aPKC[97,98]. CDC42 then binds PAR6, resulting in the activation of aPKC and subsequent phosphorylation of PAR3, which destabilizes the PAR3/aPKC interaction and excludes PAR3 from the apical complex[97,99]. With PAR3 excluded, PAR6 can then bind the C-terminal tail of CRB, which was brought to the plasma membrane via an unknown process, accumulating PAR6-aPKC to the apical plasma membrane[100,101]. With PAR6 bound to CRB, aPKC is placed in the vicinity of the CRB tail and phosphorylates it[102]. The phosphorylated CRB tail excludes a competitive binding partner Moesin and binds PALS1 instead[103], forming the basis for the complete Crb complex at the apical plasma membrane.

The complexity of the establishment of apical cell polarity allows for multiple opportunities for regulatory mechanisms to intervene and prevent, reverse, or enhance the process.

For example, several phosphorylation steps are required for apical polarity to be established, and one can expect that a balance of phosphatases, kinases, and kinase inhibitors can alter the course and direction of events. Additionally, each protein in the Crb complex is capable of multiple other protein-protein interactions, likely contributing to substrate and binding site competition. For instance, at the level of the CRB protein alone, the C-terminal tail of CRB can bind either aPKC[102], PAR6[104], Moesin[103], or PALS1[78]. Additionally, PATJ regulates levels of CRB phosphorylation via competitive binding to aPKC[102]. Gate-dependent access to binding sites have also been established: a Phe residue, unique to the PALS1 PDZ domain when compared against other protein PDZ domains, can adopt a rotamer that prevents CRB access to the peptide-binding site of PALS1[105]. This complex biological process of establishing apical cell polarity is an essential component of tissue and brain development, and disruptions in many of the proteins mentioned above are associated with an array of neurodevelopmental disorders[106-114].

2.2.3 Symmetric versus asymmetric cell division

Neural development requires both symmetric and asymmetric cell divisions at precise times to give rise to the various neuronal and glial cell types found throughout the brain. A symmetric division is one that gives rise to two identical daughter cells. Asymmetric divisions occur when there is an unequal distribution of cellular components between both daughter cells during mitosis and results in two cells with different fate potentials. Both neuroepithelia and radial glia are capable of both types of division, but the proportion of symmetric versus asymmetric division differs depending on the developmental timepoint[115].

There are several mechanisms that regulate which type of division a cell undergoes. These mechanisms can be either intrinsic, where features within a cell inherently promote a certain mode of division, or extrinsic, where extracellular elements influence how a cell divides. A dynamic

interplay between both intrinsic and extrinsic factors contributes to an organism's development, but experimental paradigms controlling one aspect allows for a greater understanding of the other. An example of intrinsic factors influencing cell division is that apical AJ protein expression is required for the ability to undergo symmetric mitotic divisions and thus maintain their stem and progenitor cell identity[60,87-89]. Examples of extrinsic factors influencing the mode of cell division include changes in Notch signaling which switches neural stem cell division from symmetric to asymmetric[64], and that lysophosphatidic acid promotes self renewal by upregulating apical junctional proteins[116].

2.2.3.1 Protein inheritance and cell fate

Intrinsic mechanisms, such as the inheritance and expression of apical determinants, contribute to cell fate determination. Inheritance of the apical process of neuroepithelia or radial glia equates to the inheritance of apical proteins such as CRB2, PALS1, and PAR3. This inheritance is required to retain neural progenitor identity and self-renewal capacity, and their loss or lack of inheritance promotes premature cell cycle exit, neuronal differentiation, and/or cell death[87,88,117-119]. The relationship between cell fate and inheritance of the basal process of progenitors is less clear; basal process inheritance has been associated with both neuronal and radial glial cell fate[120-123]. This discrepancy may reflect the difficulties in determining which daughter cell truly inherits the process, as the basal process does not retract before cell division but instead remains attached to the pial surface and becomes extremely thin as cytoplasmic contents shift apically during mitosis[120,124].

2.2.3.2 Mitotic spindle orientation

A major mechanism for cells to control the inheritance of apical determinants is to regulate the orientation of the mitotic spindle[125]. After chromosomes and the centrosome are duplicated

during the cell cycle and the nuclear envelope breaks down, the centrosomes orient themselves at opposite poles where three types of microtubules are nucleated that make up and stabilize the spindle: 1) Kinetochore microtubules physically interact with the chromosomes at the mitotic cleavage plane and form a structural basis for pulling sister chromatids apart; 2) Non-kinetochore microtubules separate sister chromatids from one another at the metaphase plate and help to stabilize the spindle structure; and 3) Astral microtubules project from the centrosomes in the opposite direction and contact the cell cortex, and thus are the primary determinants of spindle orientation[126,127]. This orientation can be planar (i.e. horizontal, not to be confused with planar polarity), perpendicular, or oblique (diagonal) to a reference surface such as an apical or basement membrane, and are typically assessed experimentally through staining centrosome markers such as γ-tubulin or centrin.

Cell polarity proteins, the lateral LGN/NuMA complex in which LGN modulates NuMA binding to astral spindle microtubules, and dynein-driven pulling forces on these microtubules coordinate to instruct the orientation of cell division[128-135]. Many of these protein-protein interactions occur specifically during mitosis and competitive interactions, posttranslational modifications, or alternate protein localizations prevent their occurrence during interphase[128,130]. This reflects a high degree of control that can be influenced at various stages of development, and dysfunctional regulatory mechanisms may lead to disease states.

Polarity protein inheritance can further combine with the effects of extrinsic factors via the differential exposure of daughter cell membranes to the stem and progenitor cell biochemical niche that is the developing ventricle. For instance, PALS1 and PTEN inheritance coordinate the restriction of insulin-like growth factor 1 (IGF1) receptor localization to the apical membrane, allowing apical progenitors to receive maximal CSF-derived IGF signaling and sustain their

proliferative capacity[136]. Additionally, sonic hedgehog (Shh), another signaling molecule present in the CSF, is required for symmetric mitotic divisions and equal inheritance of apical determinants by promoting their recruitment to the centrosomes[137,138]. With an oblique or perpendicular mitotic spindle orientation, molecules such as IGF1 and Shh from the CSF reach each daughter cell in unequal proportions, and the cell that receives more signaling molecules retains more proliferative capacity than the other[125].

Taken together, apicobasal polarity has a profound influence on the exit or continuance of the cell cycle, as well as the ultimate differentiated fate of mitotic cell progeny. A model is presented in **Figure 1.3** to illustrate these developmentally critical cell division concepts. Apical progenitors, given their proximity to the stem and progenitor cell niche and expression of apical determinants, proliferate and self-renew more frequently than basal progenitors[139,140]. Basal progenitors may also symmetrically divide, but often both daughter cells are post-mitotic[46], whereas symmetric division of apical progenitors ensures cell cycle maintenance[139].

2.3 Objectives and Rationale

Our lab previously published a brief description of 4 cases of children with microcephaly and epileptic encephalopathy from 2 consanguineous families with rare homozygous *DENND5A* variants, establishing a role for *DENND5A* during neurodevelopment[141]. Shortly thereafter, another lab conducting a clinical genomic study on children with intellectual disability mentioned two additional consanguineous families with rare homozygous DENND5A variants[142]. Neither study described these cases in detail nor examined the functional consequence of these variants. Following these initial publications, several physicians and genetic counselors reached out to us to inform us about their patients with *DENND5A* variants. To our surprise, many of these newer patients harbored missense variants that appear with relatively high allele frequency.

My project was first and foremost to investigate the genotype-phenotype relationship between *DENND5A* variants and neurodevelopmental disease, using missense variants found in patients to guide our cell biological study. Consequently, an additional rationale for this project was to gain insight on the basic cell biological processes that DENND5A is involved in. Although we know that DENND5A functions as a guanine nucleotide exchange factor for Rab GTPases based on homology with other DENN domain-containing proteins[143], that loss of DENND5A enhances ERK signaling and neurite outgrowth[141], and that cell division[144,145], migration[144], and transferrin receptor recycling[145] is affected when DENND5A is depleted, none of these studies investigated the precise impact that these processes have on development. For example, does enhanced neurite outgrowth in cultured neurons reflect increased or premature neuronal differentiation? Do the cell division abnormalities observed in cancer cell lines translate to the proliferative properties of neural progenitor cells, and if so, do they point toward over- or under-proliferation? Is apoptosis, cell proliferation defects, and/or premature differentiation primarily

responsible for the observed microcephaly? These and many more questions remained unanswered and became the basis for my research.

Finally, after years of communicating with clinicians and families, the importance of genetic counseling and the future potential for precision therapy in treating *DENND5A*-related DEE also became a driving force for all work done in this thesis. Although precision therapies for DEEs are currently rare, that does not mean they are impossible, as cutting-edge research found that a single dose of RNA-binding oligonucleotides administered to a mouse model of *DNM1*-DEE after birth significantly improved developmental outcomes[37]. The distant possibility of ameliorating a future child's epilepsy and/or developmental outcomes remains a key motivator for both myself and the families involved in this research, and basic cell biological research is a necessary prerequisite step.

2.4 Figures

Figure 1.1

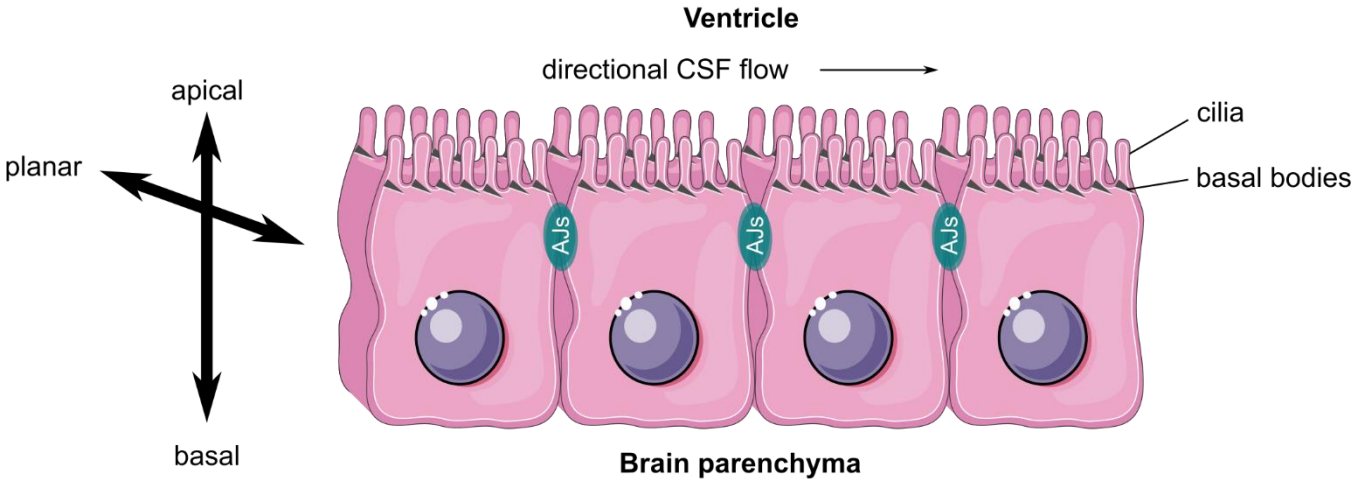

Figure 1.1: Schematic illustrating apico-basal and planar polarity axes in the context of ependymal cells lining the lateral ventricle. Adherens junctions (AJs) connect adjacent cells at their apical membranes to create a paracellular barrier between the ventricle and brain parenchyma. The basal bodies of cilia orient themselves in a uniform direction along a planar axis to ensure directional cerebrospinal fluid (CSF) flow.

Figure 1.2

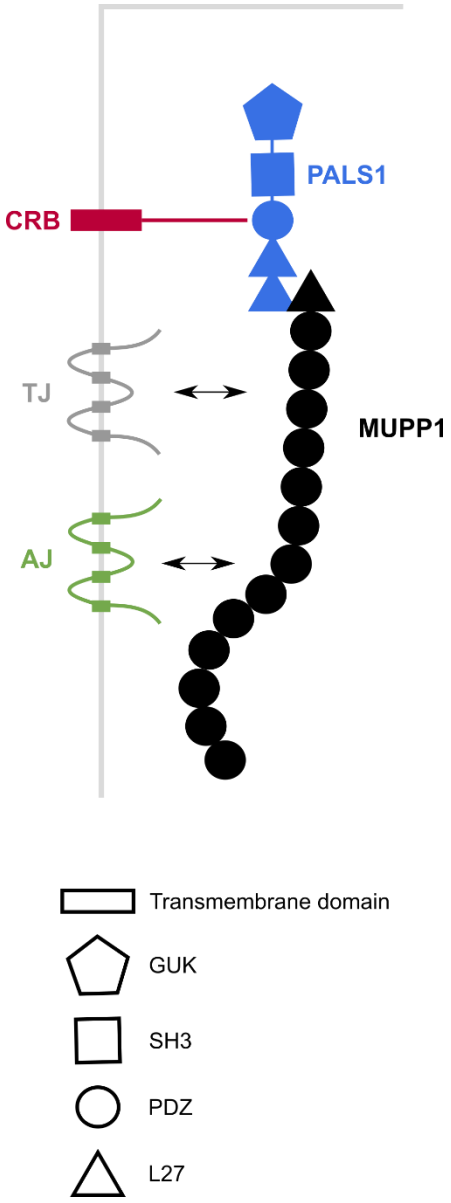

Figure 1.2: Schematic showing the apical polarity Crumbs complex containing MUPP1.

Figure 1.3

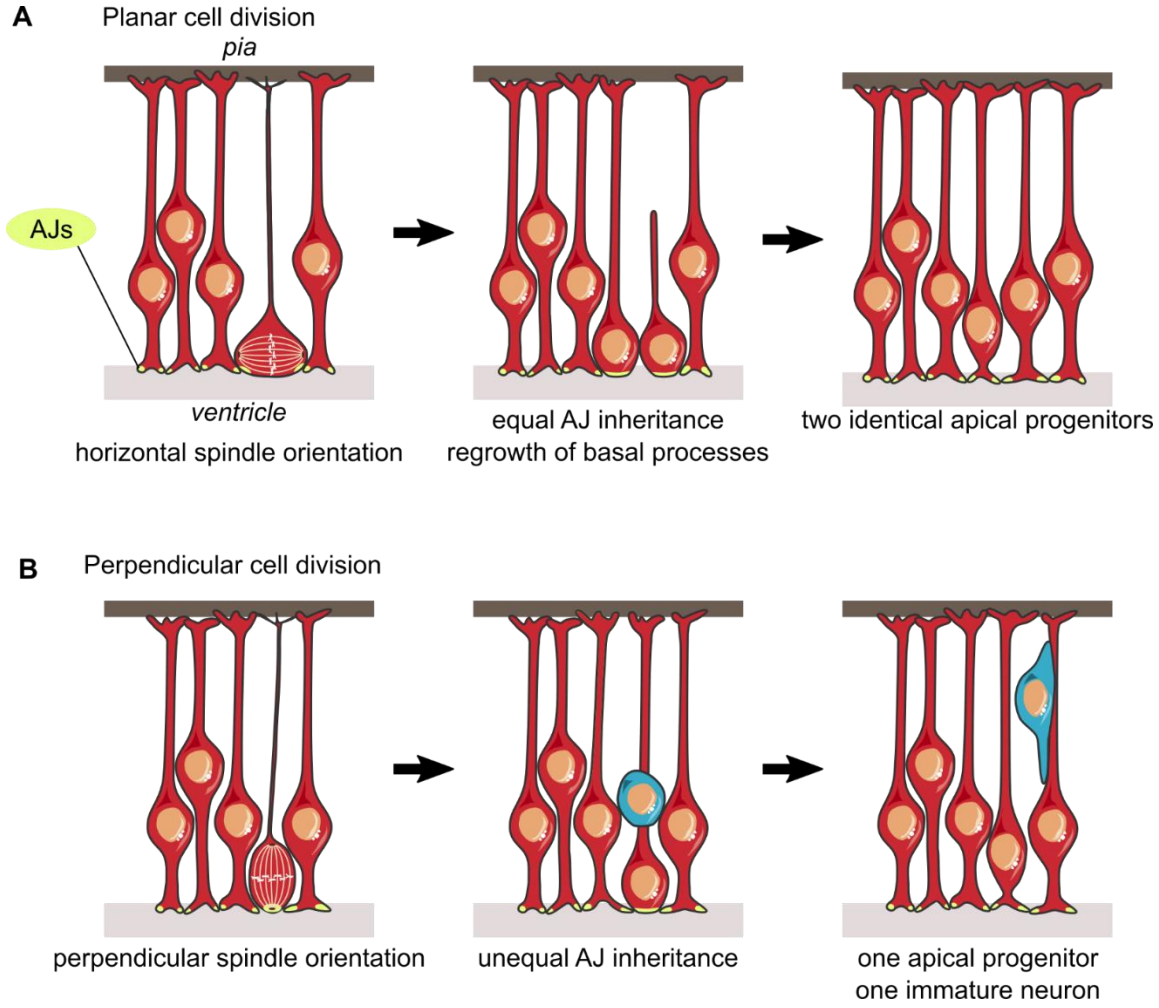

Figure 1.2: Schematic illustrating **A,** planar and **B,** perpendicular cell division of apical progenitor cells during cortical development and their effects on cell fate.

2.5 References

1. Scheffer IE, Berkovic S, Capovilla G, et al. ILAE classification of the epilepsies: Position paper of the ILAE Commission for Classification and Terminology. *Epilepsia*. Apr 2017;58(4):512-521. doi:10.1111/epi.13709

2. Raga S, Specchio N, Rheims S, Wilmshurst JM. Developmental and epileptic encephalopathies: recognition and approaches to care. *Epileptic Disord*. Feb 1 2021;23(1):40-52. doi:10.1684/epd.2021.1244

3. Gowda VK, Kulhalli P, Vamyanmane DK. Neurological Manifestations of Congenital Cytomegalovirus Infection at a Tertiary Care Centre from Southern India. *J Neurosci Rural Pract*. Jan 2021;12(1):133-136. doi:10.1055/s-0040-1721557

4. Lockrow J, Tully H, Saneto RP. Epileptic spasms as the presenting seizure type in a patient with a new "O" of TORCH, congenital Zika virus infection. *Epilepsy Behav Case Rep*. 2019;11:1-3. doi:10.1016/j.ebcr.2018.09.002

5. Helbig KL, Lauerer RJ, Bahr JC, et al. De Novo Pathogenic Variants in CACNA1E Cause Developmental and Epileptic Encephalopathy with Contractures, Macrocephaly, and Dyskinesias. *Am J Hum Genet*. Nov 1 2018;103(5):666-678. doi:10.1016/j.ajhg.2018.09.006

6. Li D, Yuan H, Ortiz-Gonzalez XR, et al. GRIN2D Recurrent De Novo Dominant Mutation Causes a Severe Epileptic Encephalopathy Treatable with NMDA Receptor Channel Blockers. *Am J Hum Genet*. Oct 6 2016;99(4):802-816. doi:10.1016/j.ajhg.2016.07.013

7. Kim HJ, Yang D, Kim SH, et al. Clinical characteristics of KCNQ2 encephalopathy. *Brain Dev*. Feb 2021;43(2):244-250. doi:10.1016/j.braindev.2020.08.015

8. Kim HJ, Yang D, Kim SH, et al. The phenotype and treatment of SCN2A-related developmental and epileptic encephalopathy. *Epileptic Disord*. Oct 1 2020;22(5):563-570. doi:10.1684/epd.2020.1199

9. Martinez-Esteve Melnikova A, Pijuan J, Aparicio J, et al. The p.Glu787Lys variant in the GRIA3 gene causes developmental and epileptic encephalopathy mimicking structural epilepsy in a female patient. *Eur J Med Genet*. Mar 2022;65(3):104442. doi:10.1016/j.ejmg.2022.104442

10. Liu CJ, Dib-Hajj SD, Renganathan M, Cummins TR, Waxman SG. Modulation of the cardiac sodium channel Nav1.5 by fibroblast growth factor homologous factor 1B. *J Biol Chem*. Jan 10 2003;278(2):1029-36. doi:10.1074/jbc.M207074200

11. Fry AE, Marra C, Derrick AV, et al. Missense variants in the N-terminal domain of the A isoform of FHF2/FGF13 cause an X-linked developmental and epileptic encephalopathy. *Am J Hum Genet*. Jan 7 2021;108(1):176-185. doi:10.1016/j.ajhg.2020.10.017

12. Gardella E, Marini C, Trivisano M, et al. The phenotype of SCN8A developmental and epileptic encephalopathy. *Neurology*. Sep 18 2018;91(12):e1112-e1124. doi:10.1212/WNL.0000000000006199

13. Mierzewska H, Laure-Kamionowska M, Jezela-Stanek A, Rydzanicz M, Ploski R, Szczepanik E. The neuropathological findings of developmental and epileptic encephalopathy-43 (DEE43) and delineation of a the molecular spectrum of novel case. *Seizure*. Dec 2021;93:75-80. doi:10.1016/j.seizure.2021.10.014

14. Wild B, Nelson S. STXBP1-Related Developmental and Epileptic Encephalopathy. *Pediatr Neurol Briefs*. Dec 31 2019;33:6. doi:10.15844/pedneurbriefs-33-6

15. Bott LC, Forouhan M, Lieto M, et al. Variants in ATP6V0A1 cause progressive myoclonus epilepsy and developmental and epileptic encephalopathy. *Brain Commun*. 2021;3(4):fcab245. doi:10.1093/braincomms/fcab245

16. Helbig I, Lopez-Hernandez T, Shor O, et al. A Recurrent Missense Variant in AP2M1 Impairs Clathrin-Mediated Endocytosis and Causes Developmental and Epileptic Encephalopathy. *Am J Hum Genet*. Jun 6 2019;104(6):1060-1072. doi:10.1016/j.ajhg.2019.04.001

17. Parthasarathy S, Ruggiero SM, Gelot A, et al. A recurrent de novo splice site variant involving DNM1 exon 10a causes developmental and epileptic encephalopathy through a dominant-negative mechanism. *Am J Hum Genet*. Dec 1 2022;109(12):2253-2269. doi:10.1016/j.ajhg.2022.11.002

18. Kanani F, Titheradge H, Cooper N, et al. Expanding the genotype-phenotype correlation of de novo heterozygous missense variants in YWHAG as a cause of developmental and epileptic encephalopathy. *Am J Med Genet A*. Apr 2020;182(4):713-720. doi:10.1002/ajmg.a.61483

19. Straub J, Konrad EDH, Gruner J, et al. Missense Variants in RHOBTB2 Cause a Developmental and Epileptic Encephalopathy in Humans, and Altered Levels Cause Neurological Defects in Drosophila. *Am J Hum Genet*. Jan 4 2018;102(1):44-57. doi:10.1016/j.ajhg.2017.11.008

20. Yang H, Liao H, Gan S, Xiao T, Wu L. ARHGEF9 gene variant leads to developmental and epileptic encephalopathy: Genotypic phenotype analysis and treatment exploration. *Mol Genet Genomic Med*. Jul 2022;10(7):e1967. doi:10.1002/mgg3.1967

21. Vlaskamp DRM, Shaw BJ, Burgess R, et al. SYNGAP1 encephalopathy: A distinctive generalized developmental and epileptic encephalopathy. *Neurology*. Jan 8 2019;92(2):e96-e107. doi:10.1212/WNL.0000000000006729

22. Hung KL, Lu JF, Su DJ, Hsu SJ, Wang LC. Tubulinopathy Presenting as Developmental and Epileptic Encephalopathy. *Children (Basel)*. Jul 23 2022;9(8)doi:10.3390/children9081105

23. Fichera M, Failla P, Saccuzzo L, et al. Mutations in ACTL6B, coding for a subunit of the neuron-specific chromatin remodeling complex nBAF, cause early onset severe developmental and epileptic encephalopathy with brain hypomyelination and cerebellar atrophy. *Hum Genet*. Feb 2019;138(2):187-198. doi:10.1007/s00439-019-01972-3

24. Kaur P, Neethukrishna K, Kumble A, Girisha KM, Shukla A. Identification of a novel homozygous variant confirms ITPA as a developmental and epileptic encephalopathy gene. *Am J Med Genet A*. May 2019;179(5):857-861. doi:10.1002/ajmg.a.61103

25. Trivisano M, Rivera M, Terracciano A, et al. Developmental and epileptic encephalopathy due to SZT2 genomic variants: Emerging features of a syndromic condition. *Epilepsy Behav*. Jul 2020;108:107097. doi:10.1016/j.yebeh.2020.107097

26. Carvill GL, Liu A, Mandelstam S, et al. Severe infantile onset developmental and epileptic encephalopathy caused by mutations in autophagy gene WDR45. *Epilepsia*. Jan 2018;59(1):e5-e13. doi:10.1111/epi.13957

27. Krenn M, Knaus A, Westphal DS, et al. Biallelic mutations in PIGP cause developmental and epileptic encephalopathy. *Ann Clin Transl Neurol*. May 2019;6(5):968-973. doi:10.1002/acn3.768

28. Trivisano M, De Dominicis A, Micalizzi A, et al. MED13 mutation: A novel cause of developmental and epileptic encephalopathy with infantile spasms. *Seizure*. Oct 2022;101:211-217. doi:10.1016/j.seizure.2022.09.002

29. Ziobro J, Eschbach K, Sullivan JE, Knupp KG. Current Treatment Strategies and Future Treatment Options for Dravet Syndrome. *Curr Treat Options Neurol*. Oct 13 2018;20(12):52. doi:10.1007/s11940-018-0537-y

30. Yu FH, Mantegazza M, Westenbroek RE, et al. Reduced sodium current in GABAergic interneurons in a mouse model of severe myoclonic epilepsy in infancy. *Nat Neurosci*. Sep 2006;9(9):1142-9. doi:10.1038/nn1754

31. Wang X, Bove AM, Simone G, Ma B. Molecular Bases of VEGFR-2-Mediated Physiological Function and Pathological Role. *Front Cell Dev Biol*. 2020;8:599281. doi:10.3389/fcell.2020.599281

32. Miljanovic N, Hauck SM, van Dijk RM, Di Liberto V, Rezaei A, Potschka H. Proteomic signature of the Dravet syndrome in the genetic Scn1a-A1783V mouse model. *Neurobiol Dis*. Sep 2021;157:105423. doi:10.1016/j.nbd.2021.105423

33. Doi T, Ueda Y, Tokumaru J, Willmore LJ. Molecular regulation of glutamate and GABA transporter proteins by clobazam during epileptogenesis in Fe(+++)-induced epileptic rats. *Brain Res Mol Brain Res*. Dec 14 2005;142(2):91-6. doi:10.1016/j.molbrainres.2005.09.010

34. Quilichini PP, Chiron C, Ben-Ari Y, Gozlan H. Stiripentol, a putative antiepileptic drug, enhances the duration of opening of GABA-A receptor channels. *Epilepsia*. Apr 2006;47(4):704-16. doi:10.1111/j.1528-1167.2006.00497.x

35. Liu C, Dib-Hajj SD, Waxman SG. Fibroblast growth factor homologous factor 1B binds to the C terminus of the tetrodotoxin-resistant sodium channel rNav1.9a (NaN). *J Biol Chem*. Jun 1 2001;276(22):18925-33. doi:10.1074/jbc.M101606200

36. Sochacka M, Opalinski L, Szymczyk J, et al. FHF1 is a bona fide fibroblast growth factor that activates cellular signaling in FGFR-dependent manner. *Cell Commun Signal*. May 1 2020;18(1):69. doi:10.1186/s12964-020-00573-2

37. Aimiuwu OV, Fowler AM, Sah M, et al. RNAi-Based Gene Therapy Rescues Developmental and Epileptic Encephalopathy in a Genetic Mouse Model. *Mol Ther*. Jul 8 2020;28(7):1706-1716. doi:10.1016/j.ymthe.2020.04.007

38. Thuveson M, Gaengel K, Collu GM, Chin ML, Singh J, Mlodzik M. Integrins are required for synchronous ommatidial rotation in the Drosophila eye linking planar cell polarity signalling to the extracellular matrix. *Open Biol*. Aug 30 2019;9(8):190148. doi:10.1098/rsob.190148

39. Ouyang M, Yu JY, Chen Y, Deng L, Guo CL. Cell-extracellular matrix interactions in the fluidic phase direct the topology and polarity of self-organized epithelial structures. *Cell Prolif*. Apr 2021;54(4):e13014. doi:10.1111/cpr.13014

40. Yu W, Datta A, Leroy P, et al. Beta1-integrin orients epithelial polarity via Rac1 and laminin. *Mol Biol Cell*. Feb 2005;16(2):433-45. doi:10.1091/mbc.e04-05-0435

41. Rasmussen JP, Reddy SS, Priess JR. Laminin is required to orient epithelial polarity in the C. elegans pharynx. *Development*. Jun 2012;139(11):2050-60. doi:10.1242/dev.078360

42. Navis A, Bagnat, M. Apicobasal Polarity and Lumen Formation During Development. Springer; 2015.

43. Lamus F, Martin C, Carnicero E, et al. FGF2/EGF contributes to brain neuroepithelial precursor proliferation and neurogenesis in rat embryos: the involvement of embryonic cerebrospinal fluid. *Dev Dyn*. Jan 2020;249(1):141-153. doi:10.1002/dvdy.135

44. Fame RM, Cortes-Campos C, Sive HL. Brain Ventricular System and Cerebrospinal Fluid Development and Function: Light at the End of the Tube: A Primer with Latest Insights. *Bioessays*. Mar 2020;42(3):e1900186. doi:10.1002/bies.201900186

45. Grant PK, Moens CB. The neuroepithelial basement membrane serves as a boundary and a substrate for neuron migration in the zebrafish hindbrain. *Neural Dev*. Mar 29 2010;5:9. doi:10.1186/1749-8104-5-9

46. Haubensak W, Attardo A, Denk W, Huttner WB. Neurons arise in the basal neuroepithelium of the early mammalian telencephalon: a major site of neurogenesis. *Proc Natl Acad Sci U S A*. Mar 2 2004;101(9):3196-201. doi:10.1073/pnas.0308600100

47. Adler PN. The frizzled/stan pathway and planar cell polarity in the Drosophila wing. *Curr Top Dev Biol*. 2012;101:1-31. doi:10.1016/B978-0-12-394592-1.00001-6

48. Kishimoto N, Sawamoto K. Planar polarity of ependymal cilia. *Differentiation*. Feb 2012;83(2):S86-90. doi:10.1016/j.diff.2011.10.007

49. Campbell HK, Maiers JL, DeMali KA. Interplay between tight junctions & adherens junctions. *Exp Cell Res*. Sep 1 2017;358(1):39-44. doi:10.1016/j.yexcr.2017.03.061

50. Kratzer I, Ek J, Stolp H. The molecular anatomy and functions of the choroid plexus in healthy and diseased brain. *Biochim Biophys Acta Biomembr*. Nov 1 2020;1862(11):183430. doi:10.1016/j.bbamem.2020.183430

51. Wolburg H, Lippoldt A. Tight junctions of the blood-brain barrier: development, composition and regulation. *Vascul Pharmacol*. Jun 2002;38(6):323-37. doi:10.1016/s1537-1891(02)00200-8

52. Bachmann A, Schneider M, Theilenberg E, Grawe F, Knust E. Drosophila Stardust is a partner of Crumbs in the control of epithelial cell polarity. *Nature*. Dec 6 2001;414(6864):638-43. doi:10.1038/414638a

53. Straight SW, Shin K, Fogg VC, et al. Loss of PALS1 expression leads to tight junction and polarity defects. *Mol Biol Cell*. Apr 2004;15(4):1981-90. doi:10.1091/mbc.e03-08-0620

54. Knust E, Bossinger O. Composition and formation of intercellular junctions in epithelial cells. *Science*. Dec 6 2002;298(5600):1955-9. doi:10.1126/science.1072161

55. Shin K, Straight S, Margolis B. PATJ regulates tight junction formation and polarity in mammalian epithelial cells. *J Cell Biol*. Feb 28 2005;168(5):705-11. doi:10.1083/jcb.200408064

56. Bonello T, Aguilar-Aragon M, Tournier A, Thompson BJ, Campanale JP. A picket fence function for adherens junctions in epithelial cell polarity. *Cells Dev*. Dec 2021;168:203719. doi:10.1016/j.cdev.2021.203719

57. Cohen E, Meininger V. Ultrastructural analysis of primary cilium in the embryonic nervous tissue of mouse. *Int J Dev Neurosci*. 1987;5(1):43-51. doi:10.1016/0736-5748(87)90047-5

58. Tong CK, Han YG, Shah JK, Obernier K, Guinto CD, Alvarez-Buylla A. Primary cilia are required in a unique subpopulation of neural progenitors. *Proc Natl Acad Sci U S A*. Aug 26 2014;111(34):12438-43. doi:10.1073/pnas.1321425111

59. Norden C, Young S, Link BA, Harris WA. Actomyosin is the main driver of interkinetic nuclear migration in the retina. *Cell*. Sep 18 2009;138(6):1195-208. doi:10.1016/j.cell.2009.06.032

60. Eze UC, Bhaduri A, Haeussler M, Nowakowski TJ, Kriegstein AR. Single-cell atlas of early human brain development highlights heterogeneity of human neuroepithelial cells and early radial glia. *Nat Neurosci*. Apr 2021;24(4):584-594. doi:10.1038/s41593-020-00794-1

61. Aaku-Saraste E, Oback B, Hellwig A, Huttner WB. Neuroepithelial cells downregulate their plasma membrane polarity prior to neural tube closure and neurogenesis. *Mech Dev*. Dec 1997;69(1-2):71-81. doi:10.1016/s0925-4773(97)00156-1

62. Aaku-Saraste E, Hellwig A, Huttner WB. Loss of occludin and functional tight junctions, but not ZO-1, during neural tube closure--remodeling of the neuroepithelium prior to neurogenesis. *Dev Biol*. Dec 15 1996;180(2):664-79. doi:10.1006/dbio.1996.0336

63. Willardsen MI, Link BA. Cell biological regulation of division fate in vertebrate neuroepithelial cells. *Dev Dyn*. Aug 2011;240(8):1865-79. doi:10.1002/dvdy.22684

64. Egger B, Gold KS, Brand AH. Notch regulates the switch from symmetric to asymmetric neural stem cell division in the Drosophila optic lobe. *Development*. Sep 2010;137(18):2981-7. doi:10.1242/dev.051250

65. Suter DM, Tirefort D, Julien S, Krause KH. A Sox1 to Pax6 switch drives neuroectoderm to radial glia progression during differentiation of mouse embryonic stem cells. *Stem Cells*. Jan 2009;27(1):49-58. doi:10.1634/stemcells.2008-0319

66. Kadowaki M, Nakamura S, Machon O, Krauss S, Radice GL, Takeichi M. N-cadherin mediates cortical organization in the mouse brain. *Dev Biol*. Apr 1 2007;304(1):22-33. doi:10.1016/j.ydbio.2006.12.014

67. Cappello S, Bohringer CR, Bergami M, et al. A radial glia-specific role of RhoA in double cortex formation. *Neuron*. Mar 8 2012;73(5):911-24. doi:10.1016/j.neuron.2011.12.030

68. Gil-Sanz C, Landeira B, Ramos C, Costa MR, Muller U. Proliferative defects and formation of a double cortex in mice lacking Mltt4 and Cdh2 in the dorsal telencephalon. *J Neurosci*. Aug 6 2014;34(32):10475-87. doi:10.1523/JNEUROSCI.1793-14.2014

69. Spassky N, Merkle FT, Flames N, Tramontin AD, Garcia-Verdugo JM, Alvarez-Buylla A. Adult ependymal cells are postmitotic and are derived from radial glial cells during embryogenesis. *J Neurosci*. Jan 5 2005;25(1):10-8. doi:10.1523/JNEUROSCI.1108-04.2005

70. Liu X, Bolteus AJ, Balkin DM, Henschel O, Bordey A. GFAP-expressing cells in the postnatal subventricular zone display a unique glial phenotype intermediate between radial glia and astrocytes. *Glia*. Oct 2006;54(5):394-410. doi:10.1002/glia.20392

71. Llorens-Bobadilla E, Zhao S, Baser A, Saiz-Castro G, Zwadlo K, Martin-Villalba A. Single-Cell Transcriptomics Reveals a Population of Dormant Neural Stem Cells that Become Activated upon Brain Injury. *Cell Stem Cell*. Sep 3 2015;17(3):329-40. doi:10.1016/j.stem.2015.07.002

72. Li X, Liu G, Yang L, et al. Decoding Cortical Glial Cell Development. *Neurosci Bull*. Apr 2021;37(4):440-460. doi:10.1007/s12264-021-00640-9

73. Assemat E, Bazellieres E, Pallesi-Pocachard E, Le Bivic A, Massey-Harroche D. Polarity complex proteins. *Biochim Biophys Acta*. Mar 2008;1778(3):614-30. doi:10.1016/j.bbamem.2007.08.029

74. Tepass U, Theres C, Knust E. crumbs encodes an EGF-like protein expressed on apical membranes of Drosophila epithelial cells and required for organization of epithelia. *Cell*. Jun 1 1990;61(5):787-99. doi:10.1016/0092-8674(90)90189-l

75. Banks E, Francis V, Lin S-J, et al. Loss of symmetric cell division of apical neural progenitors drives *DENND5A*-related developmental and epileptic encephalopathy. *medRxiv*. 2023-01-01 00:00:00 2023;doi:https://doi.org/10.1101/2022.08.23.22278845

76. Li Y, Wei Z, Yan Y, Wan Q, Du Q, Zhang M. Structure of Crumbs tail in complex with the PALS1 PDZ-SH3-GK tandem reveals a highly specific assembly mechanism for the apical Crumbs complex. *Proc Natl Acad Sci U S A*. Dec 9 2014;111(49):17444-9. doi:10.1073/pnas.1416515111

77. Kamberov E, Makarova O, Roh M, et al. Molecular cloning and characterization of Pals, proteins associated with mLin-7. *J Biol Chem*. Apr 14 2000;275(15):11425-31. doi:10.1074/jbc.275.15.11425

78. Roh MH, Makarova O, Liu CJ, et al. The Maguk protein, Pals1, functions as an adapter, linking mammalian homologues of Crumbs and Discs Lost. *J Cell Biol*. Apr 1 2002;157(1):161-72. doi:10.1083/jcb.200109010

79. Roh MH, Liu CJ, Laurinec S, Margolis B. The carboxyl terminus of zona occludens-3 binds and recruits a mammalian homologue of discs lost to tight junctions. *J Biol Chem*. Jul 26 2002;277(30):27501-9. doi:10.1074/jbc.M201177200

80. Haskins J, Gu L, Wittchen ES, Hibbard J, Stevenson BR. ZO-3, a novel member of the MAGUK protein family found at the tight junction, interacts with ZO-1 and occludin. *J Cell Biol*. Apr 6 1998;141(1):199-208. doi:10.1083/jcb.141.1.199

81. Adachi M, Hamazaki Y, Kobayashi Y, et al. Similar and distinct properties of MUPP1 and Patj, two homologous PDZ domain-containing tight-junction proteins. *Mol Cell Biol*. May 2009;29(9):2372-89. doi:10.1128/MCB.01505-08

82. Saugier-Veber P, Marguet F, Lecoquierre F, et al. Hydrocephalus due to multiple ependymal malformations is caused by mutations in the MPDZ gene. *Acta Neuropathol Commun*. May 1 2017;5(1):36. doi:10.1186/s40478-017-0438-4

83. Feldner A, Adam MG, Tetzlaff F, et al. Loss of Mpdz impairs ependymal cell integrity leading to perinatal-onset hydrocephalus in mice. *EMBO Mol Med*. Jul 2017;9(7):890-905. doi:10.15252/emmm.201606430

84. Yang J, Simonneau C, Kilker R, et al. Murine MPDZ-linked hydrocephalus is caused by hyperpermeability of the choroid plexus. *EMBO Mol Med*. Jan 2019;11(1)doi:10.15252/emmm.201809540

85. Serra R, Simard JM. Adherens, tight, and gap junctions in ependymal cells: A systematic review of their contribution to CSF-brain barrier. *Front Neurol*. 2023;14:1092205. doi:10.3389/fneur.2023.1092205

86. Shah PT, Stratton JA, Stykel MG, et al. Single-Cell Transcriptomics and Fate Mapping of Ependymal Cells Reveals an Absence of Neural Stem Cell Function. *Cell*. May 3 2018;173(4):1045-1057 e9. doi:10.1016/j.cell.2018.03.063

87. Kim S, Lehtinen MK, Sessa A, et al. The apical complex couples cell fate and cell survival to cerebral cortical development. *Neuron*. Apr 15 2010;66(1):69-84. doi:10.1016/j.neuron.2010.03.019

88. Boroviak T, Rashbass P. The apical polarity determinant Crumbs 2 is a novel regulator of ESC-derived neural progenitors. *Stem Cells*. Feb 2011;29(2):193-205. doi:10.1002/stem.567

89. Bendriem RM, Singh S, Aleem AA, Antonetti DA, Ross ME. Tight junction protein occludin regulates progenitor Self-Renewal and survival in developing cortex. *Elife*. Dec 3 2019;8doi:10.7554/eLife.49376

90. Prandovszky E, Horvath S, Gellert L, et al. Nectin-1 (HveC) is expressed at high levels in neural subtypes that regulate radial migration of cortical and cerebellar neurons of the developing human and murine brain. *J Neurovirol*. Apr 2008;14(2):164-72. doi:10.1080/13550280801898672

91. Riga A, Castiglioni VG, Boxem M. New insights into apical-basal polarization in epithelia. *Curr Opin Cell Biol*. Feb 2020;62:1-8. doi:10.1016/j.ceb.2019.07.017

92. Buckley CE, St Johnston D. Apical-basal polarity and the control of epithelial form and function. *Nat Rev Mol Cell Biol*. Aug 2022;23(8):559-577. doi:10.1038/s41580-022-00465-y

93. Wu H, Feng W, Chen J, Chan LN, Huang S, Zhang M. PDZ domains of Par-3 as potential phosphoinositide signaling integrators. *Mol Cell*. Dec 14 2007;28(5):886-98. doi:10.1016/j.molcel.2007.10.028

94. Feng W, Wu H, Chan LN, Zhang M. Par-3-mediated junctional localization of the lipid phosphatase PTEN is required for cell polarity establishment. *J Biol Chem*. Aug 22 2008;283(34):23440-9. doi:10.1074/jbc.M802482200

95. Maehama T, Dixon JE. The tumor suppressor, PTEN/MMAC1, dephosphorylates the lipid second messenger, phosphatidylinositol 3,4,5-trisphosphate. *J Biol Chem*. May 29 1998;273(22):13375-8. doi:10.1074/jbc.273.22.13375

96. Martin-Belmonte F, Gassama A, Datta A, et al. PTEN-mediated apical segregation of phosphoinositides controls epithelial morphogenesis through Cdc42. *Cell*. Jan 26 2007;128(2):383-97. doi:10.1016/j.cell.2006.11.051

97. Suzuki A, Yamanaka T, Hirose T, et al. Atypical protein kinase C is involved in the evolutionarily conserved par protein complex and plays a critical role in establishing epithelia-specific junctional structures. *J Cell Biol*. Mar 19 2001;152(6):1183-96. doi:10.1083/jcb.152.6.1183

98. Horikoshi Y, Suzuki A, Yamanaka T, et al. Interaction between PAR-3 and the aPKC-PAR-6 complex is indispensable for apical domain development of epithelial cells. *J Cell Sci*. May 15 2009;122(Pt 10):1595-606. doi:10.1242/jcs.043174

99. Nagai-Tamai Y, Mizuno K, Hirose T, Suzuki A, Ohno S. Regulated protein-protein interaction between aPKC and PAR-3 plays an essential role in the polarization of epithelial cells. *Genes Cells*. Nov 2002;7(11):1161-71. doi:10.1046/j.1365-2443.2002.00590.x

100. Nunes de Almeida F, Walther RF, Presse MT, Vlassaks E, Pichaud F. Cdc42 defines apical identity and regulates epithelial morphogenesis by promoting apical recruitment of Par6-aPKC and Crumbs. *Development*. Aug 12 2019;146(15)doi:10.1242/dev.175497

101. Whitney DS, Peterson FC, Kittell AW, Egner JM, Prehoda KE, Volkman BF. Binding of Crumbs to the Par-6 CRIB-PDZ Module Is Regulated by Cdc42. *Biochemistry*. Mar 15 2016;55(10):1455-61. doi:10.1021/acs.biochem.5b01342

102. Sotillos S, Diaz-Meco MT, Caminero E, Moscat J, Campuzano S. DaPKC-dependent phosphorylation of Crumbs is required for epithelial cell polarity in Drosophila. *J Cell Biol*. Aug 16 2004;166(4):549-57. doi:10.1083/jcb.200311031

103. Wei Z, Li Y, Ye F, Zhang M. Structural basis for the phosphorylation-regulated interaction between the cytoplasmic tail of cell polarity protein crumbs and the actin-binding protein moesin. *J Biol Chem*. May 1 2015;290(18):11384-92. doi:10.1074/jbc.M115.643791

104. Lemmers C, Michel D, Lane-Guermonprez L, et al. CRB3 binds directly to Par6 and regulates the morphogenesis of the tight junctions in mammalian epithelial cells. *Mol Biol Cell*. Mar 2004;15(3):1324-33. doi:10.1091/mbc.e03-04-0235

105. Ivanova ME, Fletcher GC, O'Reilly N, Purkiss AG, Thompson BJ, McDonald NQ. Structures of the human Pals1 PDZ domain with and without ligand suggest gated access of Crb to the PDZ peptide-binding groove. *Acta Crystallogr D Biol Crystallogr*. Mar 2015;71(Pt 3):555-64. doi:10.1107/S139900471402776X

106. Sterling N, Duncan AR, Park R, et al. De novo variants in MPP5 cause global developmental delay and behavioral changes. *Hum Mol Genet*. Dec 18 2020;29(20):3388-3401. doi:10.1093/hmg/ddaa224

107. Zanotta N, Panzeri E, Minghetti S, et al. A case of a childhood onset developmental encephalopathy with a novel de novo truncating variant in the Membrane Protein Palmitoylated 5 (MPP5) gene. *Seizure*. Jan 23 2023;doi:10.1016/j.seizure.2023.01.015

108. Lamont RE, Tan WH, Innes AM, et al. Expansion of phenotype and genotypic data in CRB2-related syndrome. *Eur J Hum Genet*. Oct 2016;24(10):1436-44. doi:10.1038/ejhg.2016.24

109. Slavotinek A, Kaylor J, Pierce H, et al. CRB2 mutations produce a phenotype resembling congenital nephrosis, Finnish type, with cerebral ventriculomegaly and raised alpha-fetoprotein. *Am J Hum Genet*. Jan 8 2015;96(1):162-9. doi:10.1016/j.ajhg.2014.11.013

110. Tessier A, Roux N, Boutaud L, et al. Bi-allelic variations in CRB2, encoding the crumbs cell polarity complex component 2, lead to non-communicating hydrocephalus due to atresia of the aqueduct of sylvius and central canal of the medulla. *Acta Neuropathol Commun*. Feb 20 2023;11(1):29. doi:10.1186/s40478-023-01519-8

111. Chen X, An Y, Gao Y, et al. Rare Deleterious PARD3 Variants in the aPKC-Binding Region are Implicated in the Pathogenesis of Human Cranial Neural Tube Defects Via Disrupting Apical Tight Junction Formation. *Hum Mutat*. Apr 2017;38(4):378-389. doi:10.1002/humu.23153

112. Yousaf A, Waltes R, Haslinger D, et al. Quantitative genome-wide association study of six phenotypic subdomains identifies novel genome-wide significant variants in autism spectrum disorder. *Transl Psychiatry*. Jul 5 2020;10(1):215. doi:10.1038/s41398-020-00906-2

113. Kenny EM, Cormican P, Furlong S, et al. Excess of rare novel loss-of-function variants in synaptic genes in schizophrenia and autism spectrum disorders. *Mol Psychiatry*. Aug 2014;19(8):872-9. doi:10.1038/mp.2013.127

114. Martinelli S, Krumbach OHF, Pantaleoni F, et al. Functional Dysregulation of CDC42 Causes Diverse Developmental Phenotypes. *Am J Hum Genet*. Feb 1 2018;102(2):309-320. doi:10.1016/j.ajhg.2017.12.015

115. Malatesta P, Appolloni I, Calzolari F. Radial glia and neural stem cells. *Cell Tissue Res*. Jan 2008;331(1):165-78. doi:10.1007/s00441-007-0481-8

116. Medelnik JP, Roensch K, Okawa S, et al. Signaling-Dependent Control of Apical Membrane Size and Self-Renewal in Rosette-Stage Human Neuroepithelial Stem Cells. *Stem Cell Reports*. Jun 5 2018;10(6):1751-1765. doi:10.1016/j.stemcr.2018.04.018

117. Park JY, Hughes LJ, Moon UY, et al. The apical complex protein Pals1 is required to maintain cerebellar progenitor cells in a proliferative state. *Development*. Jan 1 2016;143(1):133-46. doi:10.1242/dev.124180

118. Bultje RS, Castaneda-Castellanos DR, Jan LY, Jan YN, Kriegstein AR, Shi SH. Mammalian Par3 regulates progenitor cell asymmetric division via notch signaling in the developing neocortex. *Neuron*. Jul 30 2009;63(2):189-202. doi:10.1016/j.neuron.2009.07.004

119. Kosodo Y, Roper K, Haubensak W, Marzesco AM, Corbeil D, Huttner WB. Asymmetric distribution of the apical plasma membrane during neurogenic divisions of mammalian neuroepithelial cells. *EMBO J*. Jun 2 2004;23(11):2314-24. doi:10.1038/sj.emboj.7600223

120. Miyata T, Kawaguchi A, Okano H, Ogawa M. Asymmetric inheritance of radial glial fibers by cortical neurons. *Neuron*. Sep 13 2001;31(5):727-41. doi:10.1016/s0896-6273(01)00420-2

121. Tsunekawa Y, Britto JM, Takahashi M, Polleux F, Tan SS, Osumi N. Cyclin D2 in the basal process of neural progenitors is linked to non-equivalent cell fates. *EMBO J*. Apr 18 2012;31(8):1879-92. doi:10.1038/emboj.2012.43

122. Shitamukai A, Konno D, Matsuzaki F. Oblique radial glial divisions in the developing mouse neocortex induce self-renewing progenitors outside the germinal zone that resemble primate outer subventricular zone progenitors. *J Neurosci*. Mar 9 2011;31(10):3683-95. doi:10.1523/JNEUROSCI.4773-10.2011

123. Alexandre P, Reugels AM, Barker D, Blanc E, Clarke JD. Neurons derive from the more apical daughter in asymmetric divisions in the zebrafish neural tube. *Nat Neurosci*. Jun 2010;13(6):673-9. doi:10.1038/nn.2547

124. Noctor SC, Flint AC, Weissman TA, Dammerman RS, Kriegstein AR. Neurons derived from radial glial cells establish radial units in neocortex. *Nature*. Feb 8 2001;409(6821):714-20. doi:10.1038/35055553

125. Knoblich JA. Mechanisms of asymmetric stem cell division. *Cell*. Feb 22 2008;132(4):583-97. doi:10.1016/j.cell.2008.02.007

126. Prosser SL, Pelletier L. Mitotic spindle assembly in animal cells: a fine balancing act. *Nat Rev Mol Cell Biol*. Mar 2017;18(3):187-201. doi:10.1038/nrm.2016.162

127. Grill SW, Hyman AA. Spindle positioning by cortical pulling forces. *Dev Cell*. Apr 2005;8(4):461-5. doi:10.1016/j.devcel.2005.03.014

128. Hao Y, Du Q, Chen X, et al. Par3 controls epithelial spindle orientation by aPKC-mediated phosphorylation of apical Pins. *Curr Biol*. Oct 26 2010;20(20):1809-18. doi:10.1016/j.cub.2010.09.032

129. Durgan J, Kaji N, Jin D, Hall A. Par6B and atypical PKC regulate mitotic spindle orientation during epithelial morphogenesis. *J Biol Chem*. Apr 8 2011;286(14):12461-74. doi:10.1074/jbc.M110.174235

130. Gloerich M, Bianchini JM, Siemers KA, Cohen DJ, Nelson WJ. Cell division orientation is coupled to cell-cell adhesion by the E-cadherin/LGN complex. *Nat Commun*. Jan 3 2017;8:13996. doi:10.1038/ncomms13996

131. Peyre E, Jaouen F, Saadaoui M, et al. A lateral belt of cortical LGN and NuMA guides mitotic spindle movements and planar division in neuroepithelial cells. *J Cell Biol*. Apr 4 2011;193(1):141-54. doi:10.1083/jcb.201101039

132. Zheng Z, Zhu H, Wan Q, et al. LGN regulates mitotic spindle orientation during epithelial morphogenesis. *J Cell Biol*. Apr 19 2010;189(2):275-88. doi:10.1083/jcb.200910021

133. Konno D, Shioi G, Shitamukai A, et al. Neuroepithelial progenitors undergo LGN-dependent planar divisions to maintain self-renewability during mammalian neurogenesis. *Nat Cell Biol*. Jan 2008;10(1):93-101. doi:10.1038/ncb1673

134. Du Q, Taylor L, Compton DA, Macara IG. LGN blocks the ability of NuMA to bind and stabilize microtubules. A mechanism for mitotic spindle assembly regulation. *Curr Biol*. Nov 19 2002;12(22):1928-33. doi:10.1016/s0960-9822(02)01298-8

135. Woodruff JB, Drubin DG, Barnes G. Dynein-driven mitotic spindle positioning restricted to anaphase by She1p inhibition of dynactin recruitment. *Mol Biol Cell*. Jul 2009;20(13):3003-11. doi:10.1091/mbc.e09-03-0186

136. Lehtinen MK, Zappaterra MW, Chen X, et al. The cerebrospinal fluid provides a proliferative niche for neural progenitor cells. *Neuron*. Mar 10 2011;69(5):893-905. doi:10.1016/j.neuron.2011.01.023

137. Saade M, Gonzalez-Gobartt E, Escalona R, Usieto S, Marti E. Shh-mediated centrosomal recruitment of PKA promotes symmetric proliferative neuroepithelial cell division. *Nat Cell Biol*. Apr 27 2017;19(5):493-503. doi:10.1038/ncb3512

138. Huang X, Liu J, Ketova T, et al. Transventricular delivery of Sonic hedgehog is essential to cerebellar ventricular zone development. *Proc Natl Acad Sci U S A*. May 4 2010;107(18):8422-7. doi:10.1073/pnas.0911838107

139. Matsuzaki F, Shitamukai A. Cell Division Modes and Cleavage Planes of Neural Progenitors during Mammalian Cortical Development. *Cold Spring Harb Perspect Biol*. Sep 1 2015;7(9):a015719. doi:10.1101/cshperspect.a015719

140. Lehtinen MK, Walsh CA. Neurogenesis at the brain-cerebrospinal fluid interface. *Annu Rev Cell Dev Biol*. 2011;27:653-79. doi:10.1146/annurev-cellbio-092910-154026

141. Han C, Alkhater R, Froukh T, et al. Epileptic Encephalopathy Caused by Mutations in the Guanine Nucleotide Exchange Factor DENND5A. *Am J Hum Genet*. Dec 1 2016;99(6):1359-1367. doi:10.1016/j.ajhg.2016.10.006

142. Anazi S, Maddirevula S, Faqeih E, et al. Clinical genomics expands the morbid genome of intellectual disability and offers a high diagnostic yield. *Mol Psychiatry*. Apr 2017;22(4):615-624. doi:10.1038/mp.2016.113

143. Marat AL, Dokainish H, McPherson PS. DENN domain proteins: regulators of Rab GTPases. *J Biol Chem*. Apr 22 2011;286(16):13791-800. doi:10.1074/jbc.R110.217067

144. Li Y, Xu J, Xiong H, et al. Cancer driver candidate genes AVL9, DENND5A and NUPL1 contribute to MDCK cystogenesis. *Oncoscience*. 2014;1(12):854-865. doi:10.18632/oncoscience.107

145. Miserey-Lenkei S, Waharte F, Boulet A, et al. Rab6-interacting protein 1 links Rab6 and Rab11 function. *Traffic*. Oct 2007;8(10):1385-403. doi:10.1111/j.1600-0854.2007.00612.x

3 Chapter 2: Biallelic pathogenic variants in *DENND5A* result in a developmental disorder with distinct radiological signatures

Emily Banks[1], Vincent Francis[1], Fares Kharfallah[1], Vladimir Fonov[1], Maxime Levesque[1], Chanshuai Han[1], Gopinath Kulasekaran[1], Marius Tuznik[1], Armin Bayati[1], Reem Al-Khater[2], Fowzan S. Alkuraya[3], Loukas Argyriou[4], Meisam Babaei[5], Melanie Bahlo[6], Behnoosh Bakhshoodeh[7], Eileen Barr[8], Lauren Bartik[9,10], Mahmoud Bassiony[11], Miriam Bertrand[12], Dominique Braun[13], Rebecca Buchert[12], Mauro Budetta[14], Maxime Cadieux-Dion[15], Daniel Calame[16-18], Heidi Cope[19], Donna Cushing[20], Stephanie Efthymiou[21], Marwa A. Elmaksoud[22], Huda G. El Said[23], Tawfiq Froukh[24], Harinder K. Gill[25], Joseph G. Gleeson[26,27], Laura Gogoll[13], Elaine S.-Y. Goh[20], Vykuntaraju K Gowda[28], Tobias B. Haack[12], Mais O. Hashem[3], Stefan Hauser[29,30], Trevor L. Hoffman[31], Jacob S. Hogue[32], Akimoto Hosokawa[33], Henry Houlden[21], Stephanie Huynh[25], Ehsan G. Karimiani[34,35], Silke Kaulfuß[4], G. Christoph Korenke[36], Amy Kritzer[37], Hane Lee[38], James R. Lupski[16-18,39], Elysa J. Marco[40], Kirsty McWalter[41], Arakel Minassian[42], Berge A. Minassian[43], David Murphy[21], Juanita Neira-Fresneda[8], Hope Northrup[44], Denis Nyaga[33], Barbara Oehl-Jaschkowitz[45], Matthew Osmond[46], Richard Person[41], Davut Pehlivan[16-18], Lynette G. Sadleir[33], Carol Saunders[9,15,47], Ludger Schoels[29,30], Vandana Shashi[19], Rebecca C. Spillman[19], Varunvenkat M. Srinivasan[28], Paria N. Torbati[35], Tulay Tos[48], Undiagnosed Diseases Network[†], Maha S. Zaki[49], Dihong Zhou[9,10], Christiane Zweier[13], Thomas M. Durcan[1], Ziv Gan-Or[1,50], Massimo Avoli[1], Cesar Alves[51], Reza Maroofian[21], David A. Rudko[1], Peter S. McPherson[1].

[1] Department of Neurology and Neurosurgery, Montreal Neurological Institute, McGill University, Montréal, QC H3A 2B4, Canada

[2] Johns Hopkins Aramco Healthcare, Dhahran 34465, Saudi Arabia

[3] Department of Translational Genomics, Center for Genomic Medicine, King Faisal Specialist Hospital and Research Center, Riyadh 11211, Saudi Arabia

[4] Institute of Human Genetics, University Medical Center, Göttingen 37073, Germany

[5] Department of Pediatrics, North Khorasan University of Medical Sciences, Bojnurd, Iran

[6] Walter and Eliza Hall Institute for Medical Research, Parkville Victoria 3052, Australia

[7] Mashhad University of Medical Sciences, Mashhad, Iran

[8] Emory University, Department of Human Genetics, Atlanta, GA 30322, USA

[9] University of Missouri-Kansas City, School of Medicine, Kansas City, MO 64108, USA

[10] Department of Pediatrics, Division of Clinical Genetics, Children's Mercy Hospital, Kansas City, MO 64108, USA

[11] Faculty of Medicine, Alexandria University, Alexandria, Egypt

[12] Institute of Medical Genetics and Applied Genomics, University of Tübingen, Tübingen 72076, Germany

[13] Department of Human Genetics, Inselspital, Bern University Hospital, University of Bern, Bern, Switzerland

[14] Paediatric and Child Neurology Unit, Cava de' Tirreni AOU S. Giovanni di Dio e Ruggiero d'Aragona Hospital, Salerno, Italy

[15] Department of Pathology and Laboratory Medicine, Children's Mercy Hospital, Kansas City, MO 64108, USA

[16] Department of Pediatrics, Baylor College of Medicine, Houston, TX, USA

[17] Texas Children's Hospital, Houston, TX, USA

[18] Department of Molecular and Human Genetics, Baylor College of Medicine, Houston, TX, USA

[19] Division of Medical Genetics, Department of Pediatrics, Duke University Medical Center, Durham, NC 27710, USA

[20] Laboratory Medicine and Genetics, Trillium Health Partners, Mississauga, ON L5B 1B8, Canada

[21] Department of Neuromuscular Diseases, University College London (UCL) Institute of Neurology, Queen Square, London, WC1N 3BG, UK

[22] Neurology Unit, Department of Pediatrics, Faculty of Medicine, University of Alexandria, Alexandria, Egypt

[23] Department of Family Health, High Institute of Public Health, Faculty of Medicine, University of Alexandria, Alexandria, Egypt

[24] Department of Biotechnology and Genetic Engineering, Philadelphia University, Amman 19392, Jordan

[25] Provincial Medical Genetics Program at BC Women's Health Centre, Vancouver, BC V6H 3N1, Canada

[26] Department of Neurosciences, University of California San Diego, La Jolla, CA, USA

[27] Rady Children's Institute for Genomic Medicine, San Diego, CA, USA

[28] Department of Pediatric Neurology, Indira Gandhi Institute of Child Health, Bangalore, India

[29] Center for Neurology and Hertie Institute for Clinical Brain Research, University Tübingen, Tübingen 72076, Germany

[30] German Center of Neurodegenerative Diseases (DZNE), Tübingen 72076, Germany

[31] Southern California Kaiser Permanente Medical Group, Department of Regional Genetics, Anaheim, CA 92806, USA

[32] Madigan Army Medical Center, Tacoma, WA 98431, USA

[33] Department of Paediatrics and Child Health, University of Otago, Wellington, 6242, New Zealand

[34] Molecular and Clinical Sciences Institute, St. George's, University of London, Cranmer Terrace, London SW17 0RE, UK

[35] Department of Medical Genetics, Next Generation Genetic Polyclinic, Mashhad, Iran

[36] Department of Neuropediatrics, University Children's Hospital, Klinikum Oldenburg, Oldenburg 26133, Germany

[37] Division of Genetics and Genomics, Boston Children's Hospital, Boston, MA 02115, USA

[38] 3billion, Inc, Seoul, South Korea

[39] Human Genome Sequencing Center, Baylor College of Medicine, Houston, TX, USA

[40] Cortica Healthcare, San Rafael, CA 94903, USA

[41] GeneDx, Gaithersburg, MD 20877, USA

[42] Centre for Applied Genomics, Genetics, and Genome Biology, Hospital for Sick Children, Toronto, ON M5G 0A4, Canada

[43] UT Southwestern Medical Center, Departments of Pediatrics and Neurology, Dallas, TX 75390, USA

[44] Department of Pediatrics, McGovern Medical School at the University of Texas Health Science Center at Houston (UTHealth) and Children's Memorial Hermann Hospital, Houston, TX 77030, USA

[45] Practice of Human Genetics, Homburg (Saar), Germany

[46] Children's Hospital of Eastern Ontario Research Institute, University of Ottawa, Ottawa K1H 8L1, Canada

[47] Center for Pediatric Genomic Medicine Children's Mercy - Kansas City, Missouri, USA

[48] University of Health Sciences, Zubeyde Hanim Research and Training Hospital of Women's Health and Diseases, Department of Medical Genetics, Ankara 06080, Turkey

[49] Human Genetics and Genome Research Division, Clinical Genetics Department, National Research Centre, Cairo, Egypt

[50] Department of Human Genetics, McGill University, Montréal, QC H3A 2B4, Canada

[51] Division of Neuroradiology, The Children's Hospital of Philadelphia, Philadelphia, PA 19104, USA

[†] The full list of authors in network is listed in Chapter 2 Author Appendix (**3.6.1**).

3.1 Introduction

Homozygous pathogenic variants in *DENND5A*, a gene encoding a protein expressed at high levels in the brain during development, have previously been linked to DEE in four consanguineous families[1,2]. Many neurodevelopmental disorders have highly similar neuroanatomical features, making diagnosis based on radiological findings difficult. The previously reported *DENND5A* patients were noted to have a set of common brain abnormalities such as microcephaly, reduced cerebral cortex volume, calcifications, and enlarged lateral ventricles[1], but these characteristics are unremarkable in the context of DEEs with a structural etiology and do not hold much diagnostic value. We thus sought to investigate the clinical phenotype among individuals with biallelic *DENND5A* variants in greater detail. Additionally, previous studies have only examined patients with homozygous *DENND5A* variants from consanguineous families[1,2]. While these studies are useful since variant pathogenicity is easier to decipher, our study also examines individuals with compound heterozygous variants in *DENND5A*, of which some variants are relatively common in the general population.

We identified a cohort of 24 individuals from 22 families with biallelic *DENND5A* variants, including the individuals from the previous studies, and determined their clinical presentation through a phenotypic survey answered by their treating clinicians coupled with detailed neuroimaging analysis when possible. Severe cases from unrelated individuals show a cluster of neuroanatomical hallmarks that are, to our knowledge, unique to *DENND5A*-related DEE. We also provide clinical evidence that certain missense variants, currently classified as likely benign or variants of uncertain significance, should probably be re-classified as likely pathogenic. Conversely, we identify missense variants currently classified as variants of uncertain significance that we believe might be likely benign. The results of this study will provide genetic counselors

and physicians valuable information to reference when working with families and patients with *DENND5A* variants.

3.2 Results

3.2.1 Human cohort summary

Following our initial analysis of two families with homozygous variants in DENND5A[2], we identified a cohort of 24 people (11 F, 13 M, mean age = 9.0 years, *SD* = 6.0) from 22 families with biallelic *DENND5A* variants. Thirty unique *DENND5A* variants were identified across the 14 homozygous and 10 compound heterozygous individuals. Seven members of the cohort have at least one additional variant flagged as potentially causative. **Table 2.1** summarizes each person in the cohort, including their participant IDs, gene variant(s), predicted American College of Medical Genetics and Genomics (ACMG) variant interpretations, allele frequencies obtained from the gnomAD v2.1.1 dataset (https://gnomad.broadinstitute.org), seizure types and response to anti-seizure medications, occipitofrontal circumferences (OFCs), calculated scores corresponding to neurological and developmental phenotypes, and developmental outcomes. Pedigrees are available in **Figure S2.1** for participants 25-30, and some have affected family members not included in the cohort due to the unavailability of their clinical data. Pedigrees for participants 10, 15, and 16 were published previously[2]. None of the *DENND5A* point mutations in the cohort were found in the homozygous state among 140,000 individuals on gnomAD, a database that removes individuals affected by severe pediatric disease, indicating that biallelic pathogenic variants are likely incompatible with normal development. Twenty-five of the variants are found in the coding sequence, 2 are copy number variants (exon 1-14 duplication [NC_000011.9:(9171749_9172227)_(9316934_9321244)dup] and exon 1 deletion [NC_000011.10:g. 9262758_9268826del]), and 3 are intronic variants located in splice sites (splice donor variants c.2283+1G>T and c.949+1G>A, and polypyrimidine tract variant

c.950-20_950-17delTTTT). The coding variants span the length of the protein including 9 in the DENN domain, 2 in the RUN1 domain, 6 in the PLAT domain, 4 in the RUN2 domain, and 4 in predicted linker regions between the folded modules (**Fig. 2.1a**). [3]

Complete phenotypic data for each member of the cohort is available in Source Data. The phenotypes observed in more than 50% of individuals with biallelic *DENND5A* variants were seizures (21/24), microcephaly (16/24), ventriculomegaly (15/24), hypertonia (14/24), cerebral hypoplasia (13/24), and hyperreflexia (13/24); **Figure 2.1b**). It is important to note that participants 8 (p.K485E/p.R1159W), 19 (p.P955L/p.T136R), and 20 (exon 1-14 dup) did not present with seizures. Participant 8 had a normal brain MRI and an autism spectrum disorder diagnosis requiring low levels of support, participant 20 exhibited global developmental delay with a normal brain MRI, and participant 19 presented with moderate intellectual disability but did not undergo neuroimaging. These observations suggest that these individuals do not have *DENND5A*-related DEE and that one or more of these variants may be benign or inherently less pathogenic. [3]

Seizures were reported in 20/23 individuals, with an average age of onset of 4.8 months (*SD* = 5.9). Seizures typically onset within the first year of life with one patient experiencing their first seizure at 2 years of age. A funnel chart showing the frequencies of commonly reported seizure types is presented in **Figure 2.1c**. Focal to bilateral tonic-clonic are the most prominent seizure type, diagnosed in 9 individuals. Focal tonic seizures followed in 7 reported cases, 4 of whom were known to have impaired awareness. Among the 6 individuals presenting with epileptic spasms, 3 had a generalized onset, 2 had a focal onset, and 1 had an unknown onset. Generalized tonic-clonic seizures were reported in 5 individuals, as were focal clonic seizures. Three of the cases with focal clonic seizures had

documented impaired awareness. Three individuals had focal myoclonic seizures, of which 2 cases had impaired awareness. In general, when the information was available, most focal seizures were accompanied by an impairment in awareness, with only one case retaining awareness. Seizures were generally drug resistant, but control was achieved in 6 cases with variable antiepileptic treatment. Anti-seizure medications that helped, did not affect, and worsened seizures can be seen for each case in **Table 1**. [3]

All cases of microcephaly in the cohort were primary, with no cases of secondary microcephaly reported. Although microcephaly appears to be a major feature of *DENND5A*-related DEE, OFC percentiles ranged considerably (*M* = 18.5, *Mdn* = 2.9, *SD* = 30.2, *Min* = <1, *Max* = 97). A histogram depicting the distribution of known OFCs can be observed in **Fig. 2.1d**. One case (participant 1) of macrocephaly was reported, possibly secondary to their benign external hydrocephalus. Another case (participant 20) was noted to be "borderline" microcephalic with an OFC percentile of 4. Among the 7 individuals with normal OFCs, 6 underwent neuroimaging and 5 had clinically significant reductions in gray and/or white matter, indicating that neurodevelopment was compromised in most cases even when head circumference was within normal limits. [3]

Failure to meet key developmental milestones was almost universal in the cohort, evidenced by the fact that all but one (participant 8; p.K485E/p.R1159W) presented with or had a history of global developmental delay. Among cohort members assessed after age 5, 9 had a severe intellectual disability (ID), profound ID was reported for 3 individuals, moderate ID was observed in 2 cases, and one participant (8) had no ID. Within the cohort, 15/24 (63%) were nonverbal, 7/24 (29%) were limited to single-word speech, and 2/24 (8%) could speak in sentences. Eye contact was present in 11 of 24 cases (46%). Eight of

24 (33%) could walk independently and 11/24 (46%) were able to reach for and grasp objects. Motor skills were assessed via a scoring system across the group (section **3.8.1**), where a low score corresponds to no or minimal motor skills. Motor capabilities were more severely affected in those with microcephaly (M_{Micro} = 3.2, $M_{\text{No micro}}$ = 7.2, SD_{Micro} = 3.5, $SD_{\text{No micro}}$ = 3.4, two-tailed Mann-Whitney U, Z = -2.55, p = .011; **Fig. 2.1e**). Additionally, those with biallelic missense variants in *DENND5A* (M = 7.4, SD = 3.7) had significantly higher motor scores compared to those with either biallelic frameshift or nonsense variants (M = 3.5, SD = 3.7), as well as those with a combination of missense, frameshift, nonsense, intronic, or copy number variants (M = 2.9, SD = 3.0, Kruskal-Wallis H = 7.02, p = .03; **Fig. 2.1f**). [3]

MRIs or computed tomography (CT) scans revealed abnormalities in 20 of the 23 cases that underwent imaging. Normal MRIs were reported for participants 8, 20 and 26. We devised a scoring system (section **3.8.2**) to analyze the extent of neurological phenotypes across the group and found that variant type influences neurological phenotype severity, with more abnormalities in individuals with biallelic frameshift or nonsense variants (M = 7.6, SD = 1.6) compared to those with both biallelic missense variants (M = 2.8, SD = 1.6, p = .0004) or another combination of variant types (M = 3.8, SD = 1.9, p = .002, one-way ANOVA, $F(2, 20)$ = [12.996], p = .0002; Fig. 1g). No significant difference in neurological score was observed between those with biallelic missense variants and those with a combination of missense, nonsense, frameshift, intronic, or copy number variants (p = .657).

Not all MR/CT images were made available, but all available images are presented in **Figure 2.2** and **Figure S2.2**. Raw MRI data from 5 cases and raw CT data from 1 case were analyzed by a pediatric neuroradiologist. Of these cases, two unrelated individuals

(participants 5 and 14), both homozygous for *DENND5A* frameshift variants, showed a "complete" phenotype and had an interesting combination of neuroanatomical abnormalities. These include severe dysgenesis of the basal ganglia with an indistinct and dysplastic thalamic transition, diencephalic-mesencephalic junction dysplasia, and cortical malformations, particularly with pachygyria involving the occipital lobes, a reduced volume of the white matter with associated striatal and periventricular calcifications and ventriculomegaly, agenesis or severe dysplasia/hypoplasia of the corpus callosum, thin anterior commissure, and variable degrees of pontocerebellar hypoplasia (**Fig. 2.2a-b**). CT image analysis of another homozygous individual with severe DEE also revealed hypoplasia of the corpus callosum, mild cerebral hypoplasia, and lenticulostriate and periventricular calcifications (**Fig. S2.2a**). MRIs analyzed from two compound heterozygous cases that exhibited severe DEE showed relatively mild neuroanatomical phenotypes (participants 2 and 18; **Fig. 2.2c-d**). Raw MRI data from additional compound heterozygous cases (participants 9 and 30) were not available, but isolated images revealed mild hypoplasia of the corpus callosum (**Fig. S2.2b**) and ventriculomegaly (**Fig. S2.2c**). Participant 8 with variants p.K485E/p.R1159W, who does not present with DEE, had a normal MRI with only mild inferior cerebellar vermis hypoplasia (**Fig. S2.2d**), providing further evidence for the benign or less deleterious nature of p.R1159W, but not p.K485E, since the latter variant was found in an individual with severe DEE and mild neuroanatomical phenotypes (participant 2, p.K485E/p.R710H; **Fig. 2.2c**). [3]

DENND5A protein levels were determined in cell lines derived from 5 cohort members: 3 from neural progenitor cells (NPCs) differentiated from iPSCs, and 2 from immortalized lymphoblasts, with homozygous and compound heterozygous as well as frameshift,

nonsense, and missense variants represented. Positive controls (i.e. cells derived from healthy donors) were used in both experiments, and iPSC-derived cells were additionally compared against a negative control cell line in which KO of *DENND5A* was generated with CRISPR/Cas9 using guide RNAs targeting exon 4. NPCs express SOX1, SOX2 and Nestin, affirming their NPC identity (**Fig. S2.3**). All patient-derived cells exhibit a reduction in DENND5A protein (**Fig. S2.4a-b**), supporting that disease phenotypes are a result of protein loss of function; however, the KO-validated DENND5A antibody recognizes a region of the protein more C-terminal to the stop codon of p.K205X. RT-qPCR was thus performed, but a poor correlation between *DENND5A* mRNA and protein levels was observed as *DENND5A* mRNA expression from patient-derived cells did not differ significantly from controls (**Fig. S2.4c-d**). This includes NPCs with homozygous p.K850Sfs*11 variants, where the antibody can determine that a ~100 kDa truncated protein is not expressed because its epitope should still be detected, but mRNA levels were comparable to WT NPCs. When introduced into a FLAG-tagged DENND5A plasmid construct and overexpressed in HEK293T cells, p.K205X resulted in no detectable protein, indicating that even if a truncated protein is produced it is rapidly degraded (**Fig. S2.4e**). [3]

3.2.2 DENND5A KI mouse model

We established a mouse model to determine how biallelic pathogenic variants in DENND5A affect development.

A knock-in (KI) mouse model, homozygous for a frameshift variant (c.517_517delGA/p.D173Pfs*8) found in the first identified cases of *DENND5A*-related DEE[1] (participants 15 and 16) and conserved in mice (**Fig. 2.3a-b**), exhibits anatomical and functional phenotypes consistent with those found in our human cohort. Immunoblotting

confirmed that full-length DENND5A protein is not expressed in KI mice (**Fig. 2.3c**); however, as in the case of K205X patient-derived cells, the validated DENND5A antibody has an epitope recognizing a region more C-terminal to the stop codon. RT-qPCR revealed a significant reduction in expression of *DENND5A* mRNA in KI mouse brains compared to WT (M_{WT} = 1.0, M_{KI} = 0.67, SD_{WT} = 0.68, SD_{KI} = 0.42, two-tailed Welch's $t(13.4) = 2.20$, $p = 0.046$; **Fig. 2.3d**), suggesting nonsense-mediated RNA decay. Moreover, DENND5A protein tagged at the N-terminus with FLAG containing this mutation is degraded when overexpressed in HEK-293T cells (**Fig. S2.3c**), indicating that even if translated, the protein is likely degraded. *In vivo* 7T MRI scans revealed that *DENND5A* KI mice have significantly enlarged lateral ventricles (M_{WT} = 4.8 mm^3, M_{KI} = 6.6 mm^3, SD_{WT} = 1.3, SD_{KI} = 2.4, two-tailed Mann-Whitney U, $Z = -2.117$, $p = .034$), consistent with ventriculomegaly (**Fig. 2.3e-f**). KI mice also had lower mean and median relative brain sizes, but similar to our human cohort in which occipitofrontal circumference percentiles varied considerably, a high degree of variability was observed in the mice and the difference did not reach statistical significance (**Fig. 2.3g**). Finally, while spontaneous seizures were not observed in the KI mice, they show increased seizure susceptibility compared to WT when administered the potassium channel blocker 4-aminopyridine (M_{WT} = 23.60, M_{KI} = 11.67, SD_{WT} = 2.97, SD_{KI} = 7.20, two-tailed $t(9) = 3.445$, $p = 0.007$; **Fig 2.3h**). [3]

3.3 Discussion

Here we present a cohort of individuals with biallelic variants in *DENND5A* leading to a new form of DEE. Some key similarities and differences between *DENND5A*-DEE and other monogenic DEEs described in the literature can be noted. Although none of the neuroanatomical features that we report in *DENND5A*-DEE are unique to DEEs, we are unaware of any other monogenic DEE in the literature with the same specific combination of features as those observed here. A study examining fetuses with diencephalic-mesencephalic junction dysplasias accompanied by developmental ventriculomegaly co-presented with corpus callosum dysgenesis and pontocerebellar hypoplasia, but no microcephaly was reported and their ventriculomegaly was associated with hydrocephalus due to aqueductal stenosis, a feature not identified in our cohort[44]. There is also a considerable degree of phenotypic overlap between our cohort and one comprised of patients with pathogenic *PCDH12* variants, but these patients lacked pachygyria and often co-presented with ophthalmic abnormalities, in contrast to what was observed here[45-47]. Gyral simplification and calcifications are observed in cases with recessive variants in the tight junction protein-encoding *OCLN* gene, but severe basal ganglia or diencephalic and mesencephalic dysplasias were not reported and polymicrogyria, a key feature of *OCLN* mutations, is not observed in our study[17]. Variants in tubulin genes also result in overlapping phenotypes[48], but our cases lack the classic dysgyria pattern and instead are typically observed in the context of occipital pachygyria and differ in that our cases are associated with calcifications. Moreover, it seems that our cases have more severe basal ganglia abnormalities when compared with the typical imaging presentations associated with *TUBA1A*, *TUBB2A*, *TUBB2B*, *TUBB3*, and *TUBG1*[49-51]. Variants in *LIS1*, encoding a protein

> involved in neuronal migration, results most frequently in a posterior gradient of lissencephaly, without calcifications, and variable degrees of corpus callosum size including thin, normal, and thicker than normal tracts[52,53]. In contrast, corpus callosum volumes were either normal, reduced, or absent with no cases of increased volume in our cohort. Finally, there is a selective involvement of the cortex added to the presence of periventricular calcifications, a unique feature that brings cytomegalovirus-induced brain malformations into the differential but aligns with pseudo-TORCH syndrome diagnostic criteria in the absence of congenital infection[54,55]. These differences in neuroradiological features suggest an interesting genotype-phenotype relationship that warrants further study … [and] our radiological findings combined with clinical information in **Table 2.1** … provide physicians with valuable information to communicate with families and treatment teams on a case-by-case basis. [3]

In addition to identifying radiological features specific to *DENND5A*-related DEE, we provided the first clinical evidence for the pathogenicity (or lack thereof) of certain missense variants. Detailed MRI analysis was performed on participants 2 (p.K485E/p.R710H) and 8 (p.K485E/p.R1159W). That these two participants with very different phenotypes share a common variant, p.K485E, allows us to propose that p.K485E and p.R710H are likely pathogenic and that p.R1159W is likely benign: participant 2 exhibited mild brain abnormalities and severe DEE that requires aid for all aspects of daily living, whereas participant 8 had a normal brain MRI and an autism spectrum disorder (ASD) diagnosis requiring very low levels of support. Importantly, participant 8 also has a pathogenic heterozygous MYBPC3 variant and is compound heterozygous for variants of uncertain significance in HERC2, whereas participant 2 had no other gene variants flagged as potentially causative of disease. We believe that participant 8 is effectively heterozygous

for a pathogenic DENND5A variant (p.K485E), that p.R1159W is likely benign, and that their mild developmental phenotype may be caused by one or more of their other gene variants. While heterozygous pathogenic *DENND5A* variants do not result in developmental abnormalities, it is conceivable that a heterozygous *DENND5A* variant combined with variants in other genes could lead to ASD with a polygenic etiology.

We believe ACMG classifications for several variants should be updated to pathogenic or likely pathogenic, especially p.R517W, p.K485E, p.D541G and p.R710H, as these variants are found in individuals with brain abnormalities, severe intellectual disability, infantile seizure onset, and no other flagged gene variants. The identification of additional DENND5A-related DEE cases will prove valuable for future clinical and biological studies and thus improved treatment options and prognostic information for health care providers and families. [3]

An important limitation to our study is that detailed MRI analysis was not possible for most cases. We relied on physician-completed questionnaires based on clinical neuroimaging reports for most of the cohort, resulting in a loss of detail. In addition, diagnoses based on neuroimaging may still prove difficult, as the cluster of radiological features was only identified in two unrelated individuals homozygous for frameshift variants. We suspect that other homozygous individuals also present with the same features, but detailed analysis was not possible with the provided CT images (participant 25) or questionnaire responses. However, the phenotypic spectrum – especially neuroanatomically – is expanded significantly with the identification of compound heterozygous individuals. Therefore, care must be taken to not exclude *DENND5A*-related DEE based on lack of radiological features alone.

For families in which one parent is aware they are a carrier of a pathogenic *DENND5A* variant, genetic counselors can recommend the other parent undergo genetic testing. When both parents are carriers, *in vitro* fertilization with preimplantation genetic diagnosis can be offered. However, the presence of *DENND5A* variants of unknown clinical significance does not necessarily equate to a devastating prognosis; 13% of our small cohort do not meet criteria for DEE or even experience seizures; p.R1159W, p.P955L, p.T136R, and/or exon 1-14 duplication may be benign variants or variants that have less impact on development. The identification of additional *DENND5A*-related DEE cases will prove valuable for future clinical and biological studies and thus improved treatment options and prognostic information for health care providers and families. [3]

3.4 Chapter 2 Figures and Tables

3.4.1 Tables

ID	Sex, Age range (years)	*DENND5A* variant(s)	Predicted ACMG classification	Allele frequency	Other gene variants	Seizures (drug resistant) – age of onset	Seizure type(s)	Medications that controlled, [did not affect], or (worsened) seizures	Microcephaly (OFC %ile)	6FRUHV			Developmental outcome
										Neuro	Motor	Communication	
1	M, 6-10	p.R698W p.N1017S	*VUS* *VUS*	2.78×10^{-5} 1.59×10^{-5}	*CNOT3 (VUS)*	Y (N) – 6 mo	Unclassified (described as infantile spasms at 7mo and focal left hemisphere involvement at 15mo during acute illness)	Vigabatrin, levetiracetam, [ACTH]	N (97)	2	10	2	Moderate ID
2	F, 6-10	c.1453A>G / p.K485E c.2129G>A / p.R710H	*LB/VUS* *LB/VUS*	7.08×10^{-4} 5.17×10^{-5}	-	Y (Y) – 7 mo	Generalized epileptic spasms, generalized atonic	[prednisolone, vigabatrin, clobazam, lamotrigine, levetiracetam, felbamate, rufinamide, VNS therapy]	Y (<3)	4	0	4	Profound ID
3	M, 16-20	c.611_612insG / p.K205X	*LP*	N/A	-	Y (Y) – 12 mo	Generalized tonic-clonic	Valproic acid, lamotrigine, ativan, clobazam	Y (UK, -8.9 SD)	9	6	6	Profound ID
4[22]	F, 6-10	c.1622A>G / p.D541G	*VUS*	N/A	-	Y (Y) – 2 wk	Focal impaired awareness tonic-clonic; focal to bilateral tonic-clonic	Levetiracetam, carbamazepine, clonazepam, topiramate, vigabatrin [(phenobarbital)]	Y (<3)	3	3	0	GDD (assessed age <5 y)
5[22]	F, deceased 6-10	c.3811del / p.Q1271Rfs*67	*VUS/P*	N/A	-	Y (Y) – 2 d	Focal aware tonic-clonic; focal to bilateral tonic-clonic	Phenobarbital, levetiracetam, [carbamazepine]	Y (<3)	10	0	1	GDD (assessed age <5 y)
7	F, 11-15	c.1363T>C / p.S455P c.3733G>A / p.A1245T	*VUS* *LB/VUS*	N/A 7.96×10^{-6}	*PEX1 (P)*	Y (N) – 2 y	Focal impaired awareness automatism, clonic, and atonic; generalized tonic-clonic	No medication	N (51)	4	9	4	Severe ID
8	M, 11-15	c.1453A>G / p.K485E c.3475C>T / p.R1159W	*LB/VUS* *VUS*	7.08×10^{-4} 9.20×10^{-5}	*HERC2 (VUS), MYBPC3 (P)*	N	N/A	N/A	N (90)	1	10	9	No GDD/ID
9	F, deceased 1-5	c.950-20_950-17delTTTT c.3233G>A / p.R1078Q	*LB* *LB/VUS*	4.06×10^{-5} 2.62×10^{-4}	*TBCK (LB/VUS)*	Y (Y) – 7 mo	Focal behavior arrest; unclassified (described as infantile spasms, myoclonic, and atonic seizures)	Topiramate, ACTH, [vigabatrin, diazepam, dexamethasone, pyridoxine, CBD oil, clobazam, sabril, prednisone, levocarnitine]	N (14)	4	1	3	Severe ID
10	F, 11-15	c.2547del / p.K850Sfs*11	*P*	N/A	-	Y (UK) – 40 d	Generalized tonic-clonic	UK	Y (<1)	5	9	7	Severe ID
12	M, 1-5	c.2314C>T / p.R772X c.3013T>A / p.L1005M	*P* *VUS*	3.19×10^{-5} N/A	CNV: 697 kb gain 6q25.3	Y (N) – 3 mo	UK; seizure associated with hypoglycemia	Phenobarbital, levetiracetam, CBD oil	Y (<1)	2	2	5	GDD
14	M, 1-5	c.2180dupG / p.S728fs*34	*P*	N/A	-	Y (Y) – 8 d	Focal tonic and myoclonic; generalized absence	Levetiracetam, valproic acid	Y (<1)	10	0	1	GDD
15[21]	F, 11-15	c.517_518delGA / p.D173Qfs*8	*P*	N/A	-	Y (Y) – 1 mo	Focal impaired awareness tonic and myoclonic; focal to bilateral tonic-clonic	Temporary (~3 mo) control with lamotrigine	N (50)	7	3	3	Severe ID
16[21]	F, deceased	c.517_518delGA / p.D173Qfs*8	*P*	N/A	-	Y (Y) – 1 mo	Focal impaired awareness tonic and myoclonic; focal to bilateral tonic-clonic	Temporary (~3 mo) control with lamotrigine	Y (<2)	7	2	3	Severe ID
18	F, 16-20	c.2283+1G>T c.3018dupG / p.K1007Efs*10	*VUS/LP* *LP*	N/A N/A	-	Y (Y) – 3 wk	focal impaired awareness clonic and tonic; focal epileptic spasms; focal to bilateral tonic-clonic; focal impaired awareness behavior arrest; generalized motor onset myoclonic and tonic; unknown onset epileptic spasms; unknown onset behavior arrest	Vigabatrin, valproic acid, levetiracetam, [phenobarbital, sultiame]	Y (<1)	6	0	2	Profound ID
19	M, 6-10	c.407C>G / p.T136R c.2864C>T / p.P955L	*VUS* *VUS*	N/A 1.59×10^{-5}	*CACNA1C (LP/P)*	N	N/A	N/A	N (50)	No imaging	9	9	Moderate ID
20	M, 1-5	Exon 1-14 dup	*VUS*	N/A	-	N	N/A	N/A	N (4)	0	7	2	GDD
21	M, 16-20	c.1549C>T / p.R517W Exon 1 del	*VUS* *LP*	7.96×10^{-6} N/A	-	Y (Y) – 7 mo	Focal tonic; focal impaired awareness; focal clonic; focal to bilateral tonic-clonic	Current trial: clobazam, lamotrigine, CBD oil, [previous trials: levetiracetam, lacosamide, topiramate, sodium valproate, pyridoxine, gabapentin]	Y (<3)	4	8	6	Severe ID
22	M, 11-15	c.955C>T / p.Q319X	*P*	N/A	*CDH4 (VUS)*	Y (Y) – <1 y	Focal impaired awareness clonic; focal to bilateral tonic-clonic	Sodium valproate, phenobarbital, [levetiracetam, (carbamazepine)]	Y (<3)	4	8	2	Severe ID
23	M, 11-15	c.949+1G>A	*LP*	N/A	-	Y (Y) – 2 mo	Focal impaired awareness tonic; focal to bilateral tonic-clonic	Carbamazepine, sodium valproate, clobazam	Y (UK)	4	0	1	Severe ID
25	F, 1-5	c.3605del / p.V1202Afs*52	*LP*	N/A	-	Y (Y) – 22 d	Focal tonic; focal epileptic spasms	Vigabatrin, sodium valproate, [phenobarbital, vitamin B6, clobazam, ACTH, perimidone, levetiracetam], (phenytoin)	Y (<3)	9	0	1	GDD
26	M, 1-5	c.623G>A / p.C208Y	*VUS*	N/A	-	Y (N) – 7 mo	Generalized epileptic spasms	Omnacortil, levetiracetam	Y (<3)	1	9	7	GDD
27	M, 1-5	c.949+1G>A	*LP*	N/A	-	Y (N) – 1 d	Generalized tonic-clonic	Levetiracetam, sodium valproate	Y (<3)	5	2	0	Severe ID
28	F, 1-5	c.949+1G>A	*LP*	N/A	-	Y (N) – 1 d	Focal impaired awareness clonic; focal to bilateral tonic-clonic; generalized tonic-clonic	Levetiracetam, sodium valproate	Y (<3)	5	3	0	GDD
30	M, 1-5	c.3095G>C / p.Arg1032Thr c.3116C>A / p.Thr1039Asn	*VUS* *VUS*	N/A N/A	-	Y (Y) – 8 mo	Generalized epileptic spasms	ACTH, sodium valproate, [vigabatrin, topiramate, phensuximide, nitrazepam], (lamotrigine)	N (UK)	5	9	7	GDD

Table 2.1: Clinical summary table indicating demographics, variant details with American College of Medical Genetics and Genomics classifications predicted by Franklin/Varsome, allele frequencies, and phenotype summaries for each individual in the study.

3.4.2 Main Figures

Figure 2.1

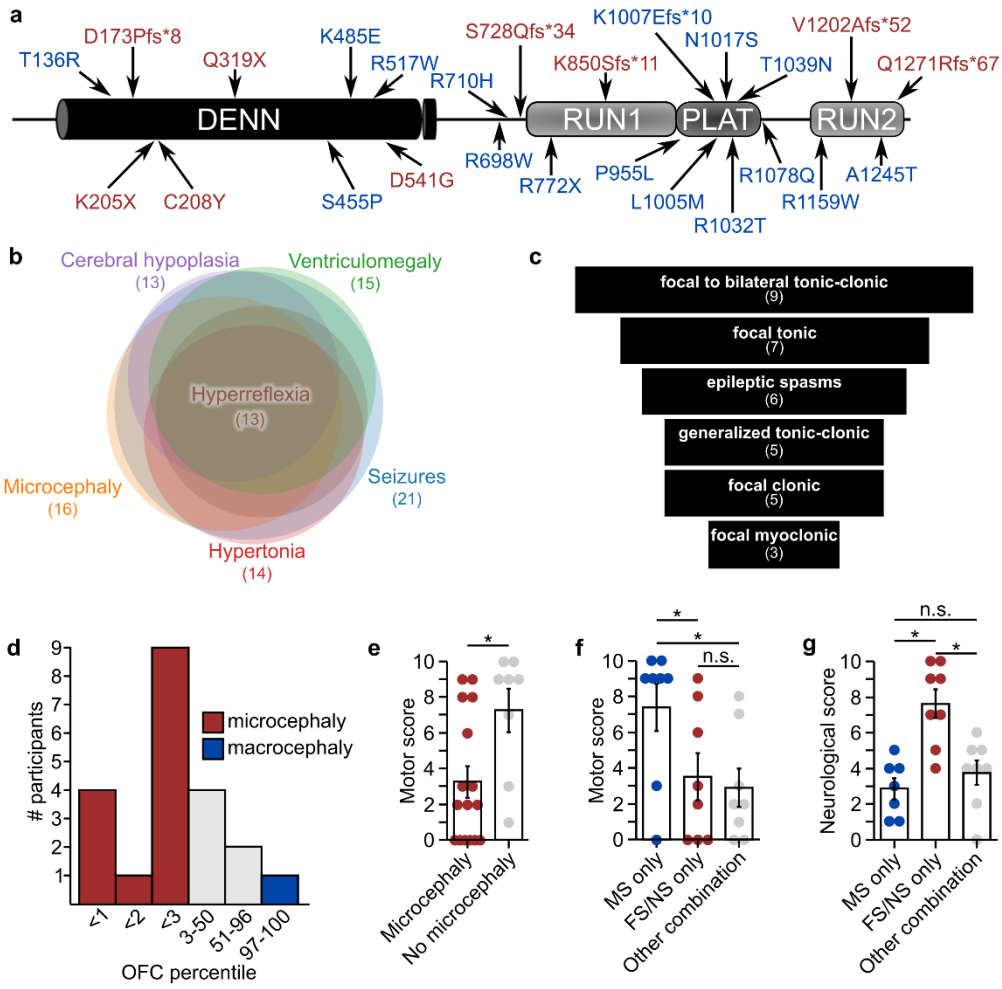

Figure 2.1: DENND5A loss of function variants influence neurodevelopment. **a,** Schematic of DENND5A protein with all coding sequence variants identified in the study. Red = found in homozygous individuals, blue = found in compound heterozygous individuals. **b,** Venn chart showing the number of people with biallelic DENND5A variants exhibiting the most frequently reported phenotypes and the degree of phenotypic overlap between cohort members. **c,** Funnel chart showing the most common seizure types present in the cohort. **d,** Histogram depicting the number of individuals in a given OFC percentile range. Note that the exact OFC percentile is not known in every case. **e,** Quantification of motor scores from $n = 16$ individuals with microcephaly and $n = 8$ individuals without microcephaly. Each dot represents one person. Data are mean ± SEM. **f,** Quantification of motor scores from $n = 8$ individuals with biallelic missense variants, $n = 8$ individuals with biallelic frameshift or nonsense variants, and $n = 8$ individuals with an allelic combination of frameshift, nonsense, missense, intronic, or copy number variants in DENND5A. Each dot represents one person. Data are mean ± SEM. **g,** Quantification of neurological scores from $n = 8$ individuals with biallelic missense variants, $n = 8$ individuals with biallelic frameshift or nonsense variants, and $n = 8$ individuals with an allelic combination of frameshift, nonsense, missense, intronic, or copy number variants in DENND5A. Each dot represents one person. Data are mean ± SEM.

Figure 2.2

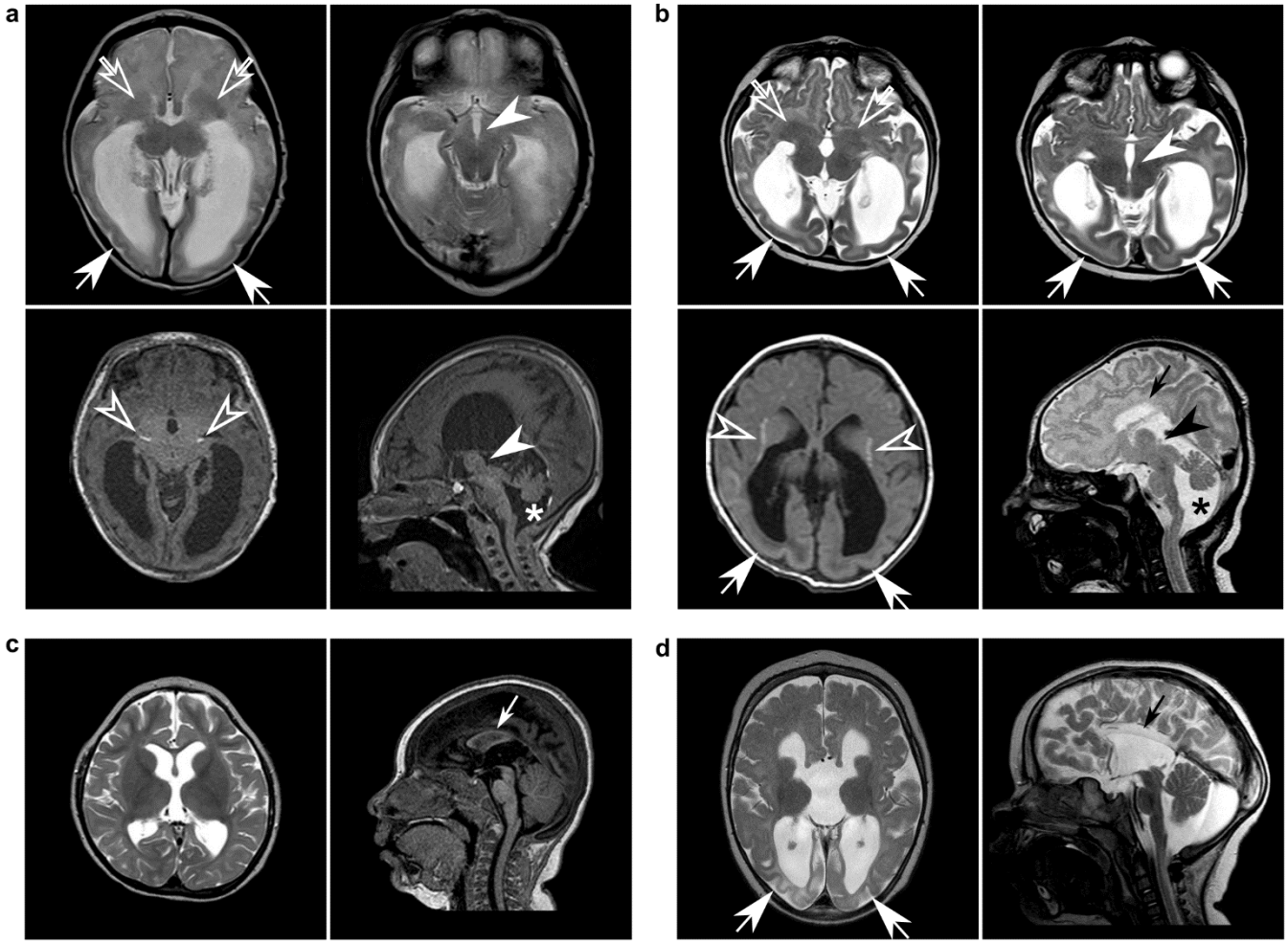

Figure 2.2: Cortical malformations, corpus callosum and anterior commissure dysgenesis, ventriculomegaly, basal ganglia dysgenesis, calcifications, and diencephalic/mesencephalic dysplasia are indicative of severe *DENND5A*-related DEE. Sample MRI slices from unrelated individuals with **a,** homozygous p.Q1271R*67 variants (participant 5); **b,** homozygous p.S728Qfs*34 variants (participant 14); **c,** compound heterozygous p.K485E/p.R710H variants (participant 2); and **d,** compound heterozygous c.2283+1G>T/p.K1007Efs*10 variants (participant 18) show many neuroanatomical phenotypes in common. Arrows = posterior gradient of pachygyria/lissencephaly; open arrows = severe basal ganglia dysmorphism; arrowheads = diencephalic/mesencephalic junction dysplasia; open arrowheads = periventricular, striatal, and diencephalic calcifications; small arrows = corpus callosum dysgenesis/agenesis; asterisks = cerebellar hypoplasia.

Figure 2.3

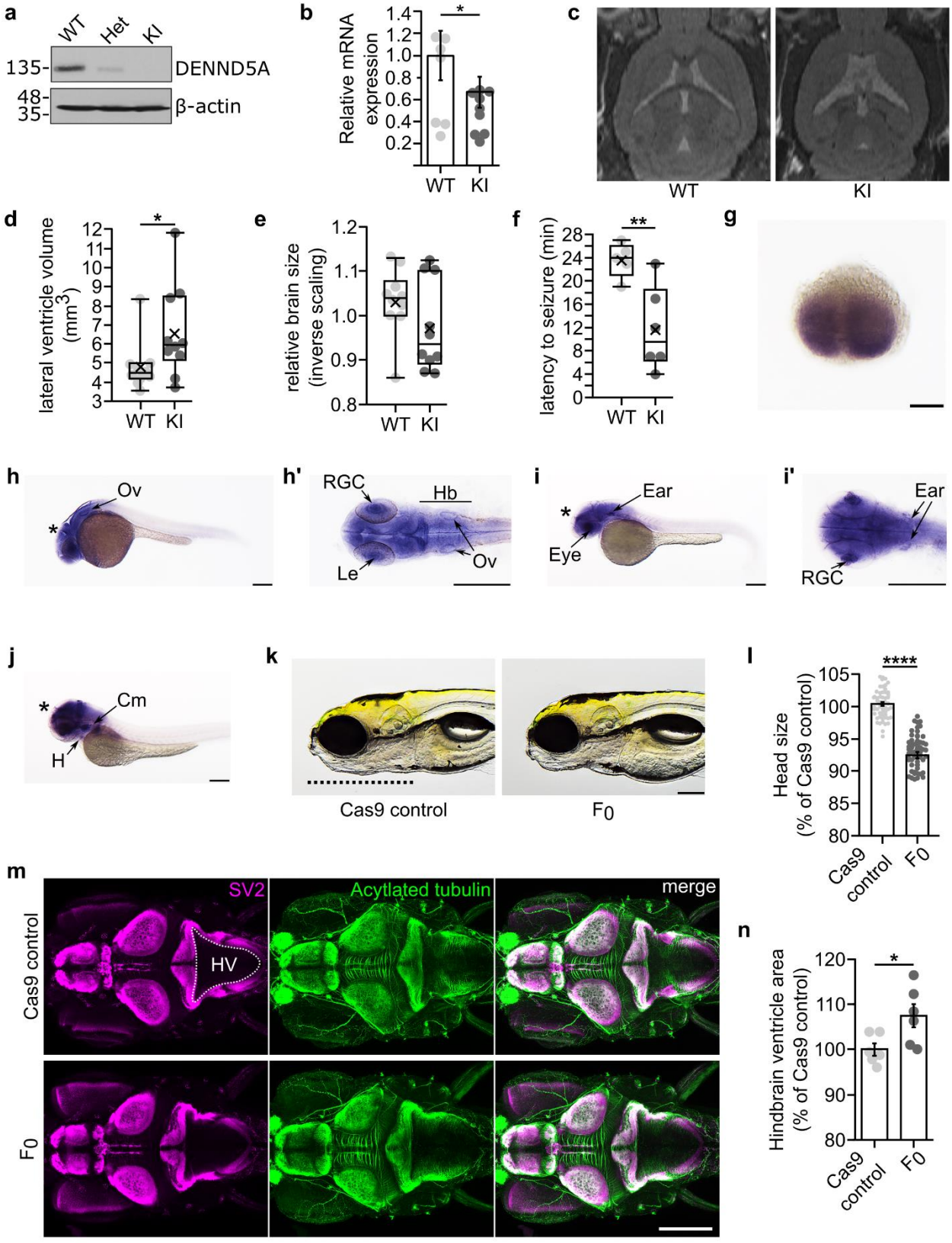
a
WT
Het
KI
135-
DENND5A
48-
35-
β-actin
b
Relative mRNA expression
1.4
1.2
1.0
0.8
0.6
0.4
0.2
*
WT
KI
c
WT
KI
d
lateral ventricle volume (mm3)
12
11
10
9
8
7
6
5
4
3
*
WT
KI
e
relative brain size (inverse scaling)
1.2
1.1
1.0
0.9
0.8
WT
KI
f
latency to seizure (min)
28
24
20
16
12
8
4
0
**
WT
KI
g
h
Ov
*
h'
RGC
Hb
Ov
Le
i
Ear
*
Eye
i'
Ear
RGC
j
Cm
*
H
k
Cas9 control
F0
l
Head size (% of Cas9 control)
105
100
95
90
85
80
****
Cas9 control
F0
m
SV2
Acytlated tubulin
merge
Cas9 control
F0
HV
n
Hindbrain ventricle area (% of Cas9 control)
120
110
100
90
80
*
Cas9 control
F0

Figure 2.3: Animal models of *DENND5A*-DEE exhibit common phenotypes observed in the human cohort. a, Mice heterozygous (Het) for p.D173Pfs*8 express full-length DENND5A protein at half the levels compared to WT mice and homozygous knock-in (KI) mice express no full-length DENND5A protein. **b,** Relative brain *DENND5A* mRNA levels measured via RT-qPCR from $n = 6$ total mice. Experiments were performed in triplicate in 3 independent experiments. Error bars = SEM. **c,** Sample images of WT and KI *in vivo* 7T MRIs. **d,** Quantification of pooled lateral ventricle volumes obtained through segmenting $n = 10$ mouse MRIs. Each dot represents one animal. X = mean. **e,** Quantification of relative brain volumes measured using MRI data from $n = 10$ mice ($M_{WT} = 1.03$, $Mdn_{WT} = 1.04$, $M_{KI} = 0.97$, $MdnKI = 0.94$, $SD_{WT} = 0.08$, $SD_{KI} = 0.10$, two-tailed Mann-Whitney U, $Z = -1.361$, $p = .174$). Each dot represents one animal. X = mean. **f,** Quantification of seizure latency after injection of 4-AP. Multiple independent experiments were performed with a total of $n = 5$ WT and $n = 6$ KI mice. Each dot represents one animal. X = mean. *(g-j)* Whole-mount *in situ* hybridization shows *dennd5a* mRNA expression at **g,** 0.75 hpf, **h,** 24 hpf, **i,** 48 hpf and **j,** 72 hpf. Asterisks = brain; Ov = otic vesicle; Le = lens; RGC = retinal ganglion cells; Hb = hindbrain; H = heart; Cm = cephalic musculature. Scale bar = 0.2 mm. **k,** Sample images of control and F_0 KO zebrafish head size. Dotted line marks the length of the head used in quantification. Scale bar = 0.2 mm. **l,** Quantification of head size in $n = 60$ larvae analyzed via two-tailed Mann-Whitney U test ($Med_{Control} = 100.432$, $Med_{F0} = 93.073$, $SD_{Control} = 2.316$, $SD_{F0} = 3.728$; $Z = -9.206$, $p < .0001$). Each dot represents one larva. Data are mean ± SEM. **m,** Representative image of larva at 6 dpf immunostained with anti-SV2 (magenta) and anti-acetylated tubulin (green). Dorsal view, anterior to the left. HV = hindbrain ventricle. Dotted line outlines hindbrain ventricle area used in quantification. **N,** Quantification of hindbrain ventricle area in $n = 6$ larvae analyzed via two-tailed student's *t*-test ($M_{Control} = 100$, $M_{F0} = 107.502$, $SD_{Control} = 3.251$, $SD_{F0} = 6.386$; $t(10) = -2.564$, $p = 0.028$). Data are mean ± SEM. Each dot represents one larva.

3.4.3 Supplementary Figures

Figure S2.1

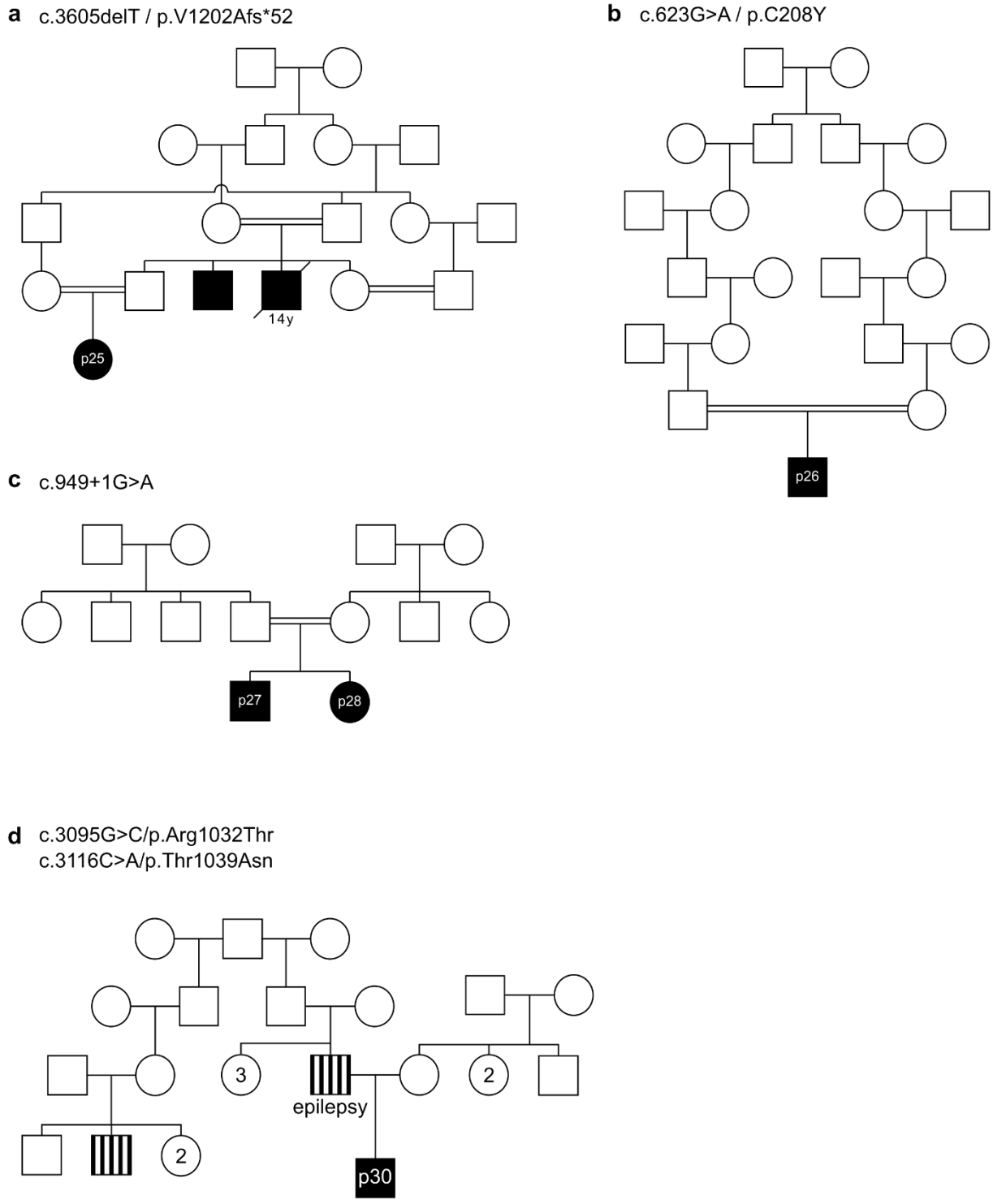

Figure S2.1: Extended pedigrees of consanguineous families demonstrate pathogenicity of select *DENND5A* variants. Pedigrees indicate affected (colored in) and unaffected (open) individuals in families carrying the variants **a,** c.3605delT/p.V1202Afs*52; **b,** c.623G>A/p.C208Y, **c,** c.949+1G>A, and d, c.3095G>C/p.R1032T and c.3116C>A/p.T1039N. Participants involved in the phenotypic study are indicated by their ID number, and the age at the time of death is indicated for a deceased individual in *(a)*.

Figure S2.2

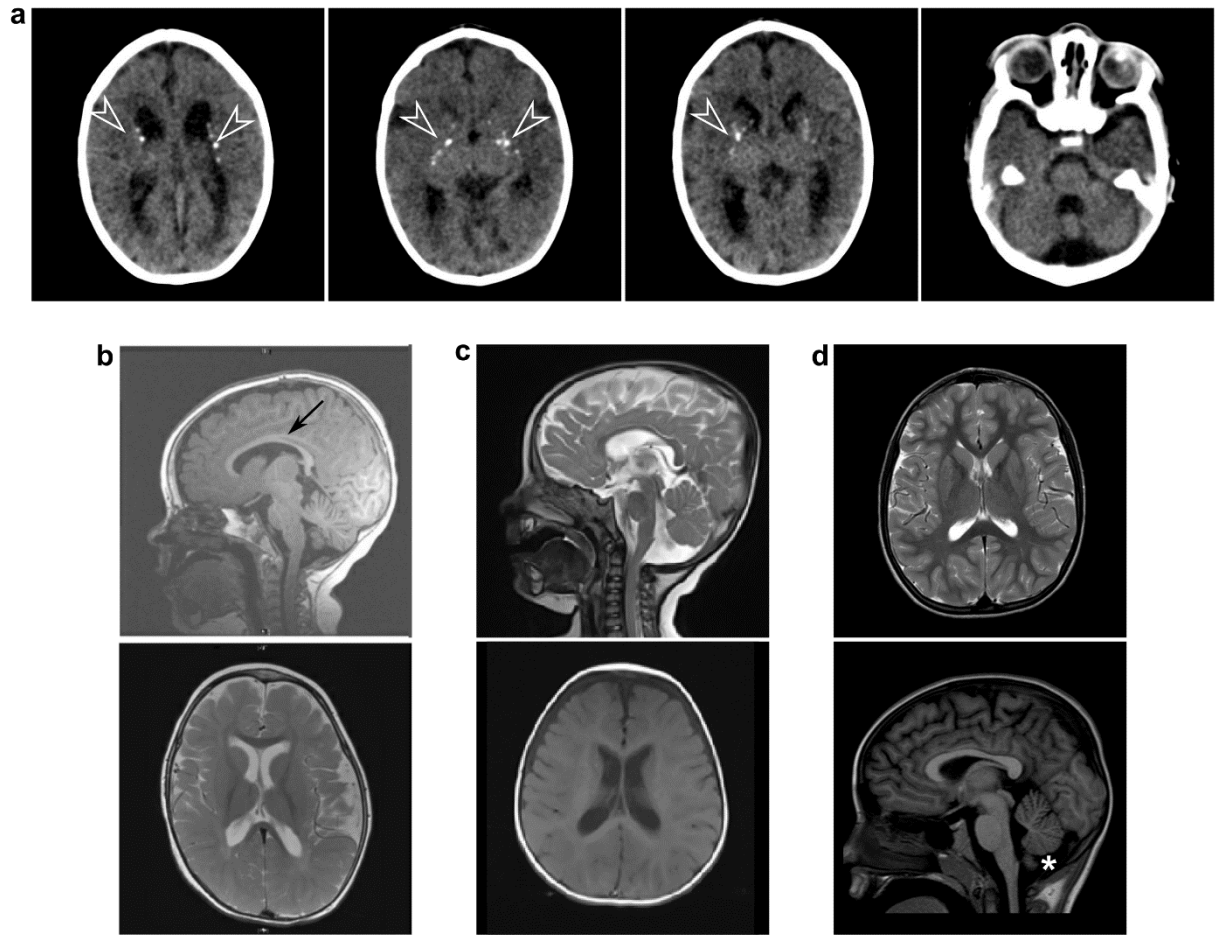

Figure S2.2: Neuroimaging of other cases with DENND5A-related DEE show varying levels of phenotypic overlap. **a,** CT from a homozygous individual with the variant p.V1202Afs*52 (participant 25) shows mild cortical volume loss, ventriculomegaly, thin corpus callosum, and lenticulostriate and periventricular calcifications (arrowheads). **b,** MRI from a compound heterozygous individual with variants c.950-20_950-17delTTTT/p.R1078Q (participant 9) shows mild corpus callosum volume loss (arrow). **c,** MRI from a compound heterozygous individual with variants p.R1032T/p.T1039N (participant 30) shows enlarged lateral ventricles. **d,** MRI from a compound heterozygous individual with variants p.K485E/p.R1159W (participant 8) shows a normal MRI with mild inferior cerebellar vermis hypoplasia (asterisk).

Figure S2.3

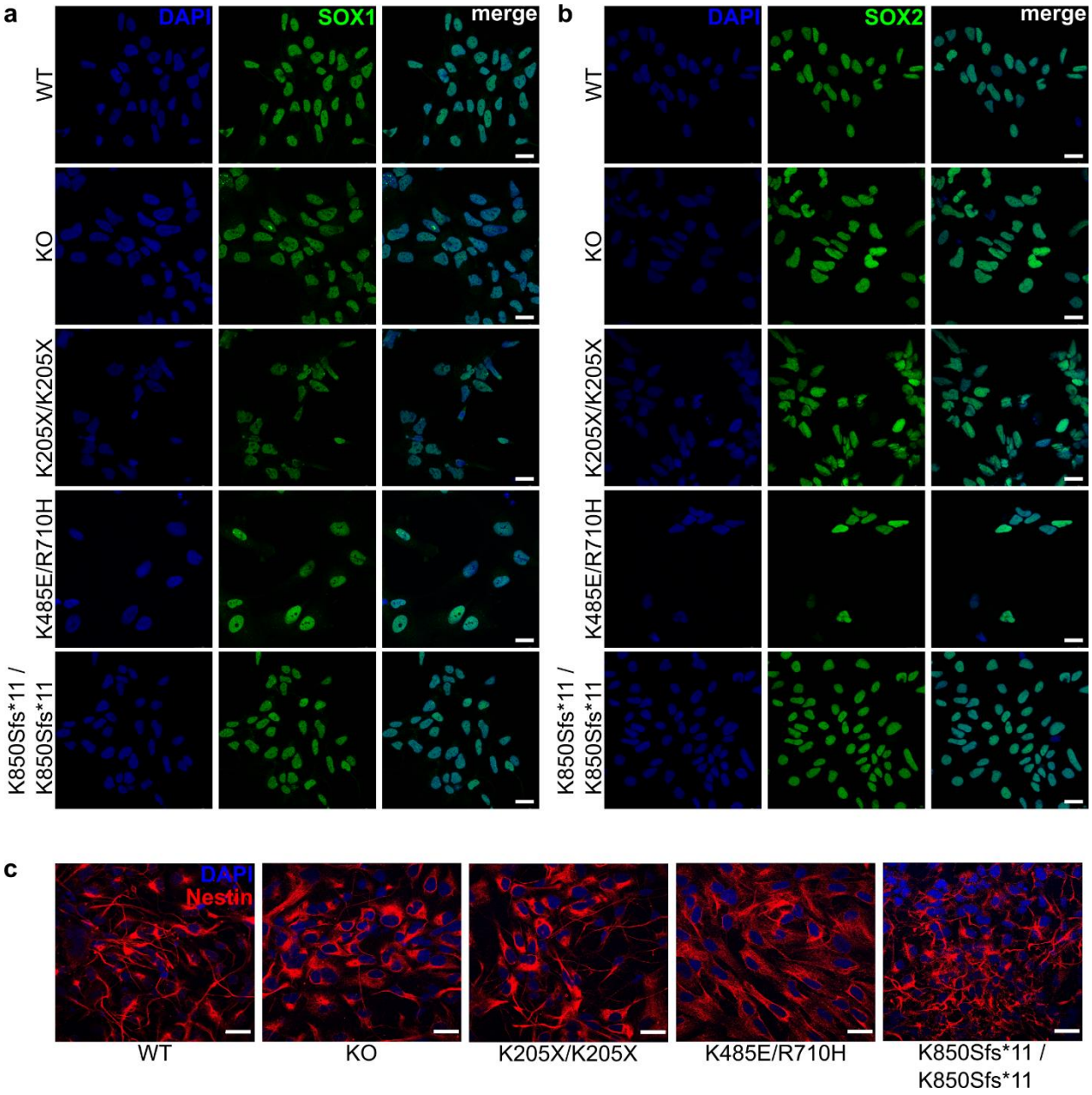

Figure S2.3: All established NPC lines express neural progenitor-specific markers. iPSCs differentiated into NPCs express **a,** SOX1 (green); **b,** SOX2 (green), and **c,** Nestin (red). Blue = DAPI. Scale bars = 20 µm.

Figure S2.4

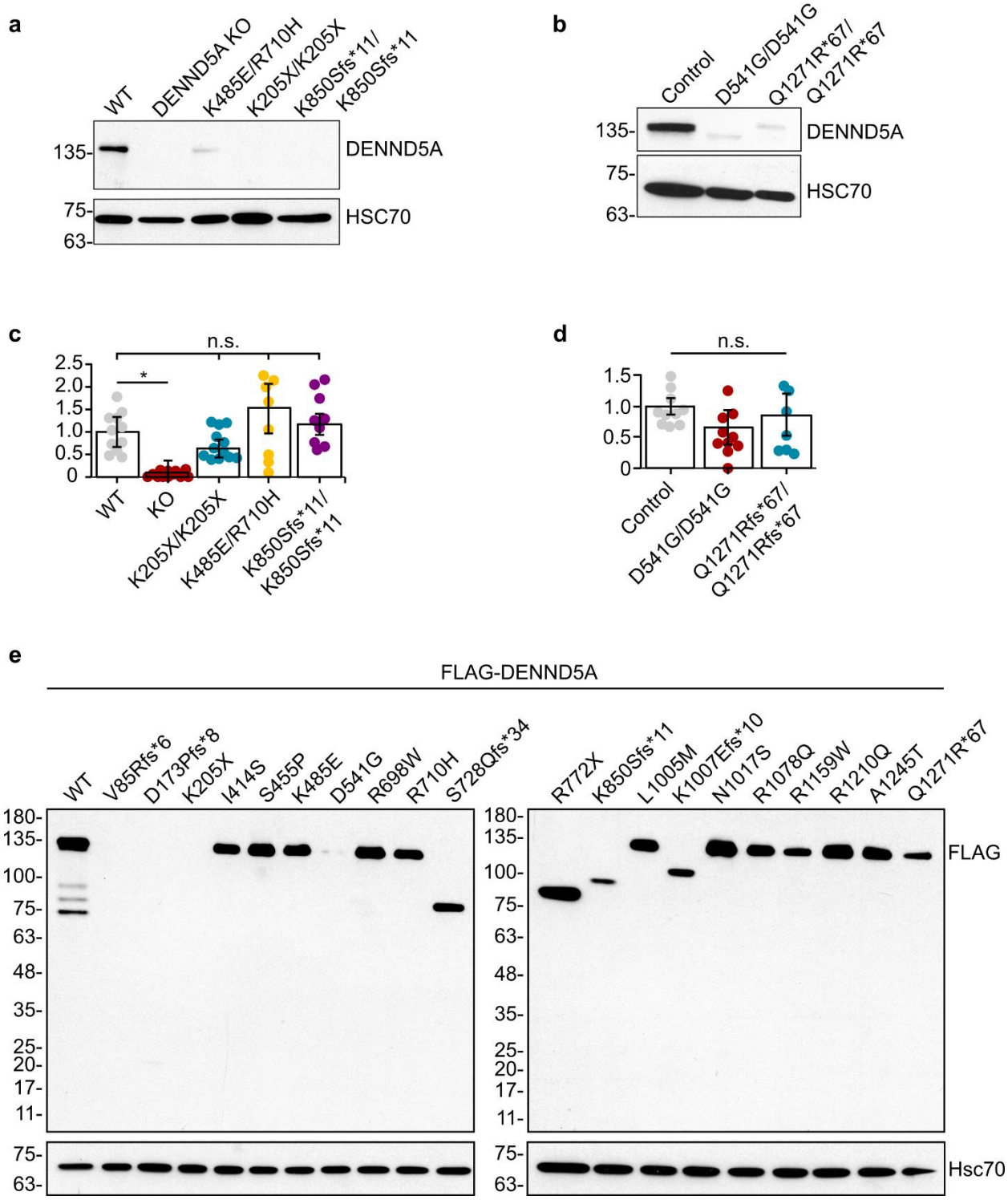

Figure S2.4: DENND5A expression varies depending on the variant. DENND5A protein expression in **a,** NPCs and **b,** lymphoblasts. Relative *DENND5A* mRNA expression measured by RT-qPCR in **c,** NPCs and **d,** lymphoblasts. Measurements were made with 4 technical replicates on $n = 3$ independent samples. Data are mean ± SEM analyzed via Kruskal-Wallis tests with Bonferroni-corrected pairwise comparisons. **c,** Overexpression of FLAG-DENND5A mutagenized to contain several variants influences protein stability and expression levels in HEK293T.

3.5 Acknowledgments

We would like to acknowledge all cohort members in this study, their families, and treating clinicians for their participation. Participant 10 was recruited as part of the German-Jordanian Autosomal Recessive Intellectual Disability project (GeJo-ARID) funded by the German Academic Exchange Service (DAAD) as part of the German-Arab Transformation Program Line4 (Project-ID 57166498). The views expressed are those of the author(s) and do not reflect the official policy of the Department of the Army, the Department of Defense or the U.S. Government. The content is solely the responsibility of the authors and does not necessarily represent the official views of the National Institutes of Health. This work was funded by a Foundation Grant from the Canadian Institutes of Health Research to PSM, and a grant from the Alain and Sandra Bouchard Foundation for Intellectual Disabilities to PSM and TMD. This work was also supported by the King Salman Center for Disability Research through Research Group no RG-2022-010 (FSA). This work was also performed under the Care4Rare Canada Consortium funded by Genome Canada and the Ontario Genomics Institute (OGI-147), the Canadian Institutes of Health Research, Ontario Research Fund, Genome Alberta, Genome British Columbia, Genome Quebec, and Children's Hospital of Eastern Ontario Foundation (DC, ESYG, MO). Research reported in this manuscript was also supported by the NIH Common Fund, through the Office of Strategic Coordination/Office of the NIH Director under Award Number(s) [U01HG007672, U01HG007943] (HC) and [NS105078, HG011758] (JRL). [3]

3.6 Author Contributions

EBan designed, performed, and analyzed most experiments. VFr performed mouse immunohistochemistry, coordinated induced seizure experiments and mouse MRIs, and maintained the mouse colony. FK established the mouse colony, performed the western blot in Fig. 3a, and coordinated mouse MRIs. VFo processed and analyzed mouse MRIs. ML performed the induced seizure experiments. CH established the iPSC lines. GK performed RT-qPCR on mouse brain tissue for Fig. 3b. MT performed the mouse MRIs. FSA generated and provided lymphoblast cell lines and contributed two clinical cases. SH and SK established iPSC lines from participants 2 and 10. RM identified many cohort members and provided pedigrees for Extended Data Fig. 1. RAK, FSA, LA, MBab, MBah, BB, EBar, LB, MBas, MBer, DB, RB, Mbu, MC-D, DCa, HC, DCu, SE, MAE, HGES, TF, HKG, JGG, LG, ESYG, VKG, TBH, MOH, TLH, JSH, AH, HH, KH, SH, EGK, GCK, AK, HL, JRL, EJM, AM, DM, JN-F, HN, DN, BO-J, MO, DP, LGS, CS, LS, VS, RCS, VMS, MSZ, DZ, and CZ completed phenotypic questionnaires and contributed to clinical phenotyping and genetic analysis. KM acted as a liaison to connect EBan with clinicans that submitted variants on ClinVar. RP analyzed clinical exomes of GeneDx-tested cases. BAM identified the initial cases. UDN is associated with the contribution of data from participant 9. TMD supervised iPSC quality control and cell line production. ZG supervised genetic analysis. MA supervised induced seizure experiments. CA analyzed participant MRIs and CTs. RM contributed many clinical cases and connected us with CA, GKV, SJL, KH, and CP. All authors reviewed the manuscript for accuracy and edited wording or data presentation according to their clinical, molecular, structural, genetic, or biological expertise. PSM supervised the study, designed experiments, secured funding, and wrote the manuscript.

3.6.1 Author Appendix

Members of the Undiagnosed Diseases Network include: Maria T. Acosta, Margaret Adam, David R. Adams, Pankaj B. Agrawal, Mercedes E. Alejandro, Justin Alvey, Laura Amendola, Ashley Andrews, Euan A. Ashley, Mahshid S. Azamian, Carlos A. Bacino, Guney Bademci, Eva Baker, Ashok Balasubramanyam, Dustin Baldridge, Jim Bale, Michael Bamshad, Deborah Barbouth, Gabriel F. Batzli, Pinar Bayrak-Toydemir, Anita Beck, Alan H. Beggs, Edward Behrens, Gill Bejerano, Jimmy Bennet, Beverly Berg-Rood, Raphael Bernier, Jonathan A. Bernstein, Gerard T. Berry, Anna Bican, Stephanie Bivona, Elizabeth Blue, John Bohnsack, Carsten Bonnenmann, Devon Bonner, Lorenzo Botto, Brenna Boyd, Lauren C. Briere, Elly Brokamp, Gabrielle Brown, Elizabeth A. Burke, Lindsay C. Burrage, Manish J. Butte, Peter Byers, William E. Byrd, John Carey, Olveen Carrasquillo, Ta Chen Peter Chang, Sirisak Chanprasert, Hsiao-Tuan Chao, Gary D. Clark, Terra R. Coakley, Laurel A. Cobban, Joy D. Cogan, F. Sessions Cole, Heather A. Colley, Cynthia M. Cooper, Heidi Cope, William J. Craigen, Andrew B. Crouse, Michael Cunningham, Precilla D'Souza, Hongzheng Dai, Surendra Dasari, Mariska Davids, Jyoti G. Dayal, Matthew Deardorff, Esteban C. Dell'Angelica, Shweta U. Dhar, Katrina Dipple, Daniel Doherty, Naghmeh Dorrani, Emilie D. Douine, David D. Draper, Laura Duncan, Dawn Earl, David J. Eckstein, Lisa T. Emrick, Christine M. Eng, Cecilia Esteves, Tyra Estwick, Marni Falk, Liliana Fernandez, Carlos Ferreira, Elizabeth L. Fieg, Paul G. Fisher, Brent L. Fogel, Irman Forghani, Laure Fresard, William A. Gahl, Ian Glass, Rena A. Godfrey, Katie Golden-Grant, Alica M. Goldman, David B. Goldstein, Alana Grajewski, Catherine A. Groden, Andrea L. Gropman, Irma Gutierrez, Sihoun Hahn, Rizwan Hamid, Neil A. Hanchard, Kelly Hassey, Nichole Hayes, Frances High, Anne Hing, Fuki M. Hisama, Ingrid A. Holm, Jason Hom, Martha Horike-

Pyne, Alden Huang, Yong Huang, Rosario Isasi, Fariha Jamal, Gail P. Jarvik, Jeffrey Jarvik, Suman Jayadev, Jean M. Johnston, Lefkothea Karaviti, Emily G. Kelley, Jennifer Kennedy, Dana Kiley, Isaac S. Kohane, Jennefer N. Kohler, Deborah Krakow, Donna M. Krasnewich, Elijah Kravets, Susan Korrick, Mary Koziura, Joel B. Krier, Seema R. Lalani, Byron Lam, Christina Lam, Brendan C. Lanpher, Ian R. Lanza, C. Christopher Lau, Kimberly LeBlanc, Brendan H. Lee, Hane Lee, Roy Levitt, Richard A. Lewis, Sharyn A. Lincoln, Pengfei Liu, Xue Zhong Liu, Nicola Longo, Sandra K. Loo, Joseph Loscalzo, Richard L. Maas, Ellen F. Macnamara, Calum A. MacRae, Valerie V. Maduro, Marta M. Majcherska, May Christine V. Malicdan, Laura A. Mamounas, Teri A. Manolio, Rong Mao, Kenneth Maravilla, Thomas C. Markello, Ronit Marom, Gabor Marth, Beth A. Martin, Martin G. Martin, Julian A. Martínez-Agosto, Shruti Marwaha, Jacob McCauley, Allyn McConkie-Rosell, Colleen E. McCormack, Alexa T. McCray, Elisabeth McGee, Heather Mefford, J. Lawrence Merritt, Matthew Might, Ghayda Mirzaa, Eva Morava-Kozicz, Paolo M. Moretti, Marie Morimoto, John J. Mulvihill, David R. Murdock, Mariko Nakano-Okuno, Avi Nath, Stan F. Nelson, John H. Newman, Sarah K. Nicholas, Deborah Nickerson, Donna Novacic, Devin Oglesbee, James P. Orengo, Laura Pace, Stephen Pak, J. Carl Pallais, Christina GS. Palmer, Jeanette C. Papp, Neil H. Parker, John A. Phillips III, Jennifer E. Posey, Lorraine Potocki, Barbara N. Pusey, Aaron Quinlan, Wendy Raskind, Archana N. Raja, Genecee Renteria, Chloe M. Reuter, Lynette Rives, Amy K. Robertson, Lance H. Rodan, Jill A. Rosenfeld, Natalie Rosenwasser, Robb K. Rowley, Maura Ruzhnikov, Ralph Sacco, Jacinda B. Sampson, Susan L. Samson, Mario Saporta, C. Ron Scott, Judy Schaechter, Timothy Schedl, Kelly Schoch, Daryl A. Scott, Prashant Sharma, Vandana Shashi, Jimann Shin, Rebecca Signer, Catherine H. Sillari, Edwin K. Silverman, Janet S. Sinsheimer, Kathy Sisco, Edward C. Smith, Kevin

S. Smith, Emily Solem, Lilianna Solnica-Krezel, Rebecca C. Spillmann, Joan M. Stoler, Nicholas Stong, Jennifer A. Sullivan, Kathleen Sullivan, Angela Sun, Shirley Sutton, David A. Sweetser, Virginia Sybert, Holly K. Tabor, Cecelia P. Tamburro, Queenie K.-G. Tan, Mustafa Tekin, Fred Telischi, Willa Thorson, Cynthia J. Tifft, Camilo Toro, Alyssa A. Tran, Brianna M. Tucker, Tiina K. Urv, Adeline Vanderver, Matt Velinder, Dave Viskochil, Tiphanie P. Vogel, Colleen E. Wahl, Stephanie Wallace, Nicole M. Walley, Chris A. Walsh, Melissa Walker, Jennifer Wambach, Jijun Wan, Lee-kai Wang, Michael F. Wangler, Patricia A. Ward, Daniel Wegner, Mark Wener, Tara Wenger, Katherine Wesseling Perry, Monte Westerfield, Matthew T. Wheeler, Jordan Whitlock, Lynne A. Wolfe, Jeremy D. Woods, Shinya Yamamoto, John Yang, Guoyun Yu, Diane B. Zastrow, Chunli Zhao, Stephan Zuchner.

3.7 Competing Interests

KM and RP are employed by GeneDx, LLC. All other authors report no conflicts of interest.

3.8 Materials and Methods

Participant Recruitment

All materials and methods for participant recruitment and clinical data collection was approved by the McGill University Health Centre research ethics board (study 2021-6324) and the McGill Faculty of Medicine and Health Sciences institutional review board (study A12-M66-21B). We originally identified four individuals, one deceased and excluded from the cohort, from two consanguineous families with homozygous *DENND5A* variants[1]. Another two homozygous individuals were briefly described by Anazi *et al.* in 2017 and

were recruited into the study[2]. We identified an additional 23 individuals with *DENND5A* variants: 15 were brought to our attention by clinicians who reached out to us after performing diagnostic whole exome sequencing on patients; 5 were identified through physician-submitted GeneMatcher[4] and ClinVar[5] database entries; and 3 were identified through word-of-mouth of the study between clinicians that already completed the survey and their colleagues with other *DENND5A* cases. Individuals with one or more variants classified as benign were not recruited. Recruitment spanned approximately four years. Six individuals were excluded from the cohort and subsequent analysis: two did not meet eligibility criteria (both are heterozygous for a *DENND5A* variant, having only one affected allele); one was excluded due to death occurring prior to clinical data collection[1]; and three were excluded because the questionnaires were not returned. [3]

Phenotypic data collection and analysis

Clinicians with patients harboring biallelic *DENND5A* variants completed an anonymized phenotypic questionnaire based on their patient's most recent clinic visit. Available anonymized MRIs, CTs, and/or or official reports were contributed if the patient underwent neuroimaging for clinical purposes. Participants were assigned a numerical ID in the order in which their questionnaires were received. For intronic variant analysis, molecular consequences were predicted using Ensembl's Variant Effect Predictor. [6] For those whose raw MRI or CT data were provided, an independent neuroradiologist re-analyzed the scans and completed the "Brain" section of the questionnaire without viewing the original submitted questionnaires. If responses to an item differed between the original clinician and the independent radiologist, the independent radiologist's response was used for analysis. Data are missing if the presence of a phenotype is officially unknown. For occipitofrontal

circumference (OFC), if percentiles were not given directly from clinicians, percentile values were derived from the age- and sex-appropriate Word Health Organization tables (https://www.who.int/tools/child-growth-standards/standards/head-circumference-for-age). The OFC percentile for one person whose measurements were taken when they were above 5 years old was derived from tables published in Adela Chirita-Emandi et al[7]. For calculating central tendency statistics, OFC percentiles given as a range (e.g. < 3 or < 1) were assigned a conservative numerical estimate (e.g. 2.9 for < 3, 0.9 for < 1). [3]

Establishment of cell lines

The control induced pluripotent stem cell (iPSC) line AIW001-02 was derived from peripheral blood mononuclear cells of a healthy female donor (Caucasian, 48 years old). The AIW001-02 cell line was generated by using the CytoTune™-iPS 2.0 Sendai Reprogramming Kit (iPSQuebec Platform, Laval University). For knockout expression of human *DENND5A*, guide RNAs (gRNAs) were designed using an online tool (https://benchling.com). Both gRNA target sites are on *DENND5A* exon 4. Synthesized gRNAs were ordered from SYNTHEGO and transfection was performed following the manufacturer's protocol. Single cell colonies were picked and amplified. Genomic DNA from the colonies was extracted with QuickExtract (Lucigen) and PCR was performed using Q5 High-Fidelity DNA Polymerase according to the manufacturer's protocol (F: GAGGATCGCCAGTGAGTGTT; R: CCCCGAGCAGTTCAAAAACC). A 238 base pair deletion was confirmed by Sanger sequencing. [3]

Human fibroblasts from DENND5A cohort members were obtained by skin biopsy (participant IDs: 2 and 10) and renal epithelial cells (participant ID: 3) from a urine sample. Cells were reprogrammed to iPSCs by electroporation with episomal plasmids (pCXLE-

hUL, pCXLE-hSK, and pCXLE-hOCT4) as previously described[8]. Generated iPSCs were functionally and genomically validated according to Hauser and Erzler[9].

Lymphoblasts were obtained from a healthy individual (control line) and two homozygous patients (participant IDs: 4 and 5). Cells were immortalized through use of the Epstein-Barr virus and generated in the lab of Dr. Fowzan Alkuraya. [3]

Cell culture

iPSCs were cultured on hESC-qualified Corning Matrigel-coated tissue culture dishes in either TeSR-E8 medium (all patient-derived iPSC lines; STEMCELL Technologies) or mTeSR1 medium (AIW001-02 WT and *DENND5A* KO; STEMCELL Technologies) with daily medium changes and mechanical removal of differentiated cells. Cells were passaged using the ReLeSR Passaging Reagent (STEMCELL Technologies) once cultures reached approximately 70% confluency. [3]

iPSCs were differentiated to neural progenitor cells (NPCs) using the STEMdiff SMADi Neural Induction Kit (STEMCELL Technologies) with daily medium changes. Induced cultures were passaged using Accumax (Millipore Sigma) once cells reached 90-95% confluency, approximately once per week. After a two week induction period, NPCs were maintained in STEMdiff Neural Progenitor Medium (STEMCELL Technologies) on poly L ornithine (PLO)- and laminin-coated plates and passaged using Accumax once cultures reached 80-95% confluency, approximately once per week. [3]

Control and patient-derived Epstein-Barr virus-induced lymphoblastoid cell lines were obtained from the laboratory of Dr. Alkuraya. Cells were cultured in suspension in RPMI 1640 medium (Gibco) supplemented with 15% fetal bovine serum (Wisent), 1% penicillin-

streptomycin (Wisent), and 1% L-glutamine (Wisent). Cells were split 1:4 once confluency reached approximately 1 x 10^6 cells/ml. [3]

HEK293-T cells were cultured in DMEM high glucose (Fisher) supplemented with 10% bovine calf serum (Fisher), 1% L-glutamine (Wisent), and 1% penicillin-streptomycin (Wisent). [3]

Plasmid cloning

DENND5A cDNA (Origene, SC121400) was cloned into the pCMV-tag2B vector to generate FLAG-DENND5A. GFP-DENND5A was made via subcloning DENND5A into the pEGFP-C1 vector. Patient variants and targeted residues for biochemical studies were introduced using the QuikChange Lightning site-directed mutagenesis kit (Agilent) following the manufacturer's protocol. … All constructs were confirmed by Sanger sequencing. [3]

RT-qPCR

RNA was extracted from NPCs and lymphocytes using the RNeasy kit (Qiagen) followed by cDNA synthesis using iScript Reverse Transcription Supermix for RT-qPCR (Bio-Rad). RT-qPCR was performed using SsoFast EvaGreen Supermix (Bio-Rad) with primers targeting human *DENND5A* (F: CTAAAGCCAGGGATGGTGCC; R: TTTCGGCATACATAGCATTCCT) and *TBP* (F: TGCACAGGAGCCAAGAGTGAA; R: CACATCACAGCTCCCCACCA). *DENND5A* levels were normalized to *TBP* levels and AIW001-02 WT NPCs or control lymphocytes. [3]

RNA from mouse brain tissue was extracted using RNeasy Lipid Tissue kit (Qiagen), followed by cDNA synthesis and RT-qPCR performed with the same reagents as above using

primers specific to the mouse genome for *DENND5A* (F: CAGTCGCTTCGCCGACTAT; R: GCACCATCCCTGGCTTTAGAA) and *GAPDH* (F: ACTCCACTCACGGCAAATTC; R: CCAGTAGACTCCACGACATACT). *DENND5A* levels were normalized to *GAPDH* levels in WT mice. [3]

Endogenous and transfected protein expression

NPCs and lymphoblasts were harvested in lysis buffer (20 mM HEPES pH 7.4, 100 mM NaCl, 0.83 mM benzamidine, 0.5 µg/ml aprotinin, 0.5 g/ml leupeptin, 0.23 mM phenylmethylsulfonyl fluoride) containing 1X LSB. Mouse brains were homogenized in lysis buffer and incubated with 1% Triton X-100 for 15 minutes at 4°C, followed by centrifugation at 239,000 x *g* for 15 minutes at 4°C. For FLAG-DENND5A expression, plasmid DNA was transfected into HEK293T cells using the calcium phosphate method and cells were harvested after 24 hours in lysis buffer containing 1X LSB. Equal protein aliquots were loaded onto an SDS-PAGE gel and analyzed via Western blot using primary antibodies against DENND5A (ThermoFisher #702789, 2.5 µg/ml), FLAG (clone M2, Sigma-Aldrich, 1:10,000), Hsc70 (clone 1B5, StressGen Biotechnologies Corp, 1:1:10,000), and β-actin (Clone C4, Sigma-Aldrich MAB1501R, 1:1000). [3]

Animal care and selection

All mouse care and experiments in the study were approved by the Montreal Neurological Institute Animal Care Committee in accordance with guidelines set by the Canadian Council on Animal Care under ethical protocol number 5734. The experimental unit for this study is a single animal. Apart from selecting animals based on *DENND5A* genotype, no exclusion criteria were set for the experiments and both male and female animals were used. [3]

Establishment of transgenic animal models

KI mice were generated by the McGill Integrated Core for Animal Modeling. Two silent mutations were introduced in L168 and L169 (CTTGCT –> TTAGCA) as well as a deletion of 2 bp in G172 to introduce a frameshift and premature stop codon in exon 4 of the *DENND5A* mouse gene. Briefly, custom sgRNAs (Synthego), Cas9 protein (IDT, Cat#1081058) and ssODN (ultramer, IDT) were microinjected into the pronucleus of C57BL/6N mouse zygotes with concentrations of 50:50:30 ng/µl respectively. Embryos were subsequently implanted in CD-1 pseudopregnant surrogate mothers according to standard procedures approved by the McGill University Animal Care Committee. Founder pups (F0) were genotyped for evidence of a deletion of 2 bp in G172 and mated to wild-type C57BL/6N (Charles River) mice for three generations. The colony was maintained by sibling mating and by crosses to C57BL/6N mice every third generation. All genomic sequencing was performed using the Big Dye Terminator Ready Reaction Mix (ABI, Carlsbad, CA, USA) at the McGill and Genome Quebec Innovation Center (Primers: ACAAGGAATGCTCTCACTGC, CACACTCCGACATGCCTTCAT [417 bp]). Obtained sequences were analyzed using an online tool (https://benchling.com). [3]

4-aminopyridine induced seizure assay

Mice were injected with the K+ channel blocker 4-aminopyridine (8 mg/kg, i.p.) (Sigma-Aldrich, Canada) to induce seizures. If no seizures were observed after 30 min, they were re-injected with a half-dose of 4-aminopyrdine (4 mg/kg, i.p.). Animals that showed no seizures after the second dose were excluded from further analysis. Seizures were identified based on behavioral symptoms such as myoclonic activity of rear and forelimbs that evolved

to rearing and loss of balance. The latency (min) from the time of the last 4-aminopyridine injection and seizure onset was calculated. [3]

7 T small animal MRI

Ten WT (3 males, 7 females, mean age = 114 days, *SD* = 12.9) and 10 KI (3 males, 7 females, mean age = 108 days, *SD* = 10.3) for a total of 20 mice were employed for high resolution, pre-clinical MR imaging experiments. Data from four animals were excluded from analysis to restrict subjects to an age range of approximately 3-4 months for consistency. For *in vivo* structural MRI, mice were anesthetized with isoflurane, placed in a plastic bed and restrained with gauze pads to minimize the possible influence of motion artifacts. For the duration of each MRI scan, mice were maintained under isoflurane gas anesthesia at approximately 37°C using a warm air blower and respiration was monitored using a pressure pad. [3]

Imaging was performed using the 7 T Bruker Pharmascan (Bruker Biosciences, Billerica, MA), ultra-high field, pre-clinical MRI system of the McConnell Brain Imaging Centre at McGill University. The Pharmascan is equipped with an AVANCE II-model spectrometer and BFG-150/90-S shielded gradient system (Resonance Research Inc., Billerica, Massachusetts). Structural MR images were acquired using a 2D Rapid Imaging with Refocused Echoes (RARE) pulse sequence with the following parameters: effective echo time (TE_{eff}): 30 ms, RARE factor: 8. In-plane resolution: 100 µm x 100 µm, slice thickness: 300 µm and receiver bandwidth: 46875 Hz. The repetition time (TR) and the number of acquired slices were varied for two pairs of WT/KI mice in order to achieve greater slice coverage along the rostro-caudal axis (TR: 4000 ms to 4750 ms, number of slices: 40 to 50). The number of averages was varied to optimize total scan time for mouse imaging under gas

anesthesia. Lateral ventricles were manually segmented in each scan by a researcher blind to animal genotypes using the ITK-SNAP software (www.itksnap.org).[10] and pooled lateral ventricle volumes were used for statistical analysis. [3]

Statistical Analysis

Continuous data were analyzed for normality and homogeneity of variance using Shapiro-Wilk tests ($n < 50$) or Kolmogorov-Smirnov ($n \geq 50$) tests and Levene tests. Student's *t*-tests were conducted when all assumptions were met. Welch's t-tests were conducted when homogeneity of variance assumptions were not met. The nonparametric equivalent (Mann-Whitney U test) was conducted when both normality of data and homogeneity of variance assumptions were not met. A p value of < 0.05 was considered statistically significant. Data were analyzed using SPSS, R version 4.1.2 with Companion to Applied Regression package version 3.0, and Tidyverse version 1.3.1 software. All statistical analyses included multiple replicates from several independent experiments. [3]

3.8.1 Motor skills scoring system

Item	Scoring
Able to reach/grasp objects	**+1** if positive
Able to roll over	**+1** if positive
Able to sit with support	**+1** if positive OR is able to sit without support
Able to sit without support	**+1** if positive
Able to stand with support	**+1** if positive OR is able to stand without support
Able to stand without support	**+1** if positive
Able to walk with support	**+1** if positive OR is able to walk without support
Able to walk without support	**+1** if positive
Muscle tone or spasm problems	**+1** if negative for all (hyperreflexia, spastic tetraplegia, clonus, and current hyper/hypotonia)
Motor regression after seizure	**+1** if negative AND could perform one of the above behaviors in past
TOTAL	**10**

Scoring system used for quantifying motor abilities. A low score reflects minimal motor abilities, a high score indicates a high degree of motor capabilities. If a child's ability to do a skill is unknown, it is counted as positive.

3.8.2 Neurological phenotype scoring system

Item	Scoring
Seizures	**+1** if positive
Reduced volume (cerebral or supratentorial parenchymal volume loss)	**+1** if positive
Cerebellum abnormalities (hypoplastic vermis, reduced volume)	**+1** if positive
Thalamus abnormalities (thalami fusion or reduced volume, massa intermedia prominence)	**+1** if positive
Basal ganglia abnormalities (dysplasia or reduced volume)	**+1** if positive
Calcifications	**+1** if positive
Ventricle or CSF abnormalities	**+1** if positive
White matter abnormalities (reduced corpus callosum or other white matter tract volume, delayed myelination or hyperintensity)	**+1** if positive
Hemorrhage or ischemic event	**+1** if positive
Cortical visual impairment	**+1** if positive
TOTAL	**10**

Scoring system used for quantifying neurological phenotypes. A low score corresponds to few neurological abnormalities, a high score indicates many neurological abnormalities.

3.9 References

1. Han C, Alkhater R, Froukh T, Minassian AG, Galati M, et al. Epileptic Encephalopathy Caused by Mutations in the Guanine Nucleotide Exchange Factor DENND5A. *Am J Hum Genet*. Dec 1 2016;99(6):1359-1367. doi:10.1016/j.ajhg.2016.10.006

2. Anazi S, Maddirevula S, Faqeih E, Alsedairy H, Alzahrani F, et al. Clinical genomics expands the morbid genome of intellectual disability and offers a high diagnostic yield. *Mol Psychiatry*. Apr 2017;22(4):615-624. doi:10.1038/mp.2016.113

3. Banks E, Francis V, Lin S-J, Kharfallah F, Fonov V, et al. Loss of symmetric cell division of apical neural progenitors drives *DENND5A*-related developmental and epileptic encephalopathy. *medRxiv*. 2023-01-01 00:00:00 2023;doi:https://doi.org/10.1101/2022.08.23.22278845

4. Sobreira N, Schiettecatte F, Valle D, Hamosh A. GeneMatcher: a matching tool for connecting investigators with an interest in the same gene. *Hum Mutat*. Oct 2015;36(10):928-30. doi:10.1002/humu.22844

5. Landrum MJ, Lee JM, Benson M, Brown GR, Chao C, et al. ClinVar: improving access to variant interpretations and supporting evidence. *Nucleic Acids Res*. Jan 4 2018;46(D1):D1062-D1067. doi:10.1093/nar/gkx1153

6. McLaren W, Pritchard B, Rios D, Chen Y, Flicek P, et al. Deriving the consequences of genomic variants with the Ensembl API and SNP Effect Predictor. *Bioinformatics*. Aug 15 2010;26(16):2069-70. doi:10.1093/bioinformatics/btq330

7. Chirita-Emandi A, Doros G, Simina IJ, Gafencu M, Puiu M. Head Circumference References for School Age Children in Western Romania. *Rev Med Chir Soc Med Nat Iasi*. Oct-Dec 2015;119(4):1083-91.

8. Okita K, Matsumura Y, Sato Y, Okada A, Morizane A, et al. A more efficient method to generate integration-free human iPS cells. *Nat Methods*. May 2011;8(5):409-12. doi:10.1038/nmeth.1591

9. Hauser S, Erzler M, Theurer Y, Schuster S, Schule R, et al. Establishment of SPAST mutant induced pluripotent stem cells (iPSCs) from a hereditary spastic paraplegia (HSP) patient. *Stem Cell Res*. Nov 2016;17(3):485-488. doi:10.1016/j.scr.2016.09.022

10. Yushkevich PA, Piven J, Hazlett HC, Smith RG, Ho S, et al. User-guided 3D active contour segmentation of anatomical structures: significantly improved efficiency and reliability. *Neuroimage*. Jul 1 2006;31(3):1116-28. doi:10.1016/j.neuroimage.2006.01.015

4 Chapter 3: Variants in *DENND5A*-related DEE patients reveal inter- and intramolecular interactions

Emily Banks[1], Jean-François Trempe[2], Peter S. McPherson[1]

[1] Department of Neurology and Neurosurgery, Montreal Neurological Institute, McGill University, Montréal, QC H3A 2B4, Canada

[2] Department of Pharmacology & Therapeutics and Centre de Recherche en Biologie Structurale, McGill University, Montréal, QC H3G 1Y6, Canada

4.1 Introduction

As described in Chapter 2, we have established, to the best of our knowledge, that biallelic pathogenic variants in *DENND5A* result in a structural DEE characterized by a unique combination of radiological features in severe cases. The pathogenic nature of frameshift and nonsense variants are rather obvious: patients lack all or part of DENND5A protein, and its absence affects intracellular processes essential for proper development. Both of the severe cases in our cohort in which neuroradiological signatures were identified were homozygous for frameshift variants. The individual with homozygous p.Q1271R*67 variants expresses substantially reduced DENND5A protein (**Fig. 2.1e**), but all protein that remains lacks a functional C-terminus due to the frameshift mutation. We did not obtain cells from the individual with homozygous p.S728Qfs*34 variants, but even in the unlikely scenario that nonsense-mediated mRNA decay or protein degradation does not occur, almost half of the DENND5A protein is missing. While a dominant negative effect due to certain variants is possible, it is more likely that DENND5A loss of function is responsible for disease states given the reduced protein levels in all tested patient-derived cells and the lack of or reduced protein levels when FLAG-tagged DENND5A containing frameshift and nonsense variants are overexpressed in mammalian cells.

The pathogenic nature of missense variants is less obvious. In fact, all missense variants found in our cohort are assigned a conservative American College of Medical Genetics and Genomics (ACMG) classification of likely benign or a variant of uncertain significance. While it is true that all individuals with missense variants tend to have milder neuroanatomical phenotypes compared to homozygous individuals with frameshift or nonsense variants, this does not always translate to better developmental outcomes. For example, participant 2 in our cohort, compound heterozygous for p.K485E and p.R710H which are both predicted to be likely benign or variants

of uncertain significance, presents with relatively mild neuroanatomical abnormalities but also severe DEE requiring assistance for all daily living activities. This individual also had no other gene variants flagged as potentially causative for their disease. Clearly, then, ACMG classifications for missense variants are unreliable without additional clinical or cell biological research. Missense variants found in patients with phenotypes overlapping with those harboring frameshift or nonsense variants provide a powerful starting ground for studying a gene's function, as the patient can guide the cell biological study of identifying how and why a particular amino acid is essential.

DENND5A is a member of a family of minimally 25 proteins bearing a differentially expressed in normal and neoplastic cells (DENN) domain. [1,2] Via the DENN domain, these proteins function as guanine nucleotide exchange factors (activators) of Rab GTPases, master regulators of membrane trafficking. [1,3] In addition to the DENN domain, DENND5A has two RUN (RPIP8 [RaP2 interacting protein 8], UNC-14 and NESCA [new molecule containing SH3 at the carboxyl-terminus]) domains. RUN domains are protein modules often associated with GTPases in the Rap and Rab families. [4] Through the most N-terminal RUN domain (RUN1), DENND5A is an effector for the active form of Rab6, giving DENND5A the basis for its original name of Rab6-interacting protein 1 (RAB6IP1). [5-7] Through the more C-terminal RUN domain (RUN2), DENND5A interacts with sorting nexin 1, a protein involved in protein trafficking between endosomes and the trans-Golgi network. [8,9] No specific protein interaction or other function has been observed with the PLAT domain (Polycystin-1, Lipoxygenase, Alpha-Toxin) of DENND5A, a little-studied beta sheet protein module involved in protein-protein and protein-lipid interactions. [10] Full-length DENND5A also interacts with GTP-Rab11, but no specific binding site has been identified. [11] Linker regions comprising strings of residues that are not predicted to form conserved tertiary

structures link the DENN-RUN1 and PLAT-RUN2 domains, but nothing is known regarding their involvement in protein-protein interactions.

Here we investigate protein-protein interactions with fragments of DENND5A, containing either the WT amino acid sequence or with individual missense variants introduced. A series of pulldown experiments in embryonic day 18 rat brain lysate followed by mass spectrometry were performed to identify novel protein-protein interactions, and to determine if these interactions are affected by missense variants found in the human cohort. While many novel protein-protein interactions were identified using various regions of DENND5A and previously discovered interactions were confirmed, we focus on one result and its subsequent biochemical and cell biological study.

4.2 Results

4.2.1 Identification of interaction between DENND5A and MUPP1/PALS1

To better understand molecular mechanisms regulating DENND5A function,

we screened for binding partners using affinity purification with multiple regions and domains of the protein as bait. Mass spectrometry of [a GST-tagged peptide flanking the region linking the DENN and RUN1 domains] after incubation in embryonic rat brain lysate revealed members of the Crb polarity complex, MUPP1 and PALS1, as major DENND5A binding partners … (**Fig. 3.1a-b**). This interaction was confirmed with overexpressed proteins in HEK293T lysate (**Fig. 3.1c**). [12]

To elucidate which protein DENND5A binds to directly, we repeated the experiment with HEK293T lysate expressing either Pals1-FLAG, FLAG-MUPP1, or FLAG-MUPP1ΔL27. MUPP1 binds PALS1 via its L27 domain, so deleting this region should exclude endogenous PALS1. However, the DENND5A GST-tagged peptide was able to bind both PALS1-FLAG and FLAG-MUPP1ΔL27 when each were expressed alone (**Fig. 3.1d-e**), but the strongest and most reliable interaction was always observed when both were co-expressed (**Fig. 3.1c**).

4.2.2 Structural analysis of the predicted DENND5A structure provides insight on the nature of the DENND5A-MUPP1/PALS1 interaction

We [modeled] the predicted structure of DENND5A from AlphaFold[13,14] and noted that residues R701, E707, H708, R710, and R716 involved in the interaction with the polarity proteins make hydrogen bonds with residues S10-A11, R273, R129, D598, and R716 of the DENN domain (**Fig. 3.2a**), respectively, suggesting a conformational change may be necessary to expose the binding site for MUPP1/PALS1. In fact, full-length DENND5A has

limited interaction with these proteins (**Fig. 3.2d**). Because DENN domains are evolutionarily conserved protein modules that function as guanine nucleotide exchange factors for Rab GTPases[3], we aligned the co-crystal structure of DENND1B and Rab35 with the predicted DENND5A structure and found that the predicted Rab enzymatic site in DENND5A [may be occluded] by interactions between the DENN and RUN1 … domains (PDB: 3TW8[15]; **Fig. S3.1a**). In contrast, a conformational change is not necessary for the known DENND5A binding partner GTP-Rab6 to bind the RUN1 domain (PDB: 3CWZ[6]; **Fig. S3.1b**), suggesting that two functional conformations are both possible and necessary.

We next examined the intramolecular interactions blocking MUPP1/PALS1 binding in the AlphaFold structure of DENND5A and observed a cluster of highly charged residues at the interface of the DENN and RUN1 domains (**Fig. 3.2b**), suggesting that the structure can be biochemically manipulated to expose both the Rab and Crb complex binding sites. To confirm this intramolecular interaction experimentally, we performed a pull-down assay with the GST-RUN1/PLAT domains as bait in HEK293T lysate expressing either full-length FLAG-tagged DENND5A or the isolated DENN domain (aa1-680). Both DENND5A constructs bind the RUN1/PLAT domain, with a slightly stronger interaction with the isolated DENN domain (**Fig. 3.2c**). Moreover, the DENN domain interaction was impeded with charge masking from higher salt concentrations (**Fig. S3.1c**). We then performed mutagenesis experiments targeting residues involved in the intramolecular interaction. Mutating E379 [of the DENN/RUN1 interface] resulted in a weak but present interaction between full-length DENND5A and Crb complex proteins, implying that DENND5A molecules were slightly skewed toward an open conformation (**Fig. 3.2d**). R710H, [which lies in the region linking the DENN domain and the RUN1 domain], is predicted to result in

the loss of a salt bridge to D598 of the DENN domain, potentially destabilizing the closed structure (**Fig. S3.1d**). Like what was observed upon disrupting the DENN/RUN1 interaction, introducing the patient variant R710H also resulted in increased binding to MUPP1-FLAG and PALS1-FLAG (**Fig. 3.2d**). We conclude that DENND5A binds MUPP1 and PALS1 in a conformation-dependent manner, and that R710H increases the likelihood that DENND5A will adopt an open configuration. (**Fig. 3.2d**). [12]

4.3 Discussion

We provide evidence for an intramolecular interaction between the DENN and RUN1 domains of DENND5A, and that this interaction must be disrupted for apical polarity proteins to bind DENND5A. Additionally, structural modeling shows that the steady-state conformation of DENND5A prohibits a Rab substrate from associating with the conserved enzymatic pocket of the DENN domain. This is consistent with experiments showing that another DENN domain protein, DENND3, makes intramolecular interactions to modulate its tertiary structure and regulate its GEF activity toward Rab12[16]. Similarly, we propose that conformational changes in DENND5A regulate both MUPP1/PALS1 binding as well as its GEF activity toward a Rab substrate.

Because the DENND5A GST fusion peptide flanking R710H bound FLAG-MUPP1ΔL27, we provide preliminary evidence that DENND5A binds one of the 13 PDZ domains of MUPP1. The peptide binding to PALS1-FLAG when it is expressed alone may indicate that complexes comprising PALS1-FLAG and endogenous MUPP1 were formed *in vitro*, and that PALS1-FLAG was detected via the GST-tagged peptide binding endogenous MUPP1. However, these data are uncertain and unclear. Repeating the pulldown in lysate expressing various MUPP1 and PALS1 fragments can definitively clarify which protein DENND5A binds directly.

> The [low affinity] interaction between open full-length DENND5A and the apical polarity proteins may indicate that this occurs transiently in cells or only under specific circumstances. Indeed, the conformation-dependent nature of the interaction reflects the importance of these proteins remaining separate from each other under steady state conditions. … The biologically relevant mechanism for opening the DENND5A structure remains elusive, but possible candidates include posttranslational modifications or other currently unidentified protein-protein interactions. [12]

4.4 Chapter 3 Figures

4.4.1 Main Figures

Figure 3.1

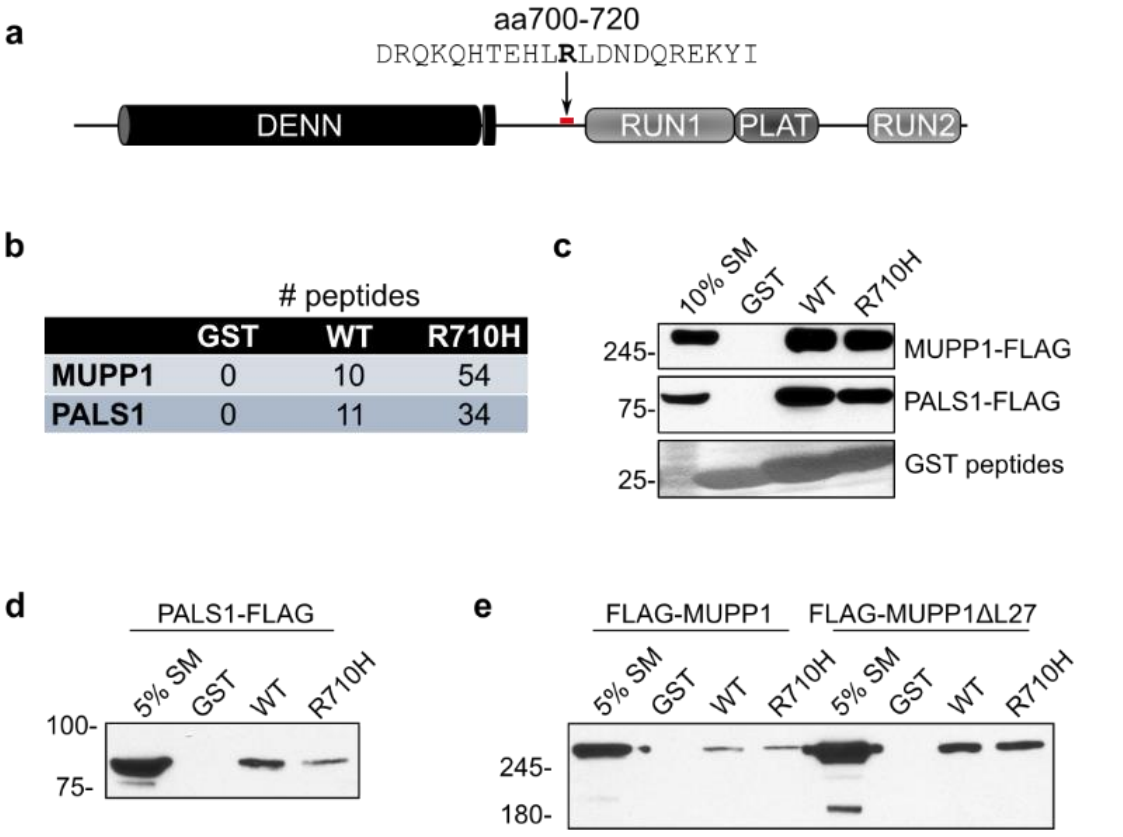

Figure 3.1: DENND5A interacts with polarity proteins MUPP1 and PALS1. a, A recombinant GST-tagged peptide containing amino acids 700-720 of human DENND5A sequence was generated for use in pulldown experiments. The bolded residue corresponds to Arg710 that is affected in the cohort (R710H). **b,** Table indicating the number of peptides corresponding to MUPP1 and PALS1 found bound to each GST fusion peptide used in the pulldown/mass spectrometry experiment. **c,** Overexpressed human MUPP1- and PALS1-FLAG bind to GST-tagged DENND5A peptides. **d,** Pulldowns in lysate expressing only PALS1-FLAG results in reduced Pals1 binding to GST-tagged peptides upon introduction of the R710H mutation. **e,** Pulldowns in lysate expressing only full-length FLAG-MUPP1 or FLAG-MUPP1 lacking its L27 domain results in similar levels of binding in both WT and R710H GST-tagged peptides.

Figure 3.2

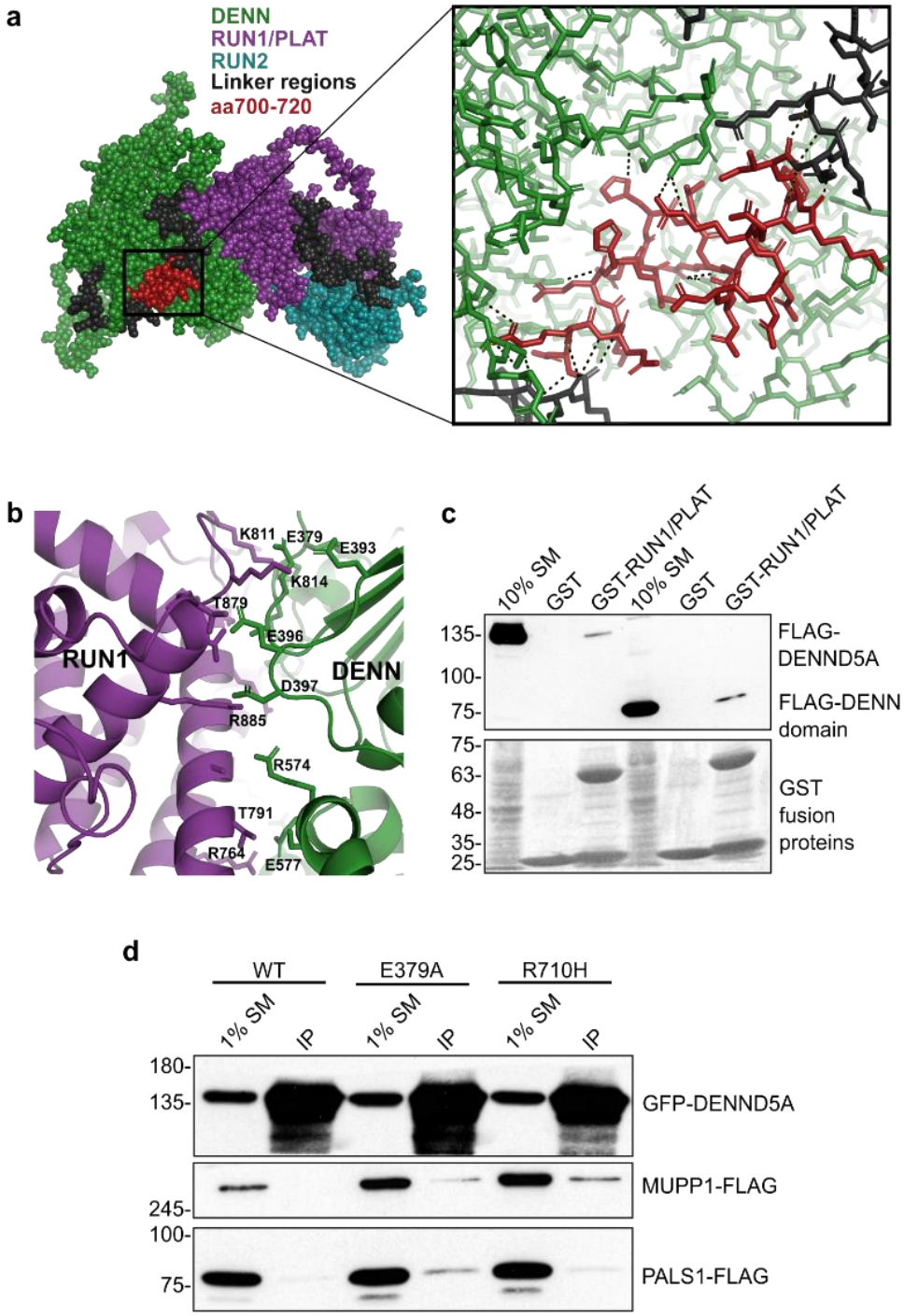

Figure 3.2: Structural basis for the interaction between DENND5A and MUPP1/PALS1. a, Residues 700-720 are shown in red in a space-fill model (left) and magnified view (right) of the predicted DENND5A protein structure from AlphaFold. Dotted lines indicate hydrogen bonds. **b,** The interface between the DENN and RUN1 domains of DENND5A comprise many charged residues. **c,** GST pulldown experiments show that FLAG-DENN and GST-RUN1/PLAT physically interact. **d,** Co-immunoprecipitations between GFP-DENND5A and MUPP1- and PALS1-FLAG show that DENND5A only binds the polarity proteins when the intramolecular DENN-RUN1 interaction is disrupted.

4.4.2 Supplementary Figures

Figure S3.1

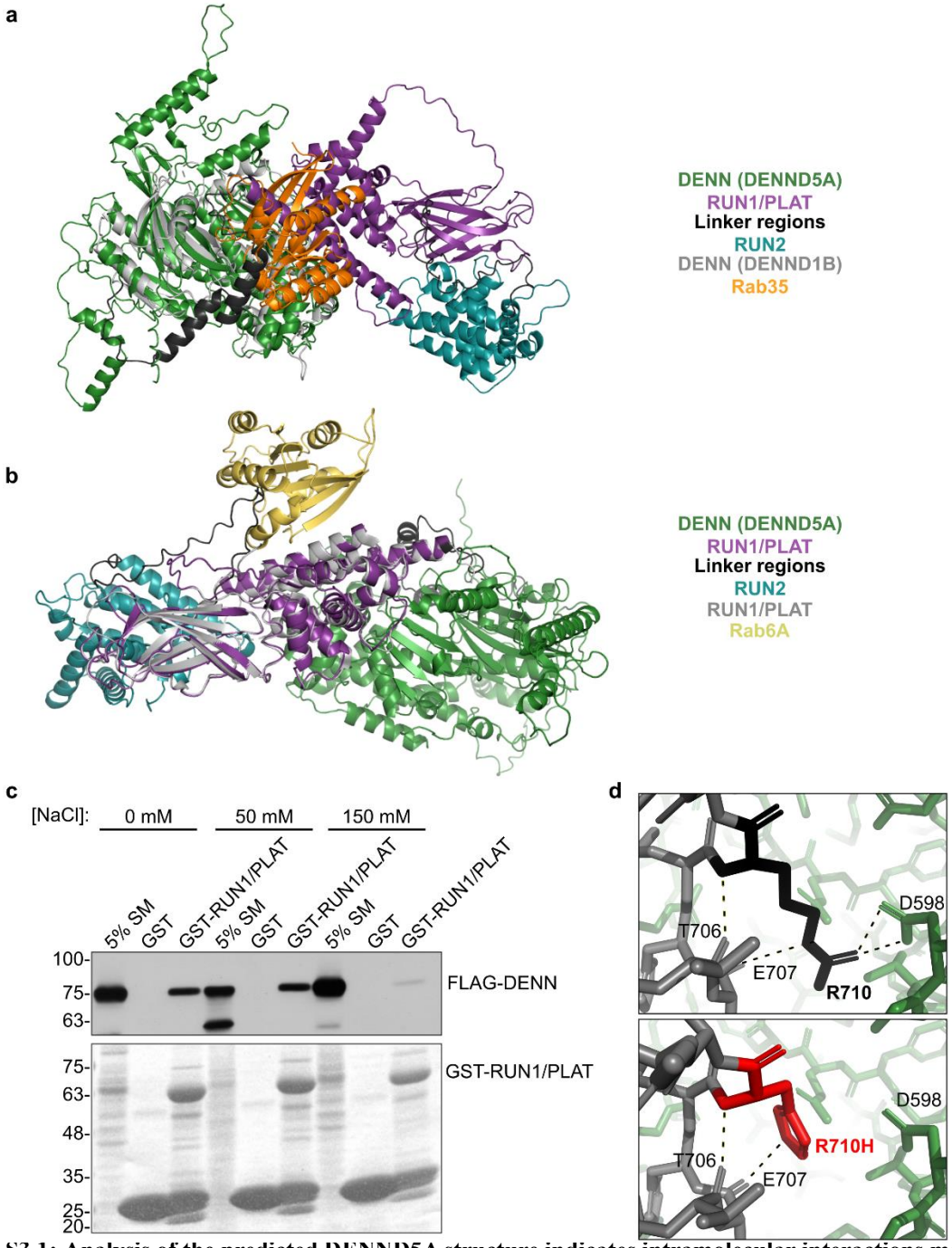

Figure S3.1: Analysis of the predicted DENND5A structure indicates intramolecular interactions may regulate other protein-protein interactions. a, Structural alignment between the predicted DENND5A structure and PDB:3TW8 (gray, yellow). **b,** Structural alignment between the predicted DENND5A structure and PDB:3CWZ (gray, yellow). **c,** Pulldown experiment showing binding capacity between GST-RUN1/PLAT and FLAG-DENN domains of DENND5A under varying NaCl concentrations. **d,** The R710H variant found in the cohort and within the region that interacts with PALS1/MUPP1 results in the removal of two hydrogen bonds with D598 of the DENN domain. Dotted lines indicate hydrogen bonds.

4.5 Author Contributions

EB designed, performed, and analyzed all experiments under the supervision of PSM. JFT identified the molecular interface between the DENN and RUN1 domains.

4.6 Competing Interests

The authors report no competing interests.

4.7 Materials and Methods

Plasmid cloning

DENND5A cDNA (Origene, SC121400) was cloned into the pCMV-tag2B vector to generate FLAG-DENND5A. GFP-DENND5A was made via subcloning DENND5A into the pEGFP-C1 vector. Patient variants and targeted residues for biochemical studies were introduced using the QuikChange Lightning site-directed mutagenesis kit (Agilent) following the manufacturer's protocol. FLAG-DENND5A DENN domain was made by subcloning aa1-680 of DENND5A into the pCMV-tag2B vector. GST-aa700-720 was made via oligo annealing followed by ligation into a pGEX-4T1 vector with a modified multiple cloning site (MCS). GST-RUN1/PLAT was created by subcloning DENND5A aa707-1090 into the pGEX-6P1 vector. MUPP1 (MPDZ) was obtained from the Harvard Medical School plasmid collection (HsCD00352820). Untagged PALS1 (MPP5) in pDONR223 was obtained from Addgene (#23447) and subcloned into a pCMV3-C-FLAG vector to generate PALS1-FLAG. The vector backbone from PALS1-FLAG was then isolated and modified to include a custom MCS via oligo annealing and ligation in order to create restriction sites suitable for subcloning MUPP1 into the vector. MUPP1 was subcloned into this modified vector to create MUPP1-FLAG. [12]

FLAG-MUPP1 and FLAG-MUPP1ΔL27 were created by subcloning into a pCMV-tag2B vector. All constructs were confirmed by Sanger sequencing.

Pulldown experiments

500 mL flasks of bacteria were induced overnight at RT to express GST-tagged proteins using 500 μM IPTG when the optical density of the cultures at 600 nm reached 0.6. Bacteria were pelleted and resuspended in PBS + protease inhibitors pH 7.4. Resuspended bacterial cells were then sonicated 3 times for 5 seconds at 70% amplitude, followed by incubation with 1% Triton X-100 for 15 minutes. Bacterial cell lysate was then spun for 5 minutes at 4°C at 11,952 x g. The supernatant was incubated with glutathione Sepharose beads pre-washed 3 times in PBS for one hour at 4°C, and beads were then briefly spun down and washed 3 times in PBS + protease inhibitors to purify GST fusion proteins. The concentration of fusion proteins was determined by running on an SDS-PAGE gel accompanied by a BSA standard curve followed by Coomassie Brilliant Blue staining. Cell lysates were then harvested for incubation with GST fusion proteins.[12]

For pulldown experiments with overexpressed proteins, HEK293-T cells were transfected using the calcium phosphate method with the appropriate plasmids and harvested the next day in lysis buffer. Cells were then sonicated once for 10 seconds at 20% amplitude, incubated in 1% Triton X-100 for 15 minutes at 4°C, and spun at 21 x g and 4°C for 15 minutes in a tabletop centrifuge. The concentration of HEK293T supernatants were analyzed via a Bradford assay, and 1 mg/ml was incubated with 20 μg (GST-aa700-720) or 100 μg (GST-RUN1/PLAT) of fusion proteins for one hour at 4°C. Following incubation, beads were washed 3 times in buffer containing 1% Triton, eluted in 1X LSB, loaded onto an SDS-

PAGE gel, and analyzed via Western blot using primary antibodies against FLAG (clone M2, Sigma-Aldrich, 1:10,000).[12]

Mass spectrometry

For the initial protein-protein interaction screen followed by mass spectrometry, 4 E18 rat brains were homogenized on ice in 1 ml lysis buffer per brain (20 mM HEPES pH 7.4, 150 mM NaCl, 0.83 mM benzamidine, 0.5 µg/ml aprotinin, 0.5 µg/ml leupeptin, and 0.23 mM phenylmethylsulfonyl fluoride) with 10 strokes using a Caframo homogenizer at 1200 rpm. Tissue homogenate was then sonicated once for 10 seconds at 20% amplitude, incubated in 1% Triton X-100 for 15 minutes at 4°C, and spun at 239,000 x g and 4°C for 15 minutes. Supernatant concentration was determined via a Bradford assay and 1 mg/ml was incubated with 50 µg GST-fusion protein overnight at 4°C. Following incubation, beads were washed 3 times in lysis buffer containing 1% Triton, then eluted in 1X Lammeli sample buffer (LSB). [12]

For each sample, proteins were loaded onto a single stacking gel band to remove lipids, detergents, and salts. The gel band was reduced with DTT, alkylated with iodoacetic acid, and digested with Trypsin. Extracted peptides were re-solubilized in 0.1% aqueous formic acid and loaded onto a Thermo Acclaim Pepmap (Thermo, 75 µM ID X 2cm C18 3 µM beads) precolumn and then onto an Acclaim Pepmap Easyspray (Thermo, 75 µM X 15cm with 2 µM C18 beads) analytical column separation using a Dionex Ultimate 3000 uHPLC at 250 nl/min with a gradient of 2-35% organic (0.1% formic acid in acetonitrile) over 2 hours. Peptides were analyzed using a Thermo Orbitrap Fusion mass spectrometer operating at 120,000 resolution (FWHM in MS1) with HCD sequencing (15,000 resolution) at top speed for all peptides with a charge of 2+ or greater. The raw data were

converted into *.mgf format (Mascot generic format) for searching using the Mascot 2.6.2 search engine (Matrix Science) against all rat protein sequences (Uniprot 2017). Search parameters for peptides > 5 residues were +/- 5 ppm on the parent ion and 0.1 amu on fragment ions. A fixed modification for carboxymethyl-Cysteine was used along with variable modifications of Oxidation (methionine) and deamination (asparagine/glutamine). At 99.0% protein and 95% peptide confidence, 1077 proteins (34,443 spectra) were identified using 1 peptide (0.0% peptide FDR and 0.40% protein FDR). The database search results were loaded onto Scaffold Q+ Scaffold_4.8.6 (Proteome Sciences) for statistical treatment and data visualization.

Co-immunoprecipitation experiments

For co-immunoprecipitation experiments, HEK293-T cells were transfected using the calcium phosphate method, harvested in lysis buffer, and sonicated once for 10 seconds at 20% amplitude, followed by incubation in 0.5% Triton X-100 for 15 minutes at 4°C. Cell lysate was then spun at 21 x *g* and 4°C for 15 minutes in a tabletop centrifuge, and 1 mg/ml of the resulting supernatant was incubated for one hour at 4°C with 25 µl ChromoTek GFP-Trap Agarose magnetic beads pre-equilibrated 3 times in lysis buffer without Triton X-100. Beads were then washed 3 times in lysis buffer containing 0.05% Triton and then eluted in 1X LSB for SDS-PAGE analysis and analyzed via Western blot using primary antibodies against FLAG (clone M2, Sigma-Aldrich, 1:10,000) and GFP (Invitrogen Cat# A-6455, 1:20,000). [12]

4.8 References

1. Allaire PD, Marat AL, Dall'Armi C, Di Paolo G, McPherson PS, et al. The Connecdenn DENN domain: a GEF for Rab35 mediating cargo-specific exit from early endosomes. *Mol Cell*. Feb 12 2010;37(3):370-82. doi:10.1016/j.molcel.2009.12.037

2. Zhang D, Iyer LM, He F, Aravind L. Discovery of Novel DENN Proteins: Implications for the Evolution of Eukaryotic Intracellular Membrane Structures and Human Disease. *Front Genet*. 2012;3:283. doi:10.3389/fgene.2012.00283

3. Marat AL, Dokainish H, McPherson PS. DENN domain proteins: regulators of Rab GTPases. *J Biol Chem*. Apr 22 2011;286(16):13791-800. doi:10.1074/jbc.R110.217067

4. Callebaut I, de Gunzburg J, Goud B, Mornon JP. RUN domains: a new family of domains involved in Ras-like GTPase signaling. *Trends Biochem Sci*. Feb 2001;26(2):79-83. doi:10.1016/s0968-0004(00)01730-8

5. Janoueix-Lerosey I, Jollivet F, Camonis J, Marche PN, Goud B. Two-hybrid system screen with the small GTP-binding protein Rab6. Identification of a novel mouse GDP dissociation inhibitor isoform and two other potential partners of Rab6. *J Biol Chem*. Jun 16 1995;270(24):14801-8. doi:10.1074/jbc.270.24.14801

6. Recacha R, Boulet A, Jollivet F, Monier S, Houdusse A, et al. Structural basis for recruitment of Rab6-interacting protein 1 to Golgi via a RUN domain. *Structure*. Jan 14 2009;17(1):21-30. doi:10.1016/j.str.2008.10.014

7. Fernandes H, Franklin E, Khan AR. Crystallization of an engineered RUN domain of Rab6-interacting protein 1/DENND5. *Acta Crystallogr Sect F Struct Biol Cryst Commun*. May 1 2011;67(Pt 5):556-60. doi:10.1107/S174430911100724X

8. Fernandes H, Franklin E, Jollivet F, Bliedtner K, Khan AR. Mapping the interactions between a RUN domain from DENND5/Rab6IP1 and sorting nexin 1. *PLoS One*. 2012;7(4):e35637. doi:10.1371/journal.pone.0035637

9. Wassmer T, Attar N, Harterink M, van Weering JR, Traer CJ, et al. The retromer coat complex coordinates endosomal sorting and dynein-mediated transport, with carrier recognition by the trans-Golgi network. *Dev Cell*. Jul 2009;17(1):110-22. doi:10.1016/j.devcel.2009.04.016

10. Bateman A, Sandford R. The PLAT domain: a new piece in the PKD1 puzzle. *Curr Biol*. Aug 26 1999;9(16):R588-90. doi:10.1016/s0960-9822(99)80380-7

11. Miserey-Lenkei S, Waharte F, Boulet A, Cuif MH, Tenza D, et al. Rab6-interacting protein 1 links Rab6 and Rab11 function. *Traffic*. Oct 2007;8(10):1385-403. doi:10.1111/j.1600-0854.2007.00612.x

12. Banks E, Francis V, Lin S-J, Kharfallah F, Fonov V, et al. Loss of symmetric cell division of apical neural progenitors drives *DENND5A*-related developmental and epileptic encephalopathy. *medRxiv*. 2023-01-01 00:00:00 2023;doi:https://doi.org/10.1101/2022.08.23.22278845

13. Jumper J, Evans R, Pritzel A, Green T, Figurnov M, et al. Highly accurate protein structure prediction with AlphaFold. *Nature*. Aug 2021;596(7873):583-589. doi:10.1038/s41586-021-03819-2

14. Varadi M, Anyango S, Deshpande M, Nair S, Natassia C, et al. AlphaFold Protein Structure Database: massively expanding the structural coverage of protein-sequence space with high-accuracy models. *Nucleic Acids Res*. Jan 7 2022;50(D1):D439-D444. doi:10.1093/nar/gkab1061

15. Wu X, Bradley MJ, Cai Y, Kummel D, De La Cruz EM, et al. Insights regarding guanine nucleotide exchange from the structure of a DENN-domain protein complexed with its Rab GTPase substrate. *Proc Natl Acad Sci U S A*. Nov 15 2011;108(46):18672-7. doi:10.1073/pnas.1110415108

16. Xu J, McPherson PS. Regulation of DENND3, the exchange factor for the small GTPase Rab12 through an intramolecular interaction. *J Biol Chem*. Apr 28 2017;292(17):7274-7282. doi:10.1074/jbc.M116.772434

5 Chapter 4: Loss of *DENND5A* results in loss of symmetric cell division and premature differentiation

Emily Banks[1], Vincent Francis[1], Peter S. McPherson[1]

[1] Department of Neurology and Neurosurgery, Montreal Neurological Institute, McGill University, Montréal, QC H3A 2B4, Canada

5.1 Introduction

The balance of symmetric versus asymmetric cell division in the ventricular zone (VZ) and subventricular zone (SVZ) throughout cortical development is critical to obtain the ideal number, diversity, and positioning of neurons in the mature brain. Excessive symmetric division leads to an increased number of progenitors and over-proliferation and can result in a disorganized cortex, macrocephaly, and early death[1,2]. Excessive asymmetric division will prematurely deplete progenitor pools and lead to microcephaly, which can cause seizures and cell death[3]. Two major mechanisms that drive primary microcephaly concern centrosome dynamics and cell division, including mitotic spindle orientation and cell cycle exit[5]. Given the high prevalence of microcephaly in our human cohort, we wanted to test whether *DENND5A* is involved in differentiation, which reflects cell cycle exit, and/or the ability for the cells to divide symmetrically and increase the number of progenitors.

Loss of *DENND5A* has previously been shown to result in cell division defects. A study examining *DENND5A* KD in HeLa cells observed an increase in cells arrested in metaphase leading to apoptosis or, if the cells passed the MAD2 spindle checkpoint, the generation of binucleated cells[6]. Another study examining MDCKII cystogenesis, the process of Madin-Darby canine kidney II epithelial cells forming a three-dimensional structure surrounding a central lumen, observed spindle formation abnormalities leading to disrupted lumen formation upon *DENND5A* KD[7]. Although both studies suggest a role for DENND5A in mitotic spindle formation or orientation, its implication on neural development is unknown. Li et al. [7] argue that *DENND5A* is a cancer-driving gene, and in some tissues this may be true as *DENND5A* mutations have been identified in cases of melanoma[8]. However, an implication of cancer is that cells over-proliferate

and excessively self-renew, but the microcephaly observed in our patient cohort and experience working with *DENND5A* KO cell lines disagree with this assumption.

A traditional way of assessing a cell's ability to self-renew is to perform a neurosphere formation assay; however, the formation of neurospheres depends not only on intact self-renewal mechanisms but also the integrity of cell-cell adhesions. Given that DENND5A interacts with AJ proteins MUPP1 and PALS1, care should be taken when interpreting results. Additionally, the underlying clonality assumption of the assay, that individual spheres are genetically identical, has been disproven[9]. Finally, while self-renewal is an important stem cell-defining feature, it does not necessarily equate to symmetric cell division, because self-renewal can occur during asymmetric divisions as well[10].

A more reliable method to assess a cell's ability to divide symmetrically *in vitro* is by measuring the axis of cell division in a neural rosette formation assay. Stem cells that are dissociated into a single-cell suspension and plated on a basement membrane-like surface in neural induction medium proliferate and spontaneously arrange themselves into polarized structures centered around a hollow lumen. Neural rosettes resemble neuroepithelial cells in the neural tube based on gene expression profiles, multilineage potential, morphology, cell polarization, and radial arrangement[11,12]. Symmetric divisions in this assay are identified by the parallel positioning of daughter cells (and therefore the mitotic spindle) relative to the lumen and equal inheritance of apical determinants. Conversely, a perpendicular orientation results in an asymmetric division in which only one daughter cell is in contact with the lumen and inherits apical determinants, whereas the other becomes detached from the apical surface and divides away from the center of the rosette (See **Fig. S4.1** for an illustration of these differences).

By performing a neural rosette formation assay and examining differentiation phenotypes *in vitro*, extrinsic factors such as CSF composition in animal models that may influence cell fate and cell division are eliminated, since the culture media remains constant throughout each experiment and in each condition. Here, by controlling extrinsic factors, we test the hypotheses that intrinsic factors, namely the presence or absence of *DENND5A*, influence cell differentiation and the mode of cell division during development. We then test whether these phenotypes observed *in vitro* can also be observed *ex vivo* and examine the proportions of progenitors and post-mitotic neurons in the SVZ of WT and *DENND5A* KI mice.

5.2 Results

5.2.1 Loss of DENND5A results in premature cell cycle exit and neuronal differentiation

We observed that [AIW001-02] *DENND5A* KO NPCs grow slower than WT (**Fig. 4.1a**). Interestingly, a significant difference was observed even after 24 hours (M_{WT} = 710, M_{KO} = 621, SD_{WT} = 108.8, SD_{KO} = 72.4, two-tailed $t(18) = 2.168$, $p = .044$), likely due to an increased number of apoptotic cells observed after plating KO cells. WT NPCs then rapidly increased in number whereas the number of KO NPCs remained relatively stable, producing a significant difference after 48 (M_{WT} = 1008, M_{KO} = 614, SD_{WT} = 135.6, SD_{KO} = 65.30, two-tailed Welch's $t(12.96) = 8.30$, $p < .0001$) and 72 hours (M_{WT} = 1685, M_{KO} = 683, SD_{WT} = 351.6, SD_{KO} = 35.09, two-tailed Mann-Whitney U, $Z = -3.78$, $p < .0001$). [13]

Remarkably, after passaging newly-formed NPCs into neural progenitor maintenance medium, KO NPCs develop β-III tubulin-positive processes with neuronal morphology after one day, something rarely observed in WT NPCs (M_{WT} = 10.67%, M_{KO} = 47.29%, SD_{WT} = 13.5, SD_{KO} = 21.1, two-tailed Mann-Whitney U, $Z = -3.991$, $p < .0001$; **Fig. 4.1b-c**). To determine if this premature differentiation phenotype translates to complex organisms lacking *DENND5A*, we examined the adult mouse subventricular zone, a region that normally retains GFAP-positive radial glia-like neural stem cells[14] that are the primary source of newborn neurons in the adult SVZ[15]. KI mice have a significantly higher percentage of post-mitotic neurons expressing NeuN compared to WT (M_{WT} = 39.6%, M_{KI} = 58.8%, SD_{WT} = 6.7, SD_{KI} = 6.6, two-tailed $t(10) = -4.981$, $p = 0.001$; **Fig. 4.1d-g**). While there is also a reduction in the mean proportion of GFAP-positive cells in KI SVZs, it did not reach significance (M_{WT} = 43.3%, M_{KI} = 31.9%, SD_{WT} = 12.3, SD_{KI} = 14.1, two-tailed $t(10) = 1.486$, $p = 0.168$). [13]

5.2.2 *DENND5A* is required for neurosphere formation

To assess the ability for NPCs to self-renew, we initially performed a neurosphere formation assay by plating between 5-100 NPCs per well in uncoated 96 well tissue culture dishes. WT NPCs consistently formed neurospheres of at least 50 μm after 2 weeks in culture, but no spheres were observed in *DENND5A* KO cultures regardless of the number of cells seeded (**Fig. 4.2**), pointing toward a self-renewal deficiency in *DENND5A* KO cells.

5.2.3 Loss of *DENND5A* misorients mitotic spindles

To completely remove the confounding variable of cell-cell adhesion deficits and assess with more confidence whether symmetric cell division is affected in *DENND5A* KO cells, we plated iPSCs on an adherent basement membrane-like substrate and measured the orientation of cell division in relation to the lumen in a polarized *in vitro* model of early neural development.

WT and *DENND5A* KO iPSCs were plated at low density in neural induction medium and neural rosettes were allowed to form for up to 7 days. After 1 day *in vitro* (DIV), both WT and KO rosettes had maximal OCT4 expression, a marker of pluripotency, which rapidly declined by DIV 3 and was completely abolished by DIV 5 (**Figure S4.2a**). Expression of the NPC marker SOX2 was observed after 1 DIV, reached maximal levels at DIV 3, then slightly reduced and stabilized at DIV 5-7 (**Figure S4.2b**). This characterization is in line with rosettes generated from both iPSCs and embryonic stem cells using various neural induction protocols[16-18]. In general, there were many more WT rosettes formed per coverslip compared to KO. As in the NPC proliferation experiment, this may be due to the large amount of KO cell death observed at DIV 1, reducing the number of stem cells initially available for rosette formation. WT rosettes were considerably denser than KOs, but rosette diameter, lumen area, and lumen perimeter did not differ significantly (**Figure S4.2c-e**).

PALS1 localized apically in both WT and KO rosettes (**Fig. 4.3a**), suggesting DENND5A is not involved in trafficking MUPP1/PALS1 to the apical membrane. However, the axis of cell division in relation to the lumen differed (**Fig. 4.3b**). Because F-actin accumulates apically during rosette formation[19] and outlines the cell borders of dividing cells, we used F-actin as a convenient marker of the apical surface. We thus measured the mitotic spindle angle, defined as the angle between the cleavage plane and the nearest apical membrane (**Fig. S4.3**), considering only cells with normally condensed chromatin and both centrosomes marked by γ-tubulin visible in the same plane. Although this exclusion criteria omitted many cells in WT rosettes dividing symmetrically along the z-plane or above the lumen (**Fig. S4.4a**) as well as numerous observations of dividing cells with abnormally condensed chromatin in KO rosettes (**Fig. S4.4b**), the spindle angle among cells dividing within WT (M = 57.1°, Mdn = 65.4°, SD = 25.9) and KO (M = 26.0°, Mdn = 20.1°, SD = 19.0) rosettes differed significantly according to a two-tailed Mann-Whitney U test (Z = -7.122, $p < .0001$; **Fig. 4.3c**). An overwhelming majority of KO cells divided with spindle angles <45° (**Fig. 4.3d**), indicating that *DENND5A* KO results in increased levels of oblique asymmetric cell divisions and the ability for apical progenitors to self-renew is severely compromised. [13]

5.3 Discussion

A limitation to our neurosphere formation experiment is that multiple cells per well were plated. This raises the risk that the observed spheres were not clonally derived from a single cell, but rather from multiple cells that were either inadvertently plated together as clusters, or that suspended cells in the medium grouped together prior to quantification. Indeed, unless a single cell per well is plated, the validity of the neurosphere assay to assess stem and progenitor cell self-renewal on the basis of neurosphere size and number has been criticized, as these structures are highly motile even in the absence of agitation and are prone to fuse with other cells and spheres, thereby negating the assumption that each sphere is clonal and confounding results[9]. However, the complete absence of neurospheres from *DENND5A* KO NPCs strongly indicate a self-renewal deficiency in these cells. Moreover, the limitations of the neurosphere assay were overcome with our neural rosette formation assay, where we observed a significant reduction in symmetric division based on mitotic spindle orientation in *DENND5A* KO rosettes.

"Our results suggest that DENND5A expression promotes stemness and its loss permits cell cycle exit and premature differentiation." [13] Our *in vitro* experiments excluded the potential impact of extrinsic factors on cell division and differentiation dynamics and established that *DENND5A* is necessary and sufficient for progenitors to both retain their neural stem cell identity and to divide symmetrically. The *ex vivo* examination of the adult mouse SVZ complemented our *in vitro* results, confirming that premature neuronal differentiation also occurs in a complex organism with homozygous *DENND5A* variants identified in the human cohort. Future studies should explore embryonic cortical development in WT and KI mice. Measuring the mitotic spindle angle at the embryonic VZ and comparing progenitor and neuron populations at this stage of

development will provide a more definitive mechanism underlying microcephaly due to biallelic pathogenic *DENND5A* variants.

5.4 Chapter 4 Figures

5.4.1 Main Figures

Figure 4.1

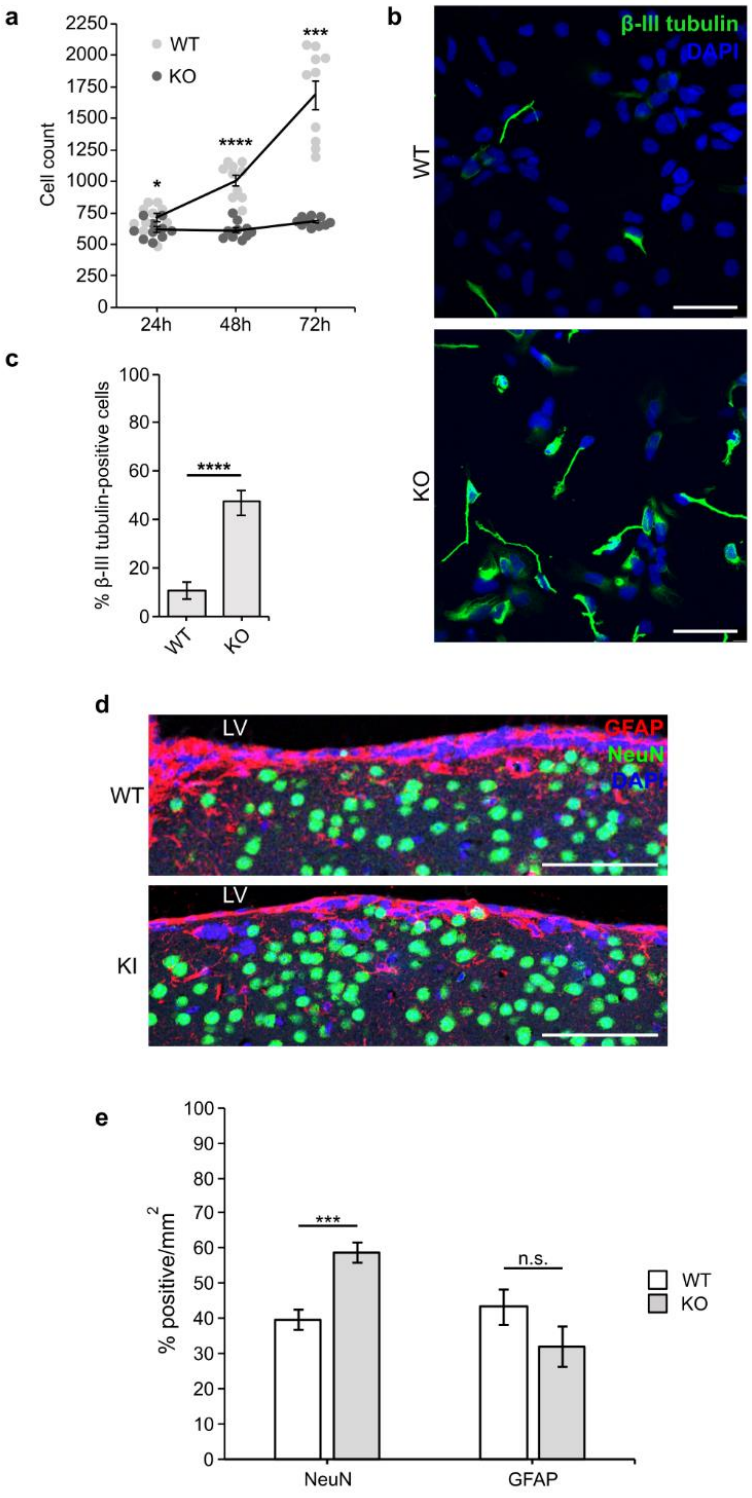

Figure 4.1: Loss of DENND5A results in premature neuronal differentiation. a, Graph showing the average number of NPCs counted per well of a 96-well plate 24, 48, and 72 hours after plating equal numbers of cells. Data are derived from 10 technical replicates from $n = 2$ independent experiments. Error bars = SEM. **b,** Immunostaining of β-III tubulin (green) and DAPI (blue) in NPCs one day after plating. Scale bar = 50 µm. **c,** Quantification of the percent of β-III tubulin-positive cells per field. A total of $n = 2267$ cells were analyzed from three independent experiments. Data are means ± SEM. **d,** Immunostaining of GFAP (red), NeuN (green), and DAPI (blue) in the SVZ of adult mice. LV = lateral ventricle. Scale bar = 100 µm. **e,** Quantification of the percentage of cells per mm^2 labeled by NeuN or GFAP from a total of $n = 4$ mice. Data are means ± SEM.

Figure 4.2

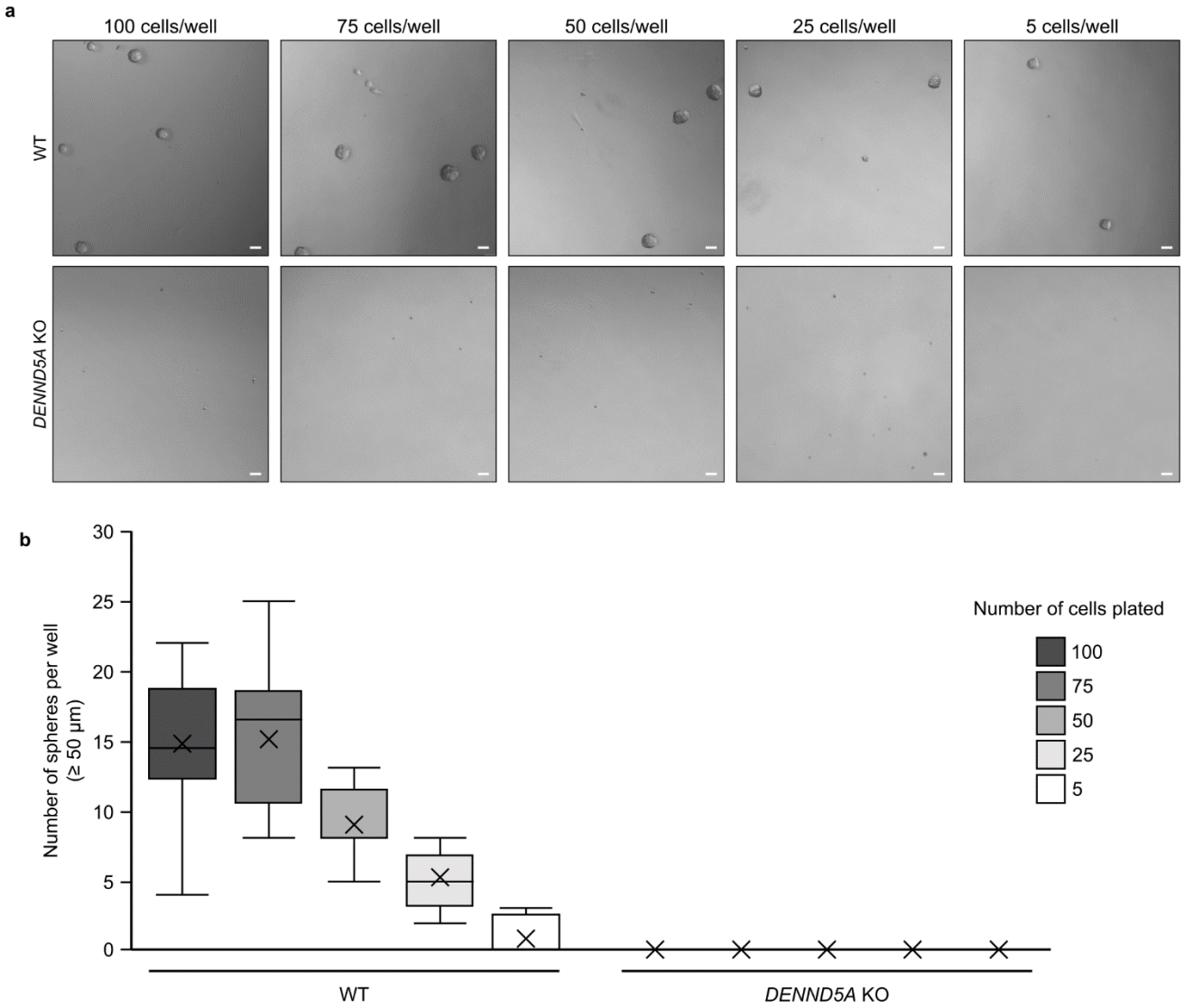

Figure 4.2: *DENND5A* KO NPCs are unable to form neurospheres. a, Representative images of neurospheres formed when 100, 75, 50, 25, or 5 cells were seeded per well of a 96 well plate. Scale bar = 50 µm. **b,** Quantification of the number of neurospheres ≥ 50 µm per well after 2 weeks in culture.

Figure 4.3

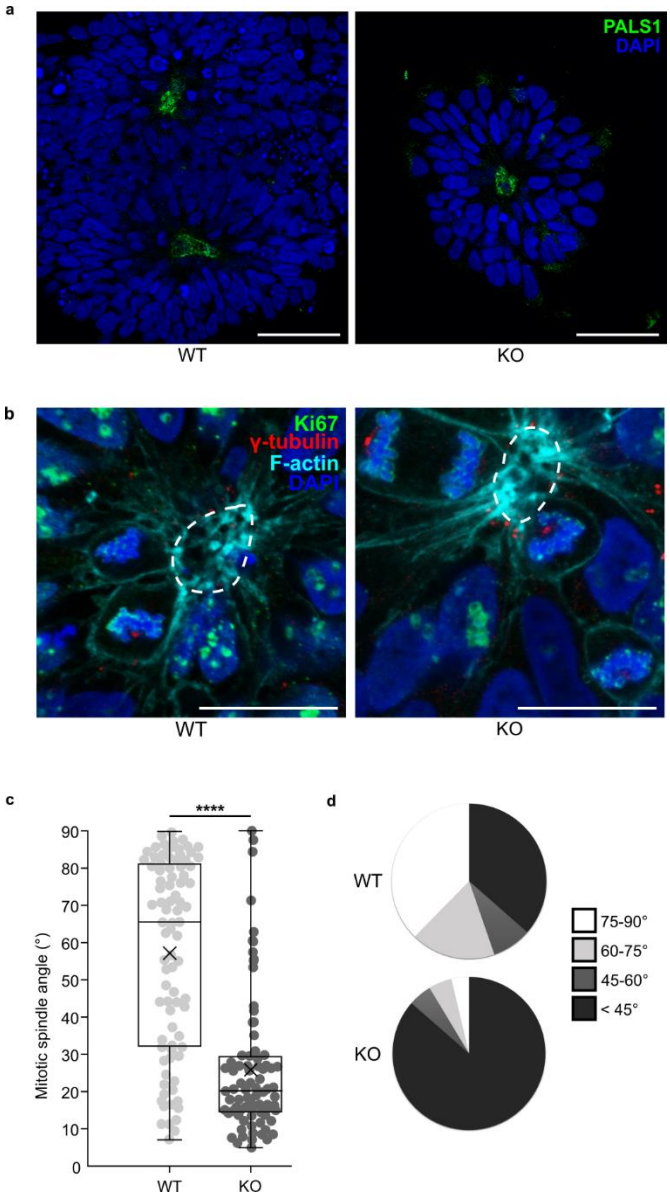

Figure 4.3: A neural rosette formation assay reveals abnormal mitotic spindle orientations upon loss of *DENND5A*. a, PALS1 staining (green) shows an apical localization in both WT and KO neural rosettes. Scale bars = 50 µm. **b,** Sample images showing the orientation of apical progenitor cell division in WT and *DENND5A* KO rosettes. Green = Ki67, red = γ-tubulin, cyan = F-actin, blue = DAPI. Scale bars = 20 µm. Dotted lines outline the lumen. **c,** Quantification of mitotic spindle angles measured from n = 85 WT and n = 81 KO dividing cells from 2 independent experiments. **d,** Pie charts showing the proportion of dividing cells with mitotic spindle angles falling within various ranges.

5.4.2 Supplementary Figures

Figure S4.1

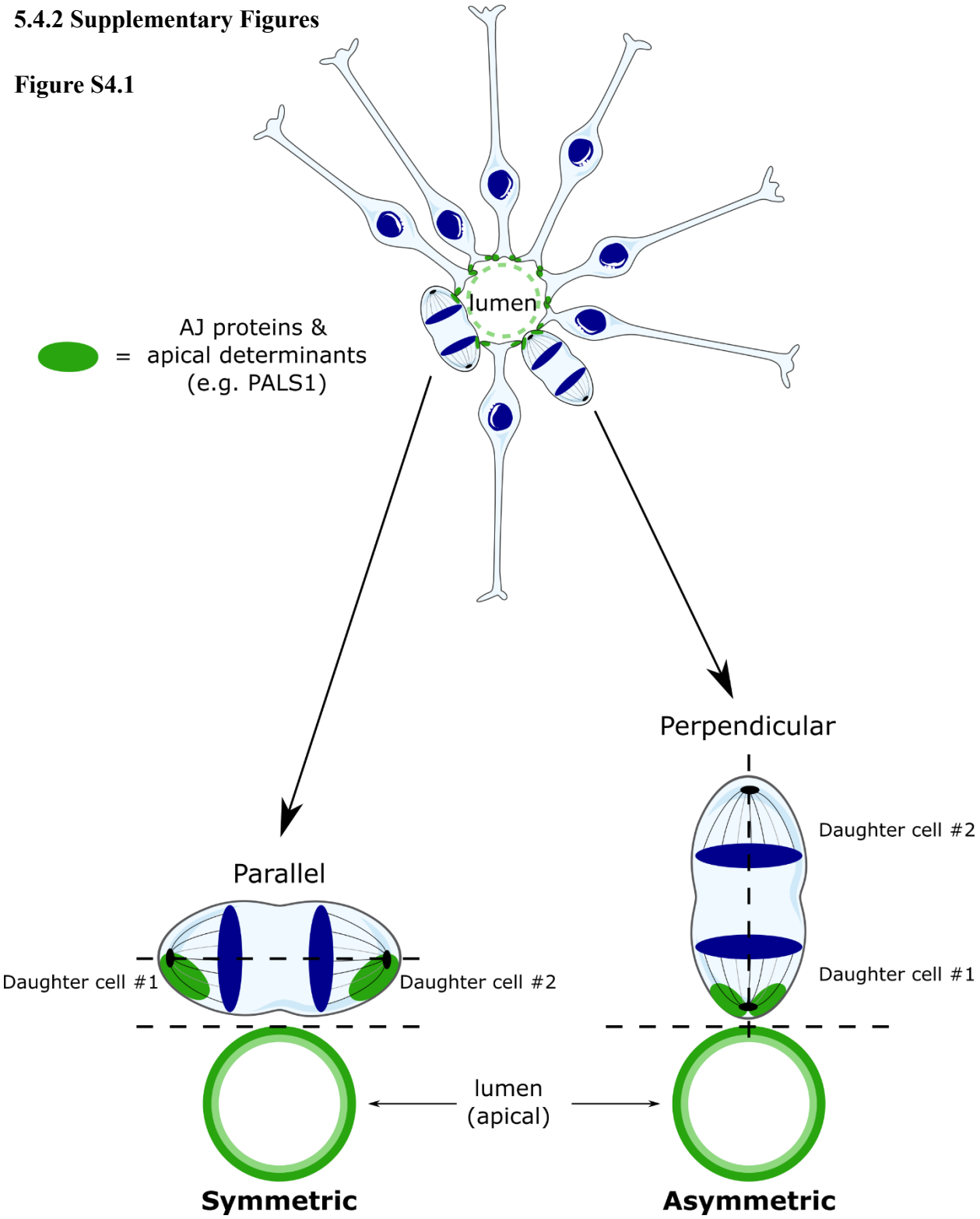

Figure S4.1: Illustration depicting the differences between symmetric and asymmetric cell divisions in the context of neural rosettes.

Figure S4.2

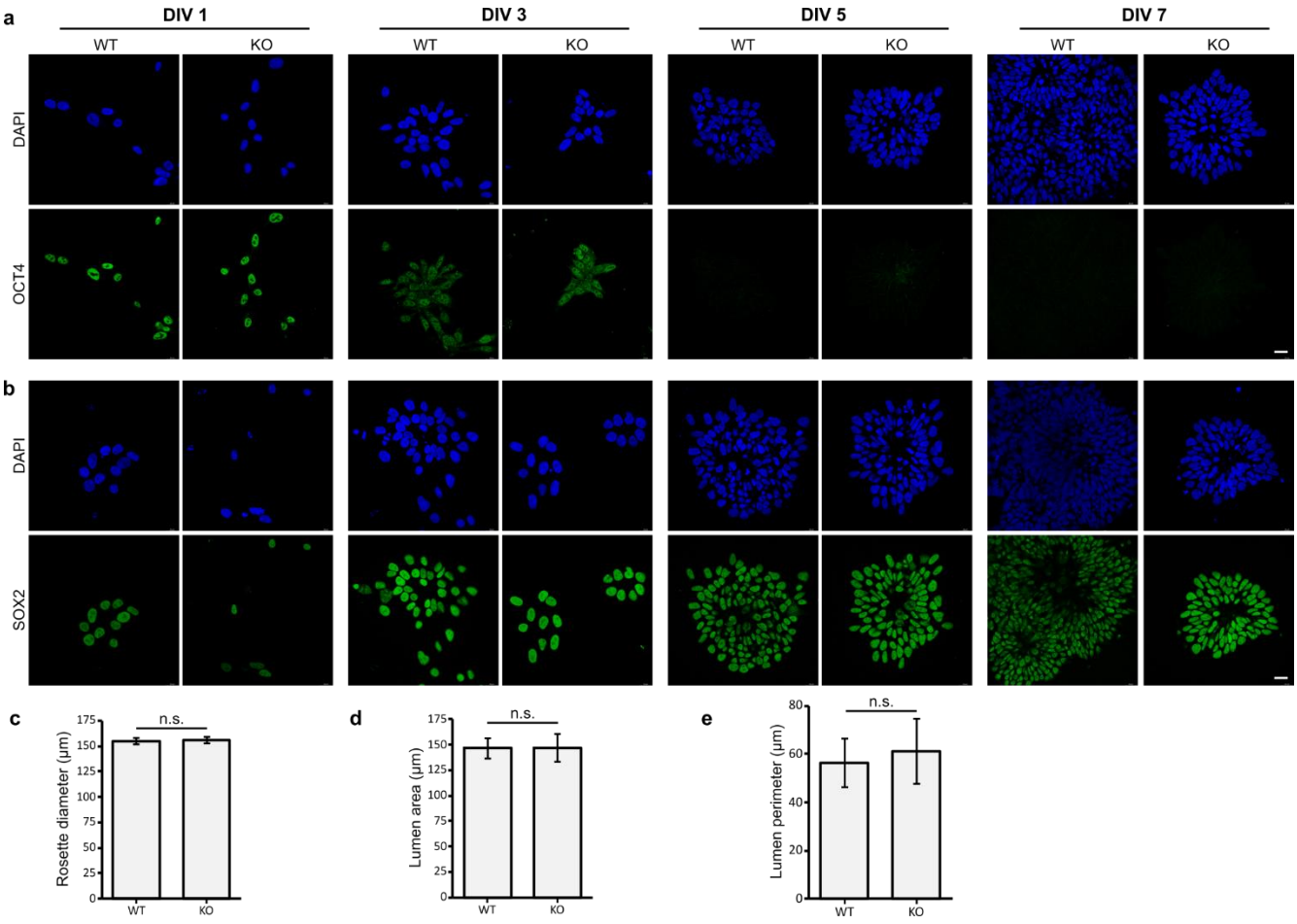

Figure S4.2: WT and *DENND5A* KO neural rosettes differ in density and cell division properties, but not in marker expression or size. Expression of a, OCT4 and b, SOX2 during neural rosette development. Blue = DAPI, green = OCT4/SOX2. Scale bars = 20 µm. c, Average diameter of individual rosettes. *n* = 159 rosettes were analyzed from 2 independent experiments. Data are mean ± SEM and analyzed via student's *t*-test. d, Average lumen area of rosettes. *n* = 294 rosettes were analyzed from 2 independent experiments. Data are mean ± SEM and analyzed via Mann-Whitney U test. e, Average lumen perimeter of rosettes. *n* = 294 rosettes were analyzed from 2 independent experiments. Data are mean ± SEM and analyzed via Mann-Whitney U test.

Figure S4.3

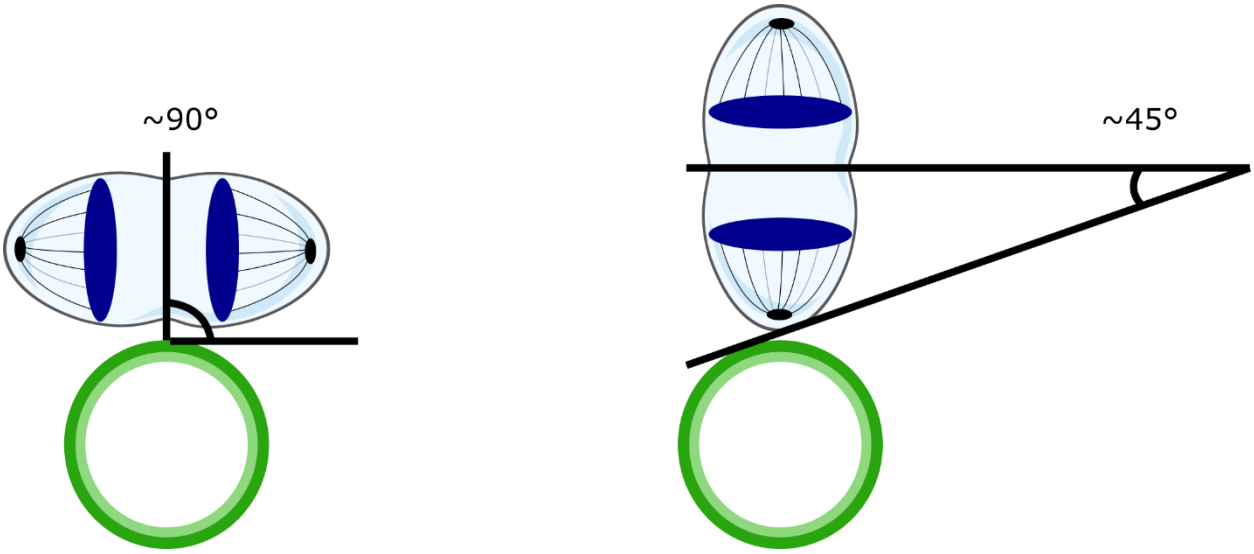

Figure S4.3: Illustration demonstrating spindle angle measurement method. Mitotic spindle angles were quantified based on Chilov et al. [4] and were defined as the angle between the plane of cleavage between two daughter cells and the nearest apical surface.

Figure S4.4

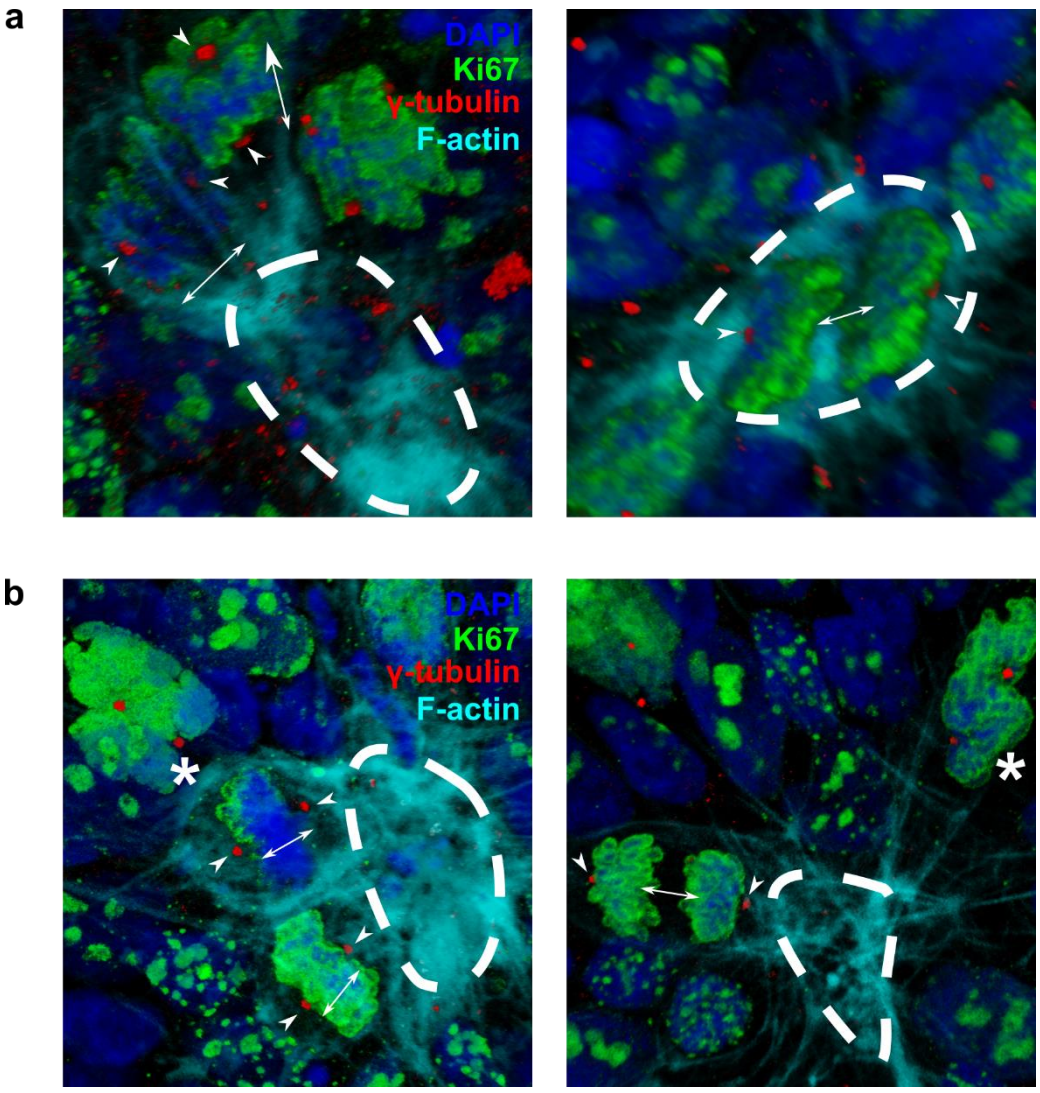

Figure S4.4: 3D images generated from z-stacks of confocal images shows that WT cells excluded from analysis still divide symmetrically, and KO cells often exhibit abnormal spindles and abnormally condensed chromatin. a, 3D-rendered images of apical progenitors of WT neural rosettes. Blue = DAPI, green = Ki67, red = -tubulin, cyan = F-actin. Arrowheads indicate centrosomes, arrows indicate orientation of cell divisions, dotted lines indicate the lumen. **b,** 3D-rendered images of apical progenitors of KO neural rosettes. Blue = DAPI, green = Ki67, red = -tubulin, cyan = F-actin. Arrowheads indicate centrosomes, arrows indicate orientation of cell

5.5 Author Contributions

VF performed IHC. EB performed all other experiments and analyzed all data under the supervision of PSM.

5.6 Competing Interests

The authors declare no competing interests.

5.7 Materials and Methods

Establishment of cell lines

The control induced pluripotent stem cell (iPSC) line AIW001-02 was derived from peripheral blood mononuclear cells of a healthy female donor (Caucasian, 48 years old). The AIW001-02 cell line was generated by using the CytoTune™-iPS 2.0 Sendai Reprogramming Kit (iPSQuebec Platform, Laval University). For knockout expression of human *DENND5A*, guide RNAs (gRNAs) were designed using an online tool (https://benchling.com). Both gRNA target sites are on *DENND5A* exon 4. Synthesized gRNAs were ordered from SYNTHEGO and transfection was performed following the manufacturer's protocol. Single cell colonies were picked and amplified. Genomic DNA from the colonies was extracted with QuickExtract (Lucigen) and PCR was performed using Q5 High-Fidelity DNA Polymerase according to the manufacturer's protocol (F: GAGGATCGCCAGTGAGTGTT; R: CCCCGAGCAGTTCAAAAACC). A 238 base pair deletion was confirmed by Sanger sequencing. … Generated iPSCs were functionally and genomically validated according to Hauser and Erzler[20]. [13]

Cell culture

iPSCs were cultured on hESC-qualified Corning Matrigel-coated tissue culture dishes in either TeSR-E8 medium (all patient-derived iPSC lines; STEMCELL Technologies) or mTeSR1 medium (AIW001-02 WT and *DENND5A* KO; STEMCELL Technologies) with daily medium changes and mechanical removal of differentiated cells. Cells were passaged using the ReLeSR Passaging Reagent (STEMCELL Technologies) once cultures reached approximately 70% confluency. [13]

iPSCs were differentiated to neural progenitor cells (NPCs) using the STEMdiff SMADi Neural Induction Kit (STEMCELL Technologies) with daily medium changes. Induced cultures were passaged using Accumax (Millipore Sigma) once cells reached 90-95% confluency, approximately once per week. After a two week induction period, NPCs were maintained in STEMdiff Neural Progenitor Medium (STEMCELL Technologies) on poly L ornithine (PLO)- and laminin-coated plates and passaged using Accumax once cultures reached 80-95% confluency, approximately once per week. Experiments examining β-III tubulin expression examined established NPC lines after one passage post-neural induction; all other experiments were performed using cells at passages 2-4. [13]

Neurosphere formation assay

5, 25, 50, 75, or 100 NPCs per well of each condition were seeded into an uncoated 96-well dish in STEMDiff Neural Progenitor Medium (STEMCell) with six replicates per experiment. 50 µl media was added every 3-4 days, and 4X images were taken of the top, bottom, left, right, and middle of each well after 2 weeks in culture using the EVOS FLc microscope. Neurospheres at least 50 µm in diameter were identified using ImageJ and counted. Data are derived from two independent experiments.

Neural rosette formation assay

iPSCs were gently dissociated into a single cell suspension and plated at low density (20,000 cells per well of a 24 well plate) onto PLO/Laminin-coated coverslips in neural induction media with SMAD inhibitor (STEMCELL Technologies #08581) containing 10 μM Y-27632 on the day of plating. Medium was changed daily and cells were fixed after 1, 3, 5, and 7 days in culture. Rosettes were stained and z-stack images in 0.5 μm increments were taken using the Leica SP8 confocal microscope. For lumen size analysis, z-plane images with the largest visible lumens were used for quantification followed by two-tailed student's *t*-tests. For rosette diameter analysis, z-plane images with the widest phalloidin staining were used for quantification followed by a two-tailed student's *t*-test. To analyze dividing cells within the rosettes, cells in metaphase, anaphase, and telophase were used for quantification. Mitotic spindle angles were measured as in Chilov et al., 2011[4] using ImageJ.[13]

Immunocytochemistry

Samples were fixed in 4% paraformaldehyde for 20 minutes at room temperature. Cells were permeabilized for 5 minutes in 0.1% Triton-X 100 and then blocked in 5% BSA and 0.01% Triton-X 100 in PBS for 30 minutes at room temperature, followed by overnight incubation at 4°C with the following antibodies: OCT4 (ab19857, 1 μg/ml), SOX1 (Invitrogen MA5-32447, 1:200), SOX2 (Abcam ab92494, 1:1000), Nestin (Invitrogen, MA1-110), β-III tubulin (Abcam ab52623, 0.1 μg/ml), Ki67 (Abcam ab15580, 0.5 μg/ml), γ-tubulin (Sigma-Aldrich T6557, 1:500), and Pals1 (Santa Cruz Biotechnology sc-365411, 1:350). After primary antibody incubation, samples were washed twice with PBS then incubated with Alexa-conjugated secondary antibodies at 1:500 dilution and phalloidin at

1:1000 dilution for 1 hour at room temperature. Cells were then washed twice in PBS, incubated with DAPI at 1:5000 dilution for 10 minutes, washed twice in PBS again, and mounted onto glass slides. [13]

Animal care and selection

All mouse care and experiments in the study were approved by the Montreal Neurological Institute Animal Care Committee in accordance with guidelines set by the Canadian Council on Animal Care under ethical protocol number 5734. The experimental unit for this study is a single animal. Apart from selecting animals based on *DENND5A* genotype, no exclusion criteria were set for the experiments and both male and female animals were used. [13]

Establishment of transgenic animal models

KI mice were generated by the McGill Integrated Core for Animal Modeling. Two silent mutations were introduced in L168 and L169 (CTTGCT –> TTAGCA) as well as a deletion of 2 bp in G172 to introduce a frameshift and premature stop codon in exon 4 of the *DENND5A* mouse gene. Briefly, custom sgRNAs (Synthego), Cas9 protein (IDT, Cat#1081058) and ssODN (ultramer, IDT) were microinjected into the pronucleus of C57BL/6N mouse zygotes with concentrations of 50:50:30 ng/µl respectively. Embryos were subsequently implanted in CD-1 pseudopregnant surrogate mothers according to standard procedures approved by the McGill University Animal Care Committee. Founder pups (F0) were genotyped for evidence of a deletion of 2 bp in G172 and mated to wild-type C57BL/6N (Charles River) mice for three generations. The colony was maintained by sibling mating and by crosses to C57BL/6N mice every third generation. All genomic sequencing was performed using the Big Dye Terminator Ready Reaction Mix (ABI, Carlsbad, CA,

USA) at the McGill and Genome Quebec Innovation Center (Primers: ACAAGGAATGCTCTCACTGC, CACACTCCGACATGCCTTCAT [417 bp]). Obtained sequences were analyzed using an online tool (https://benchling.com). [13]

Immunohistochemistry

Mouse brain sections were baked overnight at 60°C in a conventional oven. Samples were then deparaffinized and rehydrated in a series of xylene and ethanol washes, followed by antigen retrieval using citrate buffer (pH 6.0) for 10 minutes at 120°C in a decloaking chamber (Biocare Medical). Slides were then rinsed IHC buffer (PBS + 0.05% Tween-20 + 0.2% Triton X-100) and blocked for 1 hour with Protein Block (Spring Bioscience), incubated with primary antibodies overnight at 4°C, and washed with IHC buffer followed by incubation with respective secondary antibodies (Invitrogen) for 1 hour at room temperature. Coverslip mounting was done using ProLong Diamond Gold Antifade Mountant with DAPI (Invitrogen) to stain nuclei. mages were acquired using Leica SP8 laser scanning confocal microscope. Quantification of the percentage of cells per mm^2 labeled by NeuN or GFAP was based on three 10x magnification images per animal from a total of n = 4 mice. Cells within 100 μm of the ependymal layer (excluding the ependymal cells) in which DAPI signal was also evident were considered. All measurements were done using ImageJ. [13]

Statistical Analysis

Continuous data were analyzed for normality and homogeneity of variance using Shapiro-Wilk tests ($n < 50$) or Kolmogorov-Smirnov ($n \geq 50$) tests and Levene tests. Student's t-tests were conducted when all assumptions were met. Welch's t-tests were conducted when

homogeneity of variance assumptions were not met. The nonparametric equivalent (Mann-Whitney U test) was conducted when both normality of data and homogeneity of variance assumptions were not met. A p value of < 0.05 was considered statistically significant. Data were analyzed using SPSS. … All statistical analyses included multiple replicates from several independent experiments. [13]

5.8 References

1. Groszer M, Erickson R, Scripture-Adams DD, Lesche R, Trumpp A, et al. Negative regulation of neural stem/progenitor cell proliferation by the Pten tumor suppressor gene in vivo. *Science*. Dec 7 2001;294(5549):2186-9. doi:10.1126/science.1065518

2. Lehtinen MK, Zappaterra MW, Chen X, Yang YJ, Hill AD, et al. The cerebrospinal fluid provides a proliferative niche for neural progenitor cells. *Neuron*. Mar 10 2011;69(5):893-905. doi:10.1016/j.neuron.2011.01.023

3. Gruber R, Zhou Z, Sukchev M, Joerss T, Frappart PO, et al. MCPH1 regulates the neuroprogenitor division mode by coupling the centrosomal cycle with mitotic entry through the Chk1-Cdc25 pathway. *Nat Cell Biol*. Sep 25 2011;13(11):1325-34. doi:10.1038/ncb2342

4. Chilov D, Sinjushina N, Rita H, Taketo MM, Makela TP, et al. Phosphorylated beta-catenin localizes to centrosomes of neuronal progenitors and is required for cell polarity and neurogenesis in developing midbrain. *Dev Biol*. Sep 1 2011;357(1):259-68. doi:10.1016/j.ydbio.2011.06.029

5. Jean F, Stuart A, Tarailo-Graovac M. Dissecting the Genetic and Etiological Causes of Primary Microcephaly. *Front Neurol*. 2020;11:570830. doi:10.3389/fneur.2020.570830

6. Miserey-Lenkei S, Waharte F, Boulet A, Cuif MH, Tenza D, et al. Rab6-interacting protein 1 links Rab6 and Rab11 function. *Traffic*. Oct 2007;8(10):1385-403. doi:10.1111/j.1600-0854.2007.00612.x

7. Li Y, Xu J, Xiong H, Ma Z, Wang Z, et al. Cancer driver candidate genes AVL9, DENND5A and NUPL1 contribute to MDCK cystogenesis. *Oncoscience*. 2014;1(12):854-865. doi:10.18632/oncoscience.107

8. Yang M, Johnsson P, Brautigam L, Yang XR, Thrane K, et al. Novel loss-of-function variant in DENND5A impedes melanosomal cargo transport and predisposes to familial cutaneous melanoma. *Genet Med*. Jan 2022;24(1):157-169. doi:10.1016/j.gim.2021.09.003

9. Singec I, Knoth R, Meyer RP, Maciaczyk J, Volk B, et al. Defining the actual sensitivity and specificity of the neurosphere assay in stem cell biology. *Nat Methods*. Oct 2006;3(10):801-6. doi:10.1038/nmeth926

10. Peyre E, Morin X. An oblique view on the role of spindle orientation in vertebrate neurogenesis. *Dev Growth Differ*. Apr 2012;54(3):287-305. doi:10.1111/j.1440-169X.2012.01350.x

11. Elkabetz Y, Panagiotakos G, Al Shamy G, Socci ND, Tabar V, et al. Human ES cell-derived neural rosettes reveal a functionally distinct early neural stem cell stage. *Genes Dev*. Jan 15 2008;22(2):152-65. doi:10.1101/gad.1616208

12. Wilson PG, Stice SS. Development and differentiation of neural rosettes derived from human embryonic stem cells. *Stem Cell Rev*. 2006;2(1):67-77. doi:10.1007/s12015-006-0011-1

13. Banks E, Francis V, Lin S-J, Kharfallah F, Fonov V, et al. Loss of symmetric cell division of apical neural progenitors drives *DENND5A*-related developmental and epileptic encephalopathy. *medRxiv*. 2023-01-01 00:00:00 2023;doi:https://doi.org/10.1101/2022.08.23.22278845

14. Liu X, Bolteus AJ, Balkin DM, Henschel O, Bordey A. GFAP-expressing cells in the postnatal subventricular zone display a unique glial phenotype intermediate between radial glia and astrocytes. *Glia*. Oct 2006;54(5):394-410. doi:10.1002/glia.20392

15. Garcia AD, Doan NB, Imura T, Bush TG, Sofroniew MV. GFAP-expressing progenitors are the principal source of constitutive neurogenesis in adult mouse forebrain. *Nat Neurosci*. Nov 2004;7(11):1233-41. doi:10.1038/nn1340

16. Boroviak T, Rashbass P. The apical polarity determinant Crumbs 2 is a novel regulator of ESC-derived neural progenitors. *Stem Cells*. Feb 2011;29(2):193-205. doi:10.1002/stem.567

17. Zhang XZ, Huo HQ, Zhu YQ, Feng HY, Jiao J, et al. Folic Acid Rescues Valproic Acid-Induced Morphogenesis Inhibition in Neural Rosettes Derived From Human Pluripotent Stem Cells. *Front Cell Neurosci*. 2022;16:888152. doi:10.3389/fncel.2022.888152

18. Fedorova V, Vanova T, Elrefae L, Pospisil J, Petrasova M, et al. Differentiation of neural rosettes from human pluripotent stem cells in vitro is sequentially regulated on a molecular level and accomplished by the mechanism reminiscent of secondary neurulation. *Stem Cell Res*. Oct 2019;40:101563. doi:10.1016/j.scr.2019.101563

19. Townshend RF, Shao Y, Wang S, Cortez CL, Esfahani SN, et al. Effect of Cell Spreading on Rosette Formation by Human Pluripotent Stem Cell-Derived Neural Progenitor Cells. *Front Cell Dev Biol*. 2020;8:588941. doi:10.3389/fcell.2020.588941

20. Hauser S, Erzler M, Theurer Y, Schuster S, Schule R, et al. Establishment of SPAST mutant induced pluripotent stem cells (iPSCs) from a hereditary spastic paraplegia (HSP) patient. *Stem Cell Res*. Nov 2016;17(3):485-488. doi:10.1016/j.scr.2016.09.022

6 Chapter 5: Discussion

6.1 Cell biological explanations for clinical phenotypes

Our study has identified a cluster of neuroanatomical signatures that may distinguish *DENND5A*-related DEE from other monogenic DEEs. **Table 5.1** summarizes 13 monogenic disorders mentioned throughout this thesis and compares the clinical similarities and differences between those disorders and *DENND5A*-related DEE. Differences between disorders are even more distinguishable by comparing the tissue expression of these genes and the effects on cellular processes when they are disrupted. **Table 5.2** lists the same genes as **Table 5.1** and compares their mRNA or protein expression on the tissue, cellular, and subcellular levels as well as their cell biological functions on key developmental processes that DENND5A is involved in. Interestingly, according to the Human Protein Atlas, DENND5A mRNA expression is detected ubiquitously in the adult brain with no obvious regions of enrichment that are consistent across datasets. DENND5A mRNA expression levels in specific brain regions have not yet been examined in the developing brain.

The monogenic DEE with the highest degree of similarity to *DENND5A*-related DEE is caused by *PCDH12* variants. *PCDH12* cases experience seizure onset within the same age range as *DENND5A* cases, exhibit very similar gray and white matter abnormalities, show brain calcifications in the same regions, and have microcephaly and non-hydrocephalic ventriculomegaly[1-5]. However, as mentioned previously, a key difference is that pachygyria is not observed in *PCDH12* cohorts. Additionally, microcephaly in *PCDH12* cases can be either primary (present at birth) or secondary (develops progressively) [1,3,4], whereas in *DENND5A* cases it is always primary. *PCDH12* patients also frequently exhibit comorbid ophthalmic abnormalities[2,6],

which are not observed in our *DENND5A* cohort. Although blindness is observed in 7 *DENND5A* cases, it is almost always associated with a cortical visual impairment, and therefore is likely due to a lack of visual perception rather than dysfunction of the eyes. We hypothesize that cortical visual impairment is a result of the predominantly occipital pachygyria.

Pathogenic *OCLN* variants also result in a DEE very similar to *DENND5A*-related DEE with some key differences. *OCLN* variants lead to a much more extensive calcification phenotype compared to *DENND5A*, which can be explained by the abundance of OCLN expression in blood vessels[7]. Compromised TJ integrity of blood vessel walls due to *OCLN* variants leads to increased permeability of the blood-brain barrier, and the resulting leakage is a primary cause of brain calcifications[8]. Additionally, polymicrogyria is a defining feature that always accompanies pathogenic *OCLN* variants[9-12], whereas it is never found in *DENND5A* cases. However, the presence of a pool of OCLN at the centrosomes during cell division and its depletion resulting in impaired chromosomal alignment and a loss of planar spindle orientation remains intriguing[13]. Indeed, we have shown that *DENND5A* KO results in the same abnormalities. Preliminary evidence from another lab member shows that a small pool of overexpressed DENND5A colocalizes with γ-tubulin at the centrosome. This begs the question of whether DENND5A regulates spindle orientation in a similar manner as OCLN. OCLN binds directly to NuMa[13], which under normal circumstances coordinates with dynein and plasma membrane-associated proteins to tightly align the mitotic spindle through pulling forces and tethering astral microtubules to the cell cortex[14-19]. DENND5A may also play a role in mitotic spindle assembly, as abnormal chromatin condensation was observed in many dividing *DENND5A* KO progenitors. However, the loss of planar spindle orientation in virtually all the remaining cells suggests a primary function in astral microtubule tethering.

Importantly, PALS1 deficiency also results in the loss of planar spindle orientation, but its relation to astral microtubules was not investigated[20]. Consistently, "microcephaly in *PALS1* conditional KO mice is due to neural progenitors prematurely exiting the cell cycle and undergoing asymmetric neurogenic cell divisions instead of symmetric proliferative divisions, resulting in the depletion of the progenitor pool and premature neuronal differentiation[21]." [22] Our discovery of the interaction between DENND5A and PALS1, one of the earliest-identified and most extensively studied apical polarity proteins[23], implies some degree of shared function. Mora-Bermúdez et al. showed that a decrease in the number of molecules that link astral microtubules to the apical cell cortex leads to a decrease in the number of apicobasal-specific astral microtubules, resulting in a weakened anchor between the spindle poles and the apical cell cortex and thus promoting an oblique or perpendicular spindle orientation[24]. We therefore hypothesize that DENND5A functions in this capacity; that the small pool of DENND5A at the centrosome radiates outward as apicobasal astral microtubules nucleate to link them with MUPP1/PALS1 at the apical cell cortex, promoting a planar spindle orientation. Future studies could quantify the number of astral microtubules in WT versus *DENND5A* KO dividing cells within rosettes. Ideally, identifying a specific antibody against endogenous DENND5A for use in immunocytochemistry would allow for direct observation of whether DENND5A tethers a subset of astral microtubules to the MUPP1/PALS1-positive apical plasma membrane. The transient existence of astral microtubules during the cell cycle, combined with how only a small pool of DENND5A exists at the centrosome, also provides an explanation for the weak conformation-dependent interaction observed between DENND5A and MUPP1/PALS1.

Symmetric planar divisions ensure not only that both daughter cells "remain in contact with the stem and progenitor cell biochemical niche found in the developing ventricle" [22], but also the

equal inheritance of apical determinants. The apical membrane of NPCs within neural rosettes is enriched in both cell junctional proteins as well as Golgi-associated proteins[25-27]. Because DENND5A is primarily a Golgi-localized protein[28] and the Golgi is confined to the apical process of apical progenitors in punctate stacks rather than a ribbon structure[29,30], one can speculate that "Golgi fragments containing DENND5A bound to PALS1/MUPP1 may thus ensure equal Golgi and AJ protein inheritance in both daughter cells of a dividing apical progenitor, affecting the resulting daughter cell fates."[22] Progenitor cells that detach from the apical ventricular surface lose their stem cell niche contact and more readily differentiate[31-33]. We have shown that apical progenitors lacking DENND5A not only divide away from the apical surface, but they also have an intrinsic propensity to exit the cell cycle and differentiate, another well-established pathological mechanism underlying primary microcephaly[34].

We have already discussed in detail that the essential role of DENND5A in symmetric cell division and maintenance of progenitor stemness contributes to the pathogenesis of microcephaly upon DENND5A loss of function. The posterior gradient of pachygyria identified in our cohort is a distinct feature, even among other structural DEEs with pachygyria, that suggests DENND5A functions very early in development, as the occipital lobe of the cortex is among the earliest to develop and mature[35,36]. Even in cases where a posterior gradient of pachygyria was not identified, cortical visual impairments and reduced optic nerve volumes were common, accounting for a combined 11 cases out of the 23 we examined. Because DENND5A is involved with symmetric, proliferative cell divisions, this suggests DENND5A function is most essential in neuroepithelia and apical radial glia. A role for DENND5A in NECs or apical radial glia carries enormous implications, as they are both the structural basis for neurogenesis as well as the progenitors that give rise to most of the postmitotic neurons and glia in the cortex. A reduced number of mitotic

neuroepithelial cell divisions leads to a reduced number of radial glia and neurons. Genetic counseling, then, should be provided for anyone that is a known carrier of a pathogenic variant, as opportunities to intervene after birth are limited even if the pathological mechanism for *DENND5A*-related DEE is completely elucidated.

Besides the significance of the posterior gradient of pachygyria, the presence of pachygyria itself is consistent with what is known about the cellular functions of DENND5A. Pachygyria and lissencephaly often arise due to abnormalities in cell migration during neurodevelopment[37]. Interestingly, *DENND5A* depletion results in increased cell migration[38]; as shown in **Table 5.2**, all other listed genetic causes of pachygyria/lissencephaly are due to reduced migration apart from *MUPP1*[39], encoding a binding partner to DENND5A. Enhanced migration of prematurely born neurons in the *DENND5A*-depleted developing brain could conceivably lead to both reduced brain volume and over-migration, manifesting as gyral simplification and a thin cortex. Classic lissencephaly due to variants in *LIS1* lead to a thickened cortex with gyral simplification[40-43], but cortical volume is reduced in volume in *DENND5A* patients. *LIS1* variants also cause reduced cell proliferation[44,45], but basal progenitors are disproportionately affected in this capacity[46]. The thick cortex in *LIS1* patients likely reflects how apical progenitors still have the opportunity to self-renew and proliferate, and migration deficits[47-49] and reduced differentiation[50,51] result in a disorganized cortex with an excessive number of cells. This contrasts with the apical progenitors of *DENND5A* patients, which preferentially divide asymmetrically and prematurely differentiate, resulting in a reduced overall number of neurons. Cell migration deficits in *DENND5A* cases, then, are probably not the primary cause of pachygyria but may contribute to cortex disorganization and seizures.

While our human cohort exhibited many overlapping phenotypes, another less common phenotype provides further evidence of abnormal apicobasal cell polarity. Participant 7 presented with periventricular gray matter heterotopias, which are accumulations of neurons in abnormal locations. Impaired AJs in radial glia causes their basal processes to retract, preventing neuronal migration and resulting in neuron aggregation near the ventricles[52]. Thus, defects in AJ assembly or maintenance in this patient may have resulted in the observed phenotype.

The distinction of DENND5A as a polarity-related protein is consistent with clinical observations published previously. Human cases with pathogenic variants in *CRB2* and *MUPP1* have been identified and exhibit ventriculomegaly and corpus callosum dysgenesis[53-57], and patients with *PALS1* variants show global developmental delay, microcephaly, and sometimes seizures[58]. Moreover, the phenotypes observed in our *DENND5A*-related DEE mouse model are consistent with those found in other mouse models targeting apical polarity proteins. *MUPP1* KO mice have enlarged lateral ventricles[59] and the cortex in *PALS1* conditional KO mice, where PALS1 was selectively depleted from cortical progenitors, fails to develop, thus leading to microcephaly[21].[22]

6.2 Role of DENND5A in membrane trafficking

As speculated above, DENND5A may be "involved in properly positioning centrosomes to align them parallel to the apical membrane during mitosis," [22] but its function likely does not end there. "The conformation-dependent [interaction between MUPP1/PALS1 and DENND5A at p.R710] may reflect a molecular mechanism to regulate the balance of symmetric versus asymmetric cell division during [development]"[22], but the weakness of this interaction and the predominance of the steady-state closed conformation suggests that the work done in this thesis represents a small proportion of the extent of the biological functions of DENND5A. An important

gap in our knowledge is the role of DENND5A in membrane trafficking, the primary focus of our laboratory. We somewhat arbitrarily chose to follow up on the MUPP1/PALS1 result among our numerous protein-protein interactions identified in our missense mutation-guided proteomic screens. Given that our lab specializes in membrane trafficking, for years we looked for evidence of DENND5A trafficking PALS1/MUPP1 throughout the cell. However, if anything we have provided evidence that DENND5A does *not* traffic PALS1/MUPP1. Apicobasal polarity appeared largely unaffected in multiple model systems: PALS1 still localized apically in *DENND5A* KD MDCK cysts, with larger PALS1 puncta concentrated at tight junctions (**Fig. S5.1a**). The distribution of MUPP1 puncta was less apically concentrated, but localization patterns did not appear to change upon *DENND5A* KD (**Fig. S5.1b**). Consistently, PALS1 still localized to the apical membrane in neural rosettes regardless of *DENND5A* depletion status (**Fig. 4.3a and Fig. S5.2**). In the context of the DENND5A/MUPP1/PALS1 interaction, it may be the case that the primary effect is one of cell division and protein inheritance, and that the trafficking of MUPP1/PALS1 to and from the apical membrane is mediated by other proteins independent of DENND5A. Perhaps if we had followed up on other novel protein-protein interactions identified in the proteomic screen we would have elucidated membrane trafficking pathways, but the cell division and differentiation phenotypes identified here enhance our understanding of the pathogenesis of microcephaly in *DENND5A*-related DEE, one of the defining clinical features of the disorder (**Fig. 2.1b**).

Regardless, it remains true that DENND5A contains a DENN domain that functions as a guanine nucleotide exchange factor and is associated with several Rab GTPases. DENND5A binds both GTP-Rab6 and GTP-Rab11[28,60,61]. GTP-bound Rab6 localizes DENND5A to Golgi membranes and, importantly, can bind DENND5A regardless of its conformation (**Fig. S3.1b**).

This may allow for transient conformational shifts during cell division to allow DENND5A to bind both PALS1/MUPP1 at the cell periphery and Rab6-positive Golgi-derived vesicles to ensure proper spindle orientation and Golgi inheritance. Indeed, although DENND5A has been crystallized with co-expression of the Rab6A isoform[62], Rab6C is a primate-specific and brain-enriched isoform uniquely localized to centrosomes that controls cell cycle progression[63]. Microcephaly may be a primate-specific phenotype upon DENND5A depletion, because overall brain volumes of our KI mice did not significantly differ from WT (**Fig. 2.3g**). Future studies investigating DENND5A during cell division should therefore examine Rab6C to gain a greater understanding of the role of DENND5A and spindle formation, stabilization, or dynamism.

RAB11 also seemed to be a promising interacting partner to study because it transports PALS1 to the apical membrane in zebrafish embryos[64], but no RAB11 and PALS1 colocalization was observed in both MDCK cysts and neural rosettes regardless of *DENND5A* depletion status (**Fig. S5.1a and Fig. S5.2**), indicating that DENND5A is not involved in the RAB11-dependent trafficking of PALS1 from the Golgi to the apical plasma membrane. While there was an apparent decrease in overall RAB11 expression in *DENND5A* KD MDCK cysts (**Fig. S5.1a**), RAB11 remained apically localized. No obvious changes in RAB11 staining were observed in the rosettes (**Fig. S5.2**).

DENND5A also interacts with SNX1, a component of the retromer complex which transports cargo from endosomes to the Golgi[65], via its C-terminal RUN domain[66,67]. A study in Drosophila discovered that CRB is recycled from the apical membrane to the Golgi via the retromer[68]. Although we did not assess CRB recycling directly due to difficulties finding a KO-validated antibody and because CRB overexpression leads to problems with apicobasal polarity[69], CRB and PALS1 are codependent and the localization/expression of one affects the

localization/expression of the other[21,64,70,71]. We thus interpret the lack of difference in PALS1 staining in both WT and *DENND5A* depleted MDCK cysts and neural rosettes to reflect no difference in apical CRB expression as well, negating the hypothesis that DENND5A mediates CRB recycling through the retromer.

Interestingly, we also have evidence from another lab member's work that DENND5A is a GEF for Rab8 and Rab10, both of which have functions in ciliogenesis[72,73], and that a small pool of overexpressed DENND5A localizes to the γ-tubulin-positive basal bodies of primary cilia. Primary cilia are microtubule-containing protrusions of the apical plasma membrane that directly contact the CSF in the developing ventricle and uptake growth factors and other signaling molecules to affect cell proliferation and stem cell maintenance. While DENND5A may not transport the Crb complex to or from the apical plasma membrane, it is possible that it mediates its transport or function within cilia and that we did not detect it, as CRB and PALS1 are also found at the basal bodies of primary cilia[74,75] and cilia are typically 1-10 μm long[76] and easy to overlook. Moreover, the presence of DENND5A at primary cilia is consistent with a centrosome positioning function during mitosis, as the short microtubules comprising cilia are nucleated from the centrosome and both primary cilia and centrosome positioning are important for proper neurodevelopment[77].

6.3 Chapter 5 Figures and Tables

6.3.1 Tables

Table 5.1

	GDD	Seizures (onset)	Microcephaly	Ventriculomegaly	Cerebellum	Cortex	White matter	Subcortical	Calcifications	Also causes:
DENND5A	Yes	Yes (birth - 12 months)	Yes	Yes – without hydrocephalus	Hypoplastic	Reduced volume, posterior gradient of pachygyria/lissencephaly	Thin/agenesis of CC, abnormal anterior/posterior internal capsule distinction, delayed myelination	Dysmorphic basal ganglia, basal ganglia/thalamic fusion, DMJ dysplasia, brainstem abnormalities	Periventricular, basal ganglia	Melanoma
CRB2	Yes	Yes	No	Yes – with or without hydrocephalus	Hypoplastic Asymmetric	Normal	Thin CC, optic nerve abnormalities	Periventricular gray matter heterotopias	None	Retinitis pigmentosa, renal disease
Pals1	Yes	Yes (4y to adulthood)	Mostly no – 1 case of microcephaly	No – 1 case of slightly enlarged subarachnoid spaces	Normal	Mild gyral simplification	Normal	Normal	None	
MUPP1	Yes	Yes	No	Yes – with hydrocephalus	Hypoplastic	Reduced volume, frontal lissencephaly	Thin CC	Sub-commissural organ hypoplasia	None	Hearing impairment, ophthalmic abnormalities
OCLN	Yes	Yes (birth - 4 months)	Yes	Yes – without hydrocephalus	Hypoplastic	Reduced volume, polymicrogyria, posterior gyral simplification	Thin CC	Abundant calcifications	Basal ganglia, thalamus, cerebellum, brainstem, deep cortical layers, white matter	Renal failure
DNM1	Yes	Yes (6 weeks-13 months, one case of 7y onset)	Yes - secondary	Rarely – without hydrocephalus	Normal	Generalized or frontal atrophy, widened perisylvian fissure	Occasionally CC agenesis or progressive diffuse white matter/CC volume loss	Normal	None	
LIS1 (PAFAH1B1)	Yes	Yes (birth-6y)	Sometimes	Yes – with or without hydrocephalus	Mildly hypoplastic (duplication variants)	Thick cortex, posterior gradient of pachygyria/lissencephaly (haploinsufficiency); mild volume loss (duplication variants)	Thin CC and white matter volume loss (duplication variants)	Mild brainstem hypoplasia (duplication variants)	Basal ganglia (rarely)	
PCDH12	Yes	Yes (birth-12 months)	Yes – primary or secondary	Yes – without hydrocephalus	Hypoplastic	Reduced volume, hippocampal sclerosis	Thin CC, delayed myelination	Dysmorphic basal ganglia, DMJ dysplasia, brain stem abnormalities	Supratentorial, thalamus, perithalamic, basal ganglia, periventricular	Vascular ophthalmic abnormalities
TUBA1A	Yes	Yes (birth-3y)	Yes	Yes – often including 4th ventricle	Hypoplastic, dysmorphic	Pachygyria/lissencephaly, polymicrogyria	Thin/agenesis of CC, abnormal internal capsule	Basal ganglia and hippocampal dysgenesis, mild brainstem abnormalities, gray matter heterotopia	None	Fetal akinesia deformation sequence, ophthalmic abnormalities
TUBB2A	Yes	Yes (birth-5y)	Yes	Yes – often asymmetric	Hypoplastic, dysmorphic	Variable dysgyria/polymicrogyria, particularly parietal and temporal regions; pachygyria	Thin CC, delayed myelination	Dysmorphic basal ganglia, mild brainstem hypoplasia	None	
TUBB2B	Yes	Yes (birth-11mo)	Yes – often secondary	Yes	Hypoplastic, dysmorphic, nodular heterotopias	Parieto-occipital dysgyria, posterior pachygyria, polymicrogyria	Thin/agenesis of CC, internal capsule dysgenesis	Dysmorphic/fused basal ganglia, brainstem hypoplasia, thick subcortical gray matter band	None	Uner Tan syndrome, fetal akinesia deformation sequence
TUBB3	Yes	Rarely	Yes – primary or secondary	Yes – without hydrocephalus, often asymmetric, sometimes also includes 3rd or 4th ventricle	Hypoplastic, often asymmetric	Frontal lobe asymmetry and/or dysgyria, polymicrogyria, thick cortex, abnormal rotation of hippocampi, hypoplastic/absent olfactory bulbs	Thick/thin/agenesis of CC, aberrant corticospinal tract trajectory, absent long segment of dorsal language network, internal capsule dysgenesis, delayed myelination	Periventricular frontal cysts, hypoplastic or hypertrophic basal ganglia, thalamic dysplasia, brainstem hypoplasia/dysplasia; all often asymmetric	None	Ophthalmic abnormalities, hearing loss, joint contractures, cyclic vomiting, axonal sensorimotor neuropathy, mirror movements, hypohidrosis
TUBG1	Yes	Yes (birth-4y)	Yes – primary or secondary	Yes – without hydrocephalus	Hypoplastic	Posterior gradient of pachygyria, lissencephaly	Thin CC	Reduced basal ganglia volume, rarely brainstem hypoplasia	None	

GDD = Global developmental delay

CC = Corpus callosum

AC = Anterior commissure

DMJ = Diencephalic-mesencephalic junction

Comparison of clinical phenotypes in monogenic DEEs. Sources: *DENND5A*[78,79], *CRB2*[53-55,80], *PALS1*[58,81], *MUPP1*[56,57,82-84], *OCLN*[9-12], *DNM1*[85-87], *LIS1*[40-43,88-91], *PCDH12*[1-6], *TUBA1A*[92-98], *TUBB2A*[99,100], *TUBB2B*[97,98,101-109], *TUBB3*[98,110-132], *TUBG1*[133-135].

Table 5.2

	Highest Expression			Effect on phenotype after KO/KD/mutation				
	Tissue	**Cell Type**	**Subcellular localization**	**Neurite outgrowth**	**Differentiation**	**Cell proliferation**	**Mitotic spindle**	**Cell migration**
DENND5A	Brain (especially embryonic)	NPCs	Golgi	Increased	Premature differentiation	Reduced	Loss of planar orientation	Increased
CRB2	Eye, brain (especially cortex and hypothalamus), kidney	Retinal pigment epithelial cells, NPCs, neurons	Plasma membrane (TJs), cytoplasm (Rab8, VPS35 + vesicles), presynaptic terminals	Unknown	Essential for NPC survival: mouse ESCs die during neural induction; triggers epithelial-mesenchymal transition in retinal pigment epithelial cells	Increased (CRB1/2 double cKO in retina)	Unknown	Unknown
PALS1	Ubiquitous	No direct experimental comparisons	Plasma membrane (TJs and AJs)	Unknown	Premature differentiation	Reduced	Loss of planar orientation	Unaffected
MUPP1	Brain (especially choroid plexus and cortex), lung, kidney	Choroid plexus epithelial cells, neurons, ependymal cells	Plasma membrane (TJs), dendritic postsynaptic terminals	Unknown, but CASPR2/MUPP1/GPR37 complex unable to assemble in dendrites when ASD variant introduced in GPR37, resulting in reduced dendrite outgrowth	Unknown, but KD impairs Notch signaling in endothelial cells through failure to recruit ligand to AJs	Increased	Unknown	Increased
OCLN	Lung, intestines, brain (embryonic: neural tube, blood vessels, choroid plexus; adult: blood vessels and choroid plexus)	Epithelial and endothelial cells	Plasma membrane (TJs) and centrosomes	Unknown	Premature differentiation	Reduced	Loss of planar orientation, impaired spindle formation	Reduced
DNM1	Brain (expression levels of DNM1a doubled compared to DNM1b in pediatric brains)	Neurons	DNM1a: colocalizes with tubulin and plasma membrane-associated clathrin DNM1b: colocalizes with tubulin and Golgi-associated clathrin	Reduced	Unknown	Reduced due to cytokinesis failures and subsequent apoptosis	Unaffected; tetrapolar spindle formation after previous cytokinesis failure in surviving cells	Unknown
LIS1	Brain, liver, intestine	NPCs, neurons	Cytoplasmic	Reduced	Premature differentiation (hematopoietic stem cells), reduced differentiation (adult hippocampus, spermatids, osteoclasts)	Reduced, especially in basal progenitors	Reduced planar orientation	Reduced
PCDH12	Placenta, lung, heart	Vasculogenic endothelial cells	Plasma membrane (diffuse)	Reduced	Premature differentiation	Reduced	Unknown	Reduced
TUBA1A	Brain (especially embryonic), spinal cord, intestine	NPCs, neurons	Cytoplasmic	Increased branching, reduced retraction and regeneration	Conflicting evidence – premature neuronal differentiation from adult SVZ to olfactory bulb; no difference in dentate gyrus	Unaffected	Unknown	Randomized direction
TUBB2A	Brain	No direct experimental comparisons	Cytoplasmic	Unknown	Unknown	Increased	Impaired spindle formation	Reduced
TUBB2B	Thymus, brain (especially embryonic), cochlea	NPCs, embryonic post-mitotic neurons, adult macroglia, hair cells	Cytoplasmic	Unknown	Reduced differentiation	Increased, especially in basal progenitors; but also increased cell death	Spindle misorientation (in yeast)	Reduced
TUBB3	Brain, small intestine, testis	Neurons	Cytoplasmic	Reduced	Reduced differentiation	Reduced, especially in intermediate/basal progenitors	Increased length of astral microtubules with missense mutations	Reduced
TUBG1	Liver, brain, heart		Centrosomes	Reduced	Unaffected	Unaffected	Impaired spindle formation	Reduced

NPC = Neural progenitor cell
TJ = Tight junction
AJ = Adherens junction
ESC = Embryonic stem cell
KO = Knockout
KD = Knockdown
cKO = conditional knockout

Comparison of cellular phenotypes upon mutation of monogenic DEE genes. Sources: DENND5A[28,38,79], CRB2[27,80,136-139], PALS1[20,21,70,140], MUPP1[39,141-144], OCLN[7,13,145-149], DNM1[150-155], LIS1[44-51,156-159], PCDH12[4,160,161], TUBA1A[162-167], TUBB2A[168-171], TUBB2B[106,172-174], TUBB3[120,170,175-179], TUBG1[180-182].

6.3.2 Supplementary Figures

Figure S5.1

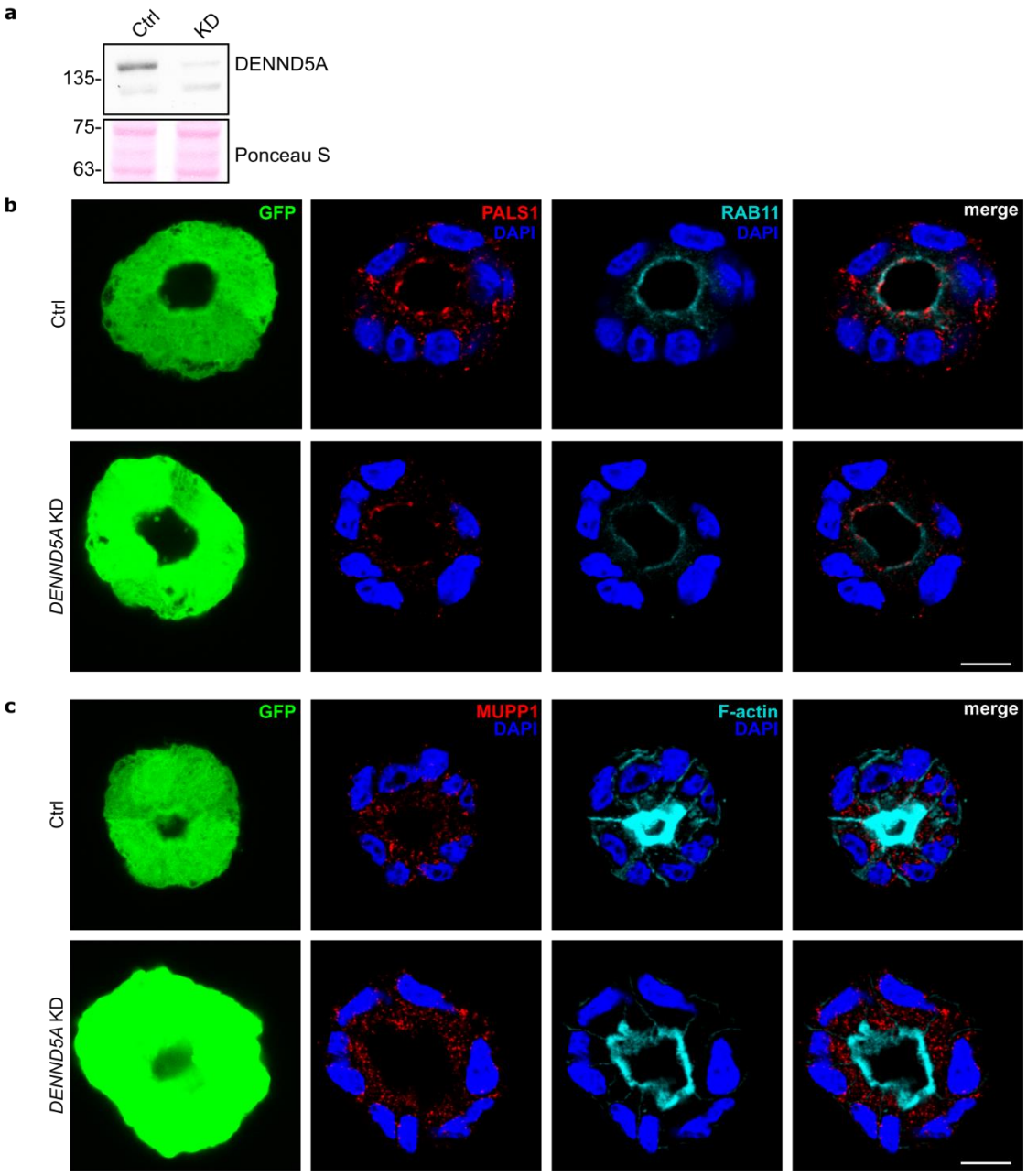

Figure S5.1: *DENND5A* KD does not result in obvious differences in PALS1/MUPP1 localization in MDCK cysts. a, Immunoblotting confirms successful lentiviral knockdown of DENND5A in MDCK cells. **b,** PALS1, RAB11 and **c,** MUPP1 distribution, visualized via immunostaining, appears largely unaffected upon *DENND5A* KD in MDCK cysts. GFP channel confirms successful transduction of GFP-tagged control or *DENND5A* KD lentivirus. Scale bar = 10 μm.

Figure S5.2

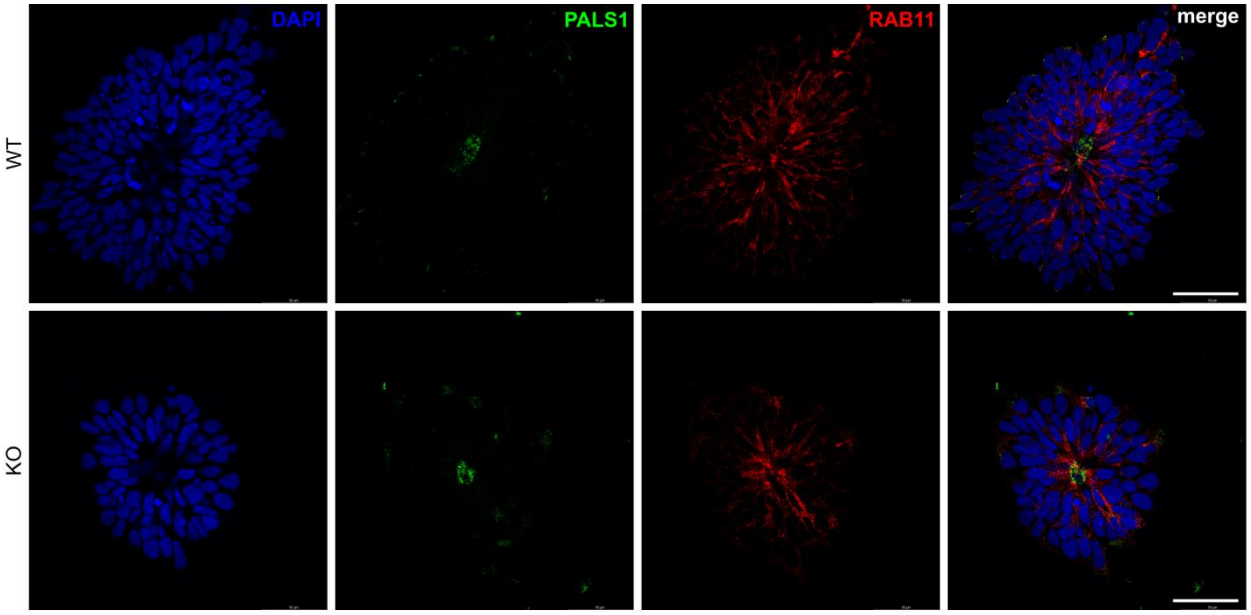

Figure S5.2: PALS1 and RAB11 expression patterns appear similar in WT and *DENND5A* KO neural rosettes. Scale bar = 50 μm.

6.4 References

1. Aran A, Rosenfeld N, Jaron R, Renbaum P, Zuckerman S, et al. Loss of function of PCDH12 underlies recessive microcephaly mimicking intrauterine infection. *Neurology*. May 24 2016;86(21):2016-24. doi:10.1212/WNL.0000000000002704

2. Accogli A, El Kosseifi C, Saint-Martin C, Addour-Boudrahem N, Riviere JB, et al. PCDH12 variants are associated with basal ganglia anomalies and exudative vitreoretinopathy. *Eur J Med Genet*. Feb 2022;65(2):104405. doi:10.1016/j.ejmg.2021.104405

3. Fazeli W, Bamborschke D, Moawia A, Bakhtiari S, Tafakhori A, et al. The phenotypic spectrum of PCDH12 associated disorders - Five new cases and review of the literature. *Eur J Paediatr Neurol*. Jan 2022;36:7-13. doi:10.1016/j.ejpn.2021.10.011

4. Guemez-Gamboa A, Caglayan AO, Stanley V, Gregor A, Zaki MS, et al. Loss of Protocadherin-12 Leads to Diencephalic-Mesencephalic Junction Dysplasia Syndrome. *Ann Neurol*. Nov 2018;84(5):638-647. doi:10.1002/ana.25327

5. Nicolas G, Sanchez-Contreras M, Ramos EM, Lemos RR, Ferreira J, et al. Brain calcifications and PCDH12 variants. *Neurol Genet*. Aug 2017;3(4):e166. doi:10.1212/NXG.0000000000000166

6. Youn EY, Parra V, Qian CX. Asynchronous presentation and evolution of homozygous PCDH12 variant-induced exudative retinopathy in two siblings. *Can J Ophthalmol*. Aug 1 2023;doi:10.1016/j.jcjo.2023.07.003

7. Virgintino D, Errede M, Robertson D, Capobianco C, Girolamo F, et al. Immunolocalization of tight junction proteins in the adult and developing human brain. *Histochem Cell Biol*. Jul 2004;122(1):51-9. doi:10.1007/s00418-004-0665-1

8. Monfrini E, Arienti F, Rinchetti P, Lotti F, Riboldi GM. Brain Calcifications: Genetic, Molecular, and Clinical Aspects. *Int J Mol Sci*. May 19 2023;24(10)doi:10.3390/ijms24108995

9. O'Driscoll MC, Daly SB, Urquhart JE, Black GC, Pilz DT, et al. Recessive mutations in the gene encoding the tight junction protein occludin cause band-like calcification with simplified gyration and polymicrogyria. *Am J Hum Genet*. Sep 10 2010;87(3):354-64. doi:10.1016/j.ajhg.2010.07.012

10. Abdel-Hamid MS, Abdel-Salam GMH, Issa MY, Emam BA, Zaki MS. Band-like calcification with simplified gyration and polymicrogyria: report of 10 new families and identification of five novel OCLN mutations. *J Hum Genet*. Apr 2017;62(5):553-559. doi:10.1038/jhg.2017.4

11. Oner TO, Unalp A, Hiz S, Bayram E, Kaytan I, et al. OCLN gene variants identified in three patients with severe neurodevelopmental disorder associated with epilepsy, intellectual

disability and malformation of cortical development. *Epileptic Disord*. Dec 1 2021;23(6):843-853. doi:10.1684/epd.2021.1349

12. Ekinci F, Yildizdas RD, Horoz OO, Herguner O, Bisgin A. A homozygote frameshift mutation in OCLN gene result in Pseudo-TORCH syndrome type I: A case report extending the phenotype with central diabetes insipidus and renal dysfunction. *Eur J Med Genet*. Jun 2020;63(6):103923. doi:10.1016/j.ejmg.2020.103923

13. Bendriem RM, Singh S, Aleem AA, Antonetti DA, Ross ME. Tight junction protein occludin regulates progenitor Self-Renewal and survival in developing cortex. *Elife*. Dec 3 2019;8doi:10.7554/eLife.49376

14. Gloerich M, Bianchini JM, Siemers KA, Cohen DJ, Nelson WJ. Cell division orientation is coupled to cell-cell adhesion by the E-cadherin/LGN complex. *Nat Commun*. Jan 3 2017;8:13996. doi:10.1038/ncomms13996

15. Peyre E, Jaouen F, Saadaoui M, Haren L, Merdes A, et al. A lateral belt of cortical LGN and NuMA guides mitotic spindle movements and planar division in neuroepithelial cells. *J Cell Biol*. Apr 4 2011;193(1):141-54. doi:10.1083/jcb.201101039

16. Zheng Z, Zhu H, Wan Q, Liu J, Xiao Z, et al. LGN regulates mitotic spindle orientation during epithelial morphogenesis. *J Cell Biol*. Apr 19 2010;189(2):275-88. doi:10.1083/jcb.200910021

17. Konno D, Shioi G, Shitamukai A, Mori A, Kiyonari H, et al. Neuroepithelial progenitors undergo LGN-dependent planar divisions to maintain self-renewability during mammalian neurogenesis. *Nat Cell Biol*. Jan 2008;10(1):93-101. doi:10.1038/ncb1673

18. Du Q, Taylor L, Compton DA, Macara IG. LGN blocks the ability of NuMA to bind and stabilize microtubules. A mechanism for mitotic spindle assembly regulation. *Curr Biol*. Nov 19 2002;12(22):1928-33. doi:10.1016/s0960-9822(02)01298-8

19. Woodruff JB, Drubin DG, Barnes G. Dynein-driven mitotic spindle positioning restricted to anaphase by She1p inhibition of dynactin recruitment. *Mol Biol Cell*. Jul 2009;20(13):3003-11. doi:10.1091/mbc.e09-03-0186

20. Yamaguchi M, Imai F, Tonou-Fujimori N, Masai I. Mutations in N-cadherin and a Stardust homolog, Nagie oko, affect cell-cycle exit in zebrafish retina. *Mech Dev*. May-Jun 2010;127(5-6):247-64. doi:10.1016/j.mod.2010.03.004

21. Kim S, Lehtinen MK, Sessa A, Zappaterra MW, Cho SH, et al. The apical complex couples cell fate and cell survival to cerebral cortical development. *Neuron*. Apr 15 2010;66(1):69-84. doi:10.1016/j.neuron.2010.03.019

22. Banks E, Francis V, Lin S-J, Kharfallah F, Fonov V, et al. Loss of symmetric cell division of apical neural progenitors drives *DENND5A*-related developmental and epileptic

encephalopathy. *medRxiv*. 2023-01-01 00:00:00 2023;doi:https://doi.org/10.1101/2022.08.23.22278845

23. Assemat E, Bazellieres E, Pallesi-Pocachard E, Le Bivic A, Massey-Harroche D. Polarity complex proteins. *Biochim Biophys Acta*. Mar 2008;1778(3):614-30. doi:10.1016/j.bbamem.2007.08.029

24. Mora-Bermudez F, Matsuzaki F, Huttner WB. Specific polar subpopulations of astral microtubules control spindle orientation and symmetric neural stem cell division. *Elife*. Jul 4 2014;3doi:10.7554/eLife.02875

25. Dreser N, Madjar K, Holzer AK, Kapitza M, Scholz C, et al. Development of a neural rosette formation assay (RoFA) to identify neurodevelopmental toxicants and to characterize their transcriptome disturbances. *Arch Toxicol*. Jan 2020;94(1):151-171. doi:10.1007/s00204-019-02612-5

26. Fedorova V, Vanova T, Elrefae L, Pospisil J, Petrasova M, et al. Differentiation of neural rosettes from human pluripotent stem cells in vitro is sequentially regulated on a molecular level and accomplished by the mechanism reminiscent of secondary neurulation. *Stem Cell Res*. Oct 2019;40:101563. doi:10.1016/j.scr.2019.101563

27. Boroviak T, Rashbass P. The apical polarity determinant Crumbs 2 is a novel regulator of ESC-derived neural progenitors. *Stem Cells*. Feb 2011;29(2):193-205. doi:10.1002/stem.567

28. Miserey-Lenkei S, Waharte F, Boulet A, Cuif MH, Tenza D, et al. Rab6-interacting protein 1 links Rab6 and Rab11 function. *Traffic*. Oct 2007;8(10):1385-403. doi:10.1111/j.1600-0854.2007.00612.x

29. Taverna E, Huttner WB. The Golgi Apparatus in Polarized Neuroepithelial Stem Cells and Their Progeny: Canonical and Noncanonical Features. *Results Probl Cell Differ*. 2019;67:359-375. doi:10.1007/978-3-030-23173-6_15

30. Taverna E, Mora-Bermudez F, Strzyz PJ, Florio M, Icha J, et al. Non-canonical features of the Golgi apparatus in bipolar epithelial neural stem cells. *Sci Rep*. Feb 16 2016;6:21206. doi:10.1038/srep21206

31. Miyamoto Y, Sakane F, Hashimoto K. N-cadherin-based adherens junction regulates the maintenance, proliferation, and differentiation of neural progenitor cells during development. *Cell Adh Migr*. 2015;9(3):183-92. doi:10.1080/19336918.2015.1005466

32. Hatakeyama J, Wakamatsu Y, Nagafuchi A, Kageyama R, Shigemoto R, et al. Cadherin-based adhesions in the apical endfoot are required for active Notch signaling to control neurogenesis in vertebrates. *Development*. Apr 2014;141(8):1671-82. doi:10.1242/dev.102988

33. Loulier K, Lathia JD, Marthiens V, Relucio J, Mughal MR, et al. beta1 integrin maintains integrity of the embryonic neocortical stem cell niche. *PLoS Biol*. Aug 2009;7(8):e1000176. doi:10.1371/journal.pbio.1000176

34. Jean F, Stuart A, Tarailo-Graovac M. Dissecting the Genetic and Etiological Causes of Primary Microcephaly. *Front Neurol*. 2020;11:570830. doi:10.3389/fneur.2020.570830

35. Napolitano R, Molloholli M, Donadono V, Ohuma EO, Wanyonyi SZ, et al. International standards for fetal brain structures based on serial ultrasound measurements from Fetal Growth Longitudinal Study of INTERGROWTH-21(st) Project. *Ultrasound Obstet Gynecol*. Sep 2020;56(3):359-370. doi:10.1002/uog.21990

36. Gogtay N, Giedd JN, Lusk L, Hayashi KM, Greenstein D, et al. Dynamic mapping of human cortical development during childhood through early adulthood. *Proc Natl Acad Sci U S A*. May 25 2004;101(21):8174-9. doi:10.1073/pnas.0402680101

37. Dobyns WB, Truwit CL. Lissencephaly and other malformations of cortical development: 1995 update. *Neuropediatrics*. Jun 1995;26(3):132-47. doi:10.1055/s-2007-979744

38. Li Y, Xu J, Xiong H, Ma Z, Wang Z, et al. Cancer driver candidate genes AVL9, DENND5A and NUPL1 contribute to MDCK cystogenesis. *Oncoscience*. 2014;1(12):854-865. doi:10.18632/oncoscience.107

39. Liu W, Huang Y, Wang D, Han F, Chen H, et al. MPDZ as a novel epigenetic silenced tumor suppressor inhibits growth and progression of lung cancer through the Hippo-YAP pathway. *Oncogene*. Jul 2021;40(26):4468-4485. doi:10.1038/s41388-021-01857-8

40. Kolbjer S, Martin DA, Pettersson M, Dahlin M, Anderlid BM. Lissencephaly in an epilepsy cohort: Molecular, radiological and clinical aspects. *Eur J Paediatr Neurol*. Jan 2021;30:71-81. doi:10.1016/j.ejpn.2020.12.011

41. Classen S, Goecke T, Drechsler M, Betz B, Nickel N, et al. A novel inverted 17p13.3 microduplication disrupting PAFAH1B1 (LIS1) in a girl with syndromic lissencephaly. *Am J Med Genet A*. Jun 2013;161A(6):1453-8. doi:10.1002/ajmg.a.35904

42. Millar DS, Tysoe C, Lazarou LP, Pilz DT, Mohammed S, et al. An isolated case of lissencephaly caused by the insertion of a mitochondrial genome-derived DNA sequence into the 5' untranslated region of the PAFAH1B1 (LIS1) gene. *Hum Genomics*. Aug 2010;4(6):384-93. doi:10.1186/1479-7364-4-6-384

43. Liu X, Shen Q, Zheng G, Guo H, Lu X, et al. Gene and Phenotype Expansion of Unexplained Early Infantile Epileptic Encephalopathy. *Front Neurol*. 2021;12:633637. doi:10.3389/fneur.2021.633637

44. Liu Z, Steward R, Luo L. Drosophila Lis1 is required for neuroblast proliferation, dendritic elaboration and axonal transport. *Nat Cell Biol*. Nov 2000;2(11):776-83. doi:10.1038/35041011

45. Zimdahl B, Ito T, Blevins A, Bajaj J, Konuma T, et al. Lis1 regulates asymmetric division in hematopoietic stem cells and in leukemia. *Nat Genet*. Mar 2014;46(3):245-52. doi:10.1038/ng.2889

46. Penisson M, Jin M, Wang S, Hirotsune S, Francis F, et al. Lis1 mutation prevents basal radial glia-like cell production in the mouse. *Hum Mol Genet*. Mar 21 2022;31(6):942-957. doi:10.1093/hmg/ddab295

47. Moore KD, Chen R, Cilluffo M, Golden JA, Phelps PE. Lis1 reduction causes tangential migratory errors in mouse spinal cord. *J Comp Neurol*. Apr 15 2012;520(6):1198-211. doi:10.1002/cne.22768

48. Reiner O, Albrecht U, Gordon M, Chianese KA, Wong C, et al. Lissencephaly gene (LIS1) expression in the CNS suggests a role in neuronal migration. *J Neurosci*. May 1995;15(5 Pt 2):3730-8. doi:10.1523/JNEUROSCI.15-05-03730.1995

49. Jheng GW, Hur SS, Chang CM, Wu CC, Cheng JS, et al. Lis1 dysfunction leads to traction force reduction and cytoskeletal disorganization during cell migration. *Biochem Biophys Res Commun*. Mar 11 2018;497(3):869-875. doi:10.1016/j.bbrc.2018.02.151

50. Nayernia K, Vauti F, Meinhardt A, Cadenas C, Schweyer S, et al. Inactivation of a testis-specific Lis1 transcript in mice prevents spermatid differentiation and causes male infertility. *J Biol Chem*. Nov 28 2003;278(48):48377-85. doi:10.1074/jbc.M309583200

51. Wang Y, Baraban SC. Granule cell dispersion and aberrant neurogenesis in the adult hippocampus of an LIS1 mutant mouse. *Dev Neurosci*. 2007;29(1-2):91-8. doi:10.1159/000096214

52. Veeraval L, O'Leary CJ, Cooper HM. Adherens Junctions: Guardians of Cortical Development. *Front Cell Dev Biol*. 2020;8:6. doi:10.3389/fcell.2020.00006

53. Tessier A, Roux N, Boutaud L, Lunel E, Hakkakian L, et al. Bi-allelic variations in CRB2, encoding the crumbs cell polarity complex component 2, lead to non-communicating hydrocephalus due to atresia of the aqueduct of sylvius and central canal of the medulla. *Acta Neuropathol Commun*. Feb 20 2023;11(1):29. doi:10.1186/s40478-023-01519-8

54. Lamont RE, Tan WH, Innes AM, Parboosingh JS, Schneidman-Duhovny D, et al. Expansion of phenotype and genotypic data in CRB2-related syndrome. *Eur J Hum Genet*. Oct 2016;24(10):1436-44. doi:10.1038/ejhg.2016.24

55. Slavotinek A, Kaylor J, Pierce H, Cahr M, DeWard SJ, et al. CRB2 mutations produce a phenotype resembling congenital nephrosis, Finnish type, with cerebral ventriculomegaly and

raised alpha-fetoprotein. *Am J Hum Genet*. Jan 8 2015;96(1):162-9. doi:10.1016/j.ajhg.2014.11.013

56. Al-Dosari MS, Al-Owain M, Tulbah M, Kurdi W, Adly N, et al. Mutation in MPDZ causes severe congenital hydrocephalus. *J Med Genet*. Jan 2013;50(1):54-8. doi:10.1136/jmedgenet-2012-101294

57. Saugier-Veber P, Marguet F, Lecoquierre F, Adle-Biassette H, Guimiot F, et al. Hydrocephalus due to multiple ependymal malformations is caused by mutations in the MPDZ gene. *Acta Neuropathol Commun*. May 1 2017;5(1):36. doi:10.1186/s40478-017-0438-4

58. Sterling N, Duncan AR, Park R, Koolen DA, Shi J, et al. De novo variants in MPP5 cause global developmental delay and behavioral changes. *Hum Mol Genet*. Dec 18 2020;29(20):3388-3401. doi:10.1093/hmg/ddaa224

59. Yang J, Simonneau C, Kilker R, Oakley L, Byrne MD, et al. Murine MPDZ-linked hydrocephalus is caused by hyperpermeability of the choroid plexus. *EMBO Mol Med*. Jan 2019;11(1)doi:10.15252/emmm.201809540

60. Recacha R, Boulet A, Jollivet F, Monier S, Houdusse A, et al. Structural basis for recruitment of Rab6-interacting protein 1 to Golgi via a RUN domain. *Structure*. Jan 14 2009;17(1):21-30. doi:10.1016/j.str.2008.10.014

61. Janoueix-Lerosey I, Jollivet F, Camonis J, Marche PN, Goud B. Two-hybrid system screen with the small GTP-binding protein Rab6. Identification of a novel mouse GDP dissociation inhibitor isoform and two other potential partners of Rab6. *J Biol Chem*. Jun 16 1995;270(24):14801-8. doi:10.1074/jbc.270.24.14801

62. Fernandes H, Franklin E, Khan AR. Crystallization of an engineered RUN domain of Rab6-interacting protein 1/DENND5. *Acta Crystallogr Sect F Struct Biol Cryst Commun*. May 1 2011;67(Pt 5):556-60. doi:10.1107/S174430911100724X

63. Young J, Menetrey J, Goud B. RAB6C is a retrogene that encodes a centrosomal protein involved in cell cycle progression. *J Mol Biol*. Mar 19 2010;397(1):69-88. doi:10.1016/j.jmb.2010.01.009

64. Hao Y, Zhou Y, Yu Y, Zheng M, Weng K, et al. Interplay of MPP5a with Rab11 synergistically builds epithelial apical polarity and zonula adherens. *Development*. Nov 19 2020;147(22)doi:10.1242/dev.184457

65. Bonifacino JS, Hurley JH. Retromer. *Curr Opin Cell Biol*. Aug 2008;20(4):427-36. doi:10.1016/j.ceb.2008.03.009

66. Fernandes H, Franklin E, Jollivet F, Bliedtner K, Khan AR. Mapping the interactions between a RUN domain from DENND5/Rab6IP1 and sorting nexin 1. *PLoS One*. 2012;7(4):e35637. doi:10.1371/journal.pone.0035637

67. Wassmer T, Attar N, Harterink M, van Weering JR, Traer CJ, et al. The retromer coat complex coordinates endosomal sorting and dynein-mediated transport, with carrier recognition by the trans-Golgi network. *Dev Cell*. Jul 2009;17(1):110-22. doi:10.1016/j.devcel.2009.04.016

68. Zhou B, Wu Y, Lin X. Retromer regulates apical-basal polarity through recycling Crumbs. *Dev Biol*. Dec 1 2011;360(1):87-95. doi:10.1016/j.ydbio.2011.09.009

69. Roh MH, Fan S, Liu CJ, Margolis B. The Crumbs3-Pals1 complex participates in the establishment of polarity in mammalian epithelial cells. *J Cell Sci*. Jul 15 2003;116(Pt 14):2895-906. doi:10.1242/jcs.00500

70. Park JY, Hughes LJ, Moon UY, Park R, Kim SB, et al. The apical complex protein Pals1 is required to maintain cerebellar progenitor cells in a proliferative state. *Development*. Jan 1 2016;143(1):133-46. doi:10.1242/dev.124180

71. Paniagua AE, Segurado A, Dolon JF, Esteve-Rudd J, Velasco A, et al. Key Role for CRB2 in the Maintenance of Apicobasal Polarity in Retinal Pigment Epithelial Cells. *Front Cell Dev Biol*. 2021;9:701853. doi:10.3389/fcell.2021.701853

72. Zhang B, Zhang T, Wang G, Wang G, Chi W, et al. GSK3beta-Dzip1-Rab8 cascade regulates ciliogenesis after mitosis. *PLoS Biol*. Apr 2015;13(4):e1002129. doi:10.1371/journal.pbio.1002129

73. Sato T, Iwano T, Kunii M, Matsuda S, Mizuguchi R, et al. Rab8a and Rab8b are essential for several apical transport pathways but insufficient for ciliogenesis. *J Cell Sci*. Jan 15 2014;127(Pt 2):422-31. doi:10.1242/jcs.136903

74. Omori Y, Malicki J. oko meduzy and related crumbs genes are determinants of apical cell features in the vertebrate embryo. *Curr Biol*. May 23 2006;16(10):945-57. doi:10.1016/j.cub.2006.03.058

75. Morthorst SK, Nielsen C, Farinelli P, Anvarian Z, Rasmussen CBR, et al. Angiomotin isoform 2 promotes binding of PALS1 to KIF13B at primary cilia and regulates ciliary length and signaling. *J Cell Sci*. Jun 15 2022;135(12)doi:10.1242/jcs.259471

76. Nishimura Y, Yamakawa D, Uchida K, Shiromizu T, Watanabe M, et al. Primary cilia and lipid raft dynamics. *Open Biol*. Aug 2021;11(8):210130. doi:10.1098/rsob.210130

77. Rao S, Ge S, Shelly M. Centrosome positioning and primary cilia assembly orchestrate neuronal development. *Frontiers in Biology : Selected Publications from Chinese Universities*. 2012;7(5):412-427. doi:10.1007/s11515-012-1231-1

78. Yang M, Johnsson P, Brautigam L, Yang XR, Thrane K, et al. Novel loss-of-function variant in DENND5A impedes melanosomal cargo transport and predisposes to familial cutaneous melanoma. *Genet Med*. Jan 2022;24(1):157-169. doi:10.1016/j.gim.2021.09.003

79. Han C, Alkhater R, Froukh T, Minassian AG, Galati M, et al. Epileptic Encephalopathy Caused by Mutations in the Guanine Nucleotide Exchange Factor DENND5A. *Am J Hum Genet*. Dec 1 2016;99(6):1359-1367. doi:10.1016/j.ajhg.2016.10.006

80. Chen X, Jiang C, Yang D, Sun R, Wang M, et al. CRB2 mutation causes autosomal recessive retinitis pigmentosa. *Exp Eye Res*. Mar 2019;180:164-173. doi:10.1016/j.exer.2018.12.018

81. Zanotta N, Panzeri E, Minghetti S, Citterio A, Giorda R, et al. A case of a childhood onset developmental encephalopathy with a novel de novo truncating variant in the Membrane Protein Palmitoylated 5 (MPP5) gene. *Seizure*. Jan 23 2023;doi:10.1016/j.seizure.2023.01.015

82. Harripaul R, Vasli N, Mikhailov A, Rafiq MA, Mittal K, et al. Mapping autosomal recessive intellectual disability: combined microarray and exome sequencing identifies 26 novel candidate genes in 192 consanguineous families. *Mol Psychiatry*. Apr 2018;23(4):973-984. doi:10.1038/mp.2017.60

83. Bharadwaj T, Schrauwen I, Rehman S, Liaqat K, Acharya A, et al. ADAMTS1, MPDZ, MVD, and SEZ6: candidate genes for autosomal recessive nonsyndromic hearing impairment. *Eur J Hum Genet*. Jan 2022;30(1):22-33. doi:10.1038/s41431-021-00913-x

84. Iyengar R, Deardorff M, Schmidt R, Nagiel A. Retinal manifestations in autosomal recessive MPDZ maculopathy: report of two cases and literature review. *Ophthalmic Genet*. Jan 3 2023:1-5. doi:10.1080/13816810.2022.2161580

85. Harms FL, Weiss D, Lisfeld J, Alawi M, Kutsche K. A deep intronic variant in DNM1 in a patient with developmental and epileptic encephalopathy creates a splice acceptor site and affects only transcript variants including exon 10a. *Neurogenetics*. Jul 2023;24(3):171-180. doi:10.1007/s10048-023-00716-w

86. Nakashima M, Kouga T, Lourenco CM, Shiina M, Goto T, et al. De novo DNM1 mutations in two cases of epileptic encephalopathy. *Epilepsia*. Jan 2016;57(1):e18-23. doi:10.1111/epi.13257

87. Yigit G, Sheffer R, Daana M, Li Y, Kaygusuz E, et al. Loss-of-function variants in DNM1 cause a specific form of developmental and epileptic encephalopathy only in biallelic state. *J Med Genet*. Jun 2022;59(6):549-553. doi:10.1136/jmedgenet-2021-107769

88. Zhang YL, Jing XY, Zhen L, Pan M, Han J, et al. Prenatal diagnosis of Miller-Dieker syndrome/PAFAH1B1-related lissencephaly: Ultrasonography and genetically investigative results. *Eur J Obstet Gynecol Reprod Biol*. Jul 2022;274:28-32. doi:10.1016/j.ejogrb.2022.04.025

89. Shi CH, Zhang S, Yang ZH, Liu YT, Li YS, et al. Identification of a novel PAFAH1B1 missense mutation as a cause of mild lissencephaly with basal ganglia calcification. *Brain Dev*. Jan 2019;41(1):29-35. doi:10.1016/j.braindev.2018.07.009

90. Simoes C, Grana M, Rodriguez S, Baltar Yanes F, Tapie A, et al. Novel frameshift mutation in LIS1 gene is a probable cause of lissencephaly: a case report. *BMC Pediatr*. Sep 14 2022;22(1):545. doi:10.1186/s12887-022-03595-6

91. Lockrow JP, Holden KR, Dwivedi A, Matheus MG, Lyons MJ. LIS1 duplication: expanding the phenotype. *J Child Neurol*. Jun 2012;27(6):791-5. doi:10.1177/0883073811425972

92. Hebebrand M, Huffmeier U, Trollmann R, Hehr U, Uebe S, et al. The mutational and phenotypic spectrum of TUBA1A-associated tubulinopathy. *Orphanet J Rare Dis*. Feb 11 2019;14(1):38. doi:10.1186/s13023-019-1020-x

93. Gardner JF, Cushion TD, Niotakis G, Olson HE, Grant PE, et al. Clinical and Functional Characterization of the Recurrent TUBA1A p.(Arg2His) Mutation. *Brain Sci*. Aug 7 2018;8(8)doi:10.3390/brainsci8080145

94. Weber M, Jaber D, Encha-Razavi F, Julien E, Grevoul-Fesquet J, et al. Broadening the phenotypic spectrum of TUBA1A tubulinopathy to syndromic arthrogryposis multiplex congenita. *Am J Med Genet A*. Aug 2022;188(8):2331-2338. doi:10.1002/ajmg.a.62866

95. Schroter J, Popp B, Brennenstuhl H, Doring JH, Donze SH, et al. Complementing the phenotypical spectrum of TUBA1A tubulinopathy and its role in early-onset epilepsies. *Eur J Hum Genet*. Mar 2022;30(3):298-306. doi:10.1038/s41431-021-01027-0

96. Myers KA, Bello-Espinosa LE, Kherani A, Wei XC, Innes AM. TUBA1A Mutation Associated With Eye Abnormalities in Addition to Brain Malformation. *Pediatr Neurol*. Nov 2015;53(5):442-4. doi:10.1016/j.pediatrneurol.2015.07.004

97. Cushion TD, Dobyns WB, Mullins JG, Stoodley N, Chung SK, et al. Overlapping cortical malformations and mutations in TUBB2B and TUBA1A. *Brain*. Feb 2013;136(Pt 2):536-48. doi:10.1093/brain/aws338

98. Romaniello R, Zucca C, Arrigoni F, Bonanni P, Panzeri E, et al. Epilepsy in Tubulinopathy: Personal Series and Literature Review. *Cells*. Jul 2 2019;8(7)doi:10.3390/cells8070669

99. Brock S, Vanderhasselt T, Vermaning S, Keymolen K, Regal L, et al. Defining the phenotypical spectrum associated with variants in TUBB2A. *J Med Genet*. Jan 2021;58(1):33-40. doi:10.1136/jmedgenet-2019-106740

100. Cai S, Li J, Wu Y, Jiang Y. De novo mutations of TUBB2A cause infantile-onset epilepsy and developmental delay. *J Hum Genet*. Jul 2020;65(7):601-608. doi:10.1038/s10038-020-0739-5

101. Dekker J, Diderich KEM, Schot R, Husen SC, Dremmen MHG, et al. A novel family illustrating the mild phenotypic spectrum of TUBB2B variants. *Eur J Paediatr Neurol*. Nov 2021;35:35-39. doi:10.1016/j.ejpn.2021.09.007

102. Wang H, Li S, Li S, Jiang N, Guo J, et al. De Novo Mutated TUBB2B Associated Pachygyria Diagnosed by Medical Exome Sequencing and Long-Range PCR. *Fetal Pediatr Pathol*. Feb 2019;38(1):63-71. doi:10.1080/15513815.2018.1538273

103. Citli S, Serdaroglu E. Maternal Germline Mosaicism of a de Novo TUBB2B Mutation Leads to Complex Cortical Dysplasia in Two Siblings. *Fetal Pediatr Pathol*. Feb 2022;41(1):155-165. doi:10.1080/15513815.2020.1753270

104. Jimenez J, Herrera DA, Vargas SA, Montoya J, Castillo M. beta-Tubulinopathy caused by a mutation of the TUBB2B gene: magnetic resonance imaging findings of the brain. *Neuroradiol J*. Apr 2019;32(2):148-150. doi:10.1177/1971400919828142

105. Guerrini R, Mei D, Cordelli DM, Pucatti D, Franzoni E, et al. Symmetric polymicrogyria and pachygyria associated with TUBB2B gene mutations. *Eur J Hum Genet*. Sep 2012;20(9):995-8. doi:10.1038/ejhg.2012.21

106. Jaglin XH, Poirier K, Saillour Y, Buhler E, Tian G, et al. Mutations in the beta-tubulin gene TUBB2B result in asymmetrical polymicrogyria. *Nat Genet*. Jun 2009;41(6):746-52. doi:10.1038/ng.380

107. Breuss MW, Nguyen T, Srivatsan A, Leca I, Tian G, et al. Uner Tan syndrome caused by a homozygous TUBB2B mutation affecting microtubule stability. *Hum Mol Genet*. Jan 15 2017;26(2):258-269. doi:10.1093/hmg/ddw383

108. Cederquist GY, Luchniak A, Tischfield MA, Peeva M, Song Y, et al. An inherited TUBB2B mutation alters a kinesin-binding site and causes polymicrogyria, CFEOM and axon dysinnervation. *Hum Mol Genet*. Dec 15 2012;21(26):5484-99. doi:10.1093/hmg/dds393

109. Laquerriere A, Gonzales M, Saillour Y, Cavallin M, Joye N, et al. De novo TUBB2B mutation causes fetal akinesia deformation sequence with microlissencephaly: An unusual presentation of tubulinopathy. *Eur J Med Genet*. Apr 2016;59(4):249-56. doi:10.1016/j.ejmg.2015.12.007

110. Jin S, Park SE, Won D, Lee ST, Han SH, et al. TUBB3 M323V Syndrome Presents with Infantile Nystagmus. *Genes (Basel)*. Apr 15 2021;12(4)doi:10.3390/genes12040575

111. Ceylan AC, Gursoy H, Yildirim N, Basmak H, Erol N, et al. Clinical heterogeneity associated with TUBB3 gene mutation in a Turkish family with congenital fibrosis of the

extraocular muscles. *Ophthalmic Genet*. May-Jun 2017;38(3):288-290. doi:10.1080/13816810.2016.1193881

112. Blumkin L, Leibovitz Z, Krajden-Haratz K, Arad A, Yosovich K, et al. Autosomal dominant TUBB3-related syndrome: Fetal, radiologic, clinical and morphological features. *Eur J Paediatr Neurol*. May 2020;26:46-60. doi:10.1016/j.ejpn.2020.03.001

113. Whitman MC, Barry BJ, Robson CD, Facio FM, Van Ryzin C, et al. TUBB3 Arg262His causes a recognizable syndrome including CFEOM3, facial palsy, joint contractures, and early-onset peripheral neuropathy. *Hum Genet*. Dec 2021;140(12):1709-1731. doi:10.1007/s00439-021-02379-9

114. Nakamura Y, Matsumoto H, Zaha K, Uematsu K, Nonoyama S. TUBB3 E410K syndrome with osteoporosis and cough syncope in a patient previously diagnosed with atypical Moebius syndrome. *Brain Dev*. Mar 2018;40(3):233-237. doi:10.1016/j.braindev.2017.12.006

115. Xue J, Song Z, Ma S, Yi Z, Yang C, et al. A Novel De Novo TUBB3 Variant Causing Developmental Delay, Epilepsy and Mild Ophthalmological Symptoms in a Chinese Child. *J Mol Neurosci*. Jan 2022;72(1):37-44. doi:10.1007/s12031-021-01909-4

116. Smith SC, Olney AH, Beavers A, Spaulding J, Nelson M, et al. The recurrent TUBB3 Gly98Ser substitution is the first described to inconsistently result in CFEOM3. *Am J Med Genet A*. Sep 2020;182(9):2161-2167. doi:10.1002/ajmg.a.61747

117. Guduru M, Powers A, Love T, Beavers A. Second trimester fetal MRI features in a fetus with TUBB3 gene mutation. *Radiol Case Rep*. Feb 2021;16(2):381-383. doi:10.1016/j.radcr.2020.11.039

118. Grant PE, Im K, Ahtam B, Laurentys CT, Chan WM, et al. Altered White Matter Organization in the TUBB3 E410K Syndrome. *Cereb Cortex*. Jul 22 2019;29(8):3561-3576. doi:10.1093/cercor/bhy231

119. Shimojima K, Okamoto N, Yamamoto T. A novel TUBB3 mutation in a sporadic patient with asymmetric cortical dysplasia. *Am J Med Genet A*. Apr 2016;170A(4):1076-9. doi:10.1002/ajmg.a.37545

120. Tischfield MA, Baris HN, Wu C, Rudolph G, Van Maldergem L, et al. Human TUBB3 mutations perturb microtubule dynamics, kinesin interactions, and axon guidance. *Cell*. Jan 8 2010;140(1):74-87. doi:10.1016/j.cell.2009.12.011

121. Dentici ML, Maglione V, Agolini E, Catena G, Capolino R, et al. TUBB3 E410K syndrome: Case report and review of the clinical spectrum of TUBB3 mutations. *Am J Med Genet A*. Aug 2020;182(8):1977-1984. doi:10.1002/ajmg.a.61719

122. Whitman MC, Andrews C, Chan WM, Tischfield MA, Stasheff SF, et al. Two unique TUBB3 mutations cause both CFEOM3 and malformations of cortical development. *Am J Med Genet A*. Feb 2016;170A(2):297-305. doi:10.1002/ajmg.a.37362

123. Hong YB, Lee JH, Park HJ, Choi YR, Hyun YS, et al. A family with axonal sensorimotor polyneuropathy with TUBB3 mutation. *Mol Med Rep*. Apr 2015;11(4):2729-34. doi:10.3892/mmr.2014.3047

124. Yeniay Sut N, Yildirim M, Bektas O, Altintas M, Teber S. The diagnostic challenges of congenital mirror movements and hand stereotypies in a case with TUBB3-associated tubulinopathy. *Acta Neurol Belg*. Feb 2022;122(1):251-253. doi:10.1007/s13760-021-01858-0

125. de Boer E, Yaldiz B, Denomme-Pichon AS, Matalonga L, Laurie S, et al. Genome-wide variant calling in reanalysis of exome sequencing data uncovered a pathogenic TUBB3 variant. *Eur J Med Genet*. Jan 2022;65(1):104402. doi:10.1016/j.ejmg.2021.104402

126. Thomas MG, Maconachie GDE, Constantinescu CS, Chan WM, Barry B, et al. Congenital monocular elevation deficiency associated with a novel TUBB3 gene variant. *Br J Ophthalmol*. Apr 2020;104(4):547-550. doi:10.1136/bjophthalmol-2019-314293

127. Fukumura S, Kato M, Kawamura K, Tsuzuki A, Tsutsumi H. A Mutation in the Tubulin-Encoding TUBB3 Gene Causes Complex Cortical Malformations and Unilateral Hypohidrosis. *Child Neurol Open*. Jan-Dec 2016;3:2329048X16665758. doi:10.1177/2329048X16665758

128. Lee YH, Park NH. A Complex Cortical Malformation Caused by a Mutation in the Tubulin-Encoding TUBB3 Gene. *Taehan Yongsang Uihakhoe Chi*. Sep 2020;81(5):1246-1249. doi:10.3348/jksr.2019.0175

129. Poirier K, Saillour Y, Bahi-Buisson N, Jaglin XH, Fallet-Bianco C, et al. Mutations in the neuronal ss-tubulin subunit TUBB3 result in malformation of cortical development and neuronal migration defects. *Hum Mol Genet*. Nov 15 2010;19(22):4462-73. doi:10.1093/hmg/ddq377

130. Jia H, Ma Q, Liang Y, Wang D, Chang Q, et al. Clinical and genetic characteristics of Chinese patients with congenital cranial dysinnervation disorders. *Orphanet J Rare Dis*. Dec 9 2022;17(1):431. doi:10.1186/s13023-022-02582-5

131. Patel RM, Liu D, Gonzaga-Jauregui C, Jhangiani S, Lu JT, et al. An exome sequencing study of Moebius syndrome including atypical cases reveals an individual with CFEOM3A and a TUBB3 mutation. *Cold Spring Harb Mol Case Stud*. Mar 2017;3(2):a000984. doi:10.1101/mcs.a000984

132. Chew S, Balasubramanian R, Chan WM, Kang PB, Andrews C, et al. A novel syndrome caused by the E410K amino acid substitution in the neuronal beta-tubulin isotype 3. *Brain*. Feb 2013;136(Pt 2):522-35. doi:10.1093/brain/aws345

133. Yuen YTK, Guella I, Roland E, Sargent M, Boelman C. Case reports: novel TUBG1 mutations with milder neurodevelopmental presentations. *BMC Med Genet*. May 31 2019;20(1):95. doi:10.1186/s12881-019-0827-6

134. Brock S, Stouffs K, Scalais E, D'Hooghe M, Keymolen K, et al. Tubulinopathies continued: refining the phenotypic spectrum associated with variants in TUBG1. *Eur J Hum Genet*. Aug 2018;26(8):1132-1142. doi:10.1038/s41431-018-0146-y

135. Poirier K, Lebrun N, Broix L, Tian G, Saillour Y, et al. Mutations in TUBG1, DYNC1H1, KIF5C and KIF2A cause malformations of cortical development and microcephaly. *Nat Genet*. Jun 2013;45(6):639-47. doi:10.1038/ng.2613

136. Paniagua AE, Herranz-Martin S, Jimeno D, Jimeno AM, Lopez-Benito S, et al. CRB2 completes a fully expressed Crumbs complex in the Retinal Pigment Epithelium. *Sci Rep*. Sep 25 2015;5:14504. doi:10.1038/srep14504

137. Dolon JF, Paniagua AE, Valle V, Segurado A, Arevalo R, et al. Expression and localization of the polarity protein CRB2 in adult mouse brain: a comparison with the CRB1(rd8) mutant mouse model. *Sci Rep*. Aug 3 2018;8(1):11652. doi:10.1038/s41598-018-30210-5

138. van den Hurk JA, Rashbass P, Roepman R, Davis J, Voesenek KE, et al. Characterization of the Crumbs homolog 2 (CRB2) gene and analysis of its role in retinitis pigmentosa and Leber congenital amaurosis. *Mol Vis*. Apr 15 2005;11:263-73.

139. Pellissier LP, Alves CH, Quinn PM, Vos RM, Tanimoto N, et al. Targeted ablation of CRB1 and CRB2 in retinal progenitor cells mimics Leber congenital amaurosis. *PLoS Genet*. 2013;9(12):e1003976. doi:10.1371/journal.pgen.1003976

140. Harms J, Luttgenau SM, Emming C, Guske J, Weber K, et al. Pals1 functions in redundancy with SMAP1 to inhibit Arf6 in order to prevent Rac1-dependent colorectal cancer cell migration and invasion. *Cancer Gene Ther*. Mar 2023;30(3):497-506. doi:10.1038/s41417-022-00570-2

141. Becamel C, Figge A, Poliak S, Dumuis A, Peles E, et al. Interaction of serotonin 5-hydroxytryptamine type 2C receptors with PDZ10 of the multi-PDZ domain protein MUPP1. *J Biol Chem*. Apr 20 2001;276(16):12974-82. doi:10.1074/jbc.M008089200

142. Sitek B, Poschmann G, Schmidtke K, Ullmer C, Maskri L, et al. Expression of MUPP1 protein in mouse brain. *Brain Res*. Apr 25 2003;970(1-2):178-87. doi:10.1016/s0006-8993(03)02338-2

143. Tanabe Y, Fujita-Jimbo E, Momoi MY, Momoi T. CASPR2 forms a complex with GPR37 via MUPP1 but not with GPR37(R558Q), an autism spectrum disorder-related mutation. *J Neurochem*. Aug 2015;134(4):783-93. doi:10.1111/jnc.13168

144. Tetzlaff F, Adam MG, Feldner A, Moll I, Menuchin A, et al. MPDZ promotes DLL4-induced Notch signaling during angiogenesis. *Elife*. Apr 5 2018;7doi:10.7554/eLife.32860

145. Hwang I, An BS, Yang H, Kang HS, Jung EM, et al. Tissue-specific expression of occludin, zona occludens-1, and junction adhesion molecule A in the duodenum, ileum, colon, kidney, liver, lung, brain, and skeletal muscle of C57BL mice. *J Physiol Pharmacol*. Feb 2013;64(1):11-8.

146. Saitou M, Ando-Akatsuka Y, Itoh M, Furuse M, Inazawa J, et al. Mammalian occludin in epithelial cells: its expression and subcellular distribution. *Eur J Cell Biol*. Jul 1997;73(3):222-31.

147. Bauer H, Stelzhammer W, Fuchs R, Weiger TM, Danninger C, et al. Astrocytes and neurons express the tight junction-specific protein occludin in vitro. *Exp Cell Res*. Aug 1 1999;250(2):434-8. doi:10.1006/excr.1999.4558

148. Wolburg H, Wolburg-Buchholz K, Liebner S, Engelhardt B. Claudin-1, claudin-2 and claudin-11 are present in tight junctions of choroid plexus epithelium of the mouse. *Neurosci Lett*. Jul 13 2001;307(2):77-80. doi:10.1016/s0304-3940(01)01927-9

149. Du D, Xu F, Yu L, Zhang C, Lu X, et al. The tight junction protein, occludin, regulates the directional migration of epithelial cells. *Dev Cell*. Jan 19 2010;18(1):52-63. doi:10.1016/j.devcel.2009.12.008

150. Ferguson SM, Brasnjo G, Hayashi M, Wolfel M, Collesi C, et al. A selective activity-dependent requirement for dynamin 1 in synaptic vesicle endocytosis. *Science*. Apr 27 2007;316(5824):570-4. doi:10.1126/science.1140621

151. Asinof S, Mahaffey C, Beyer B, Frankel WN, Boumil R. Dynamin 1 isoform roles in a mouse model of severe childhood epileptic encephalopathy. *Neurobiol Dis*. Nov 2016;95:1-11. doi:10.1016/j.nbd.2016.06.014

152. Boumil RM, Letts VA, Roberts MC, Lenz C, Mahaffey CL, et al. A missense mutation in a highly conserved alternate exon of dynamin-1 causes epilepsy in fitful mice. *PLoS Genet*. Aug 5 2010;6(8)doi:10.1371/journal.pgen.1001046

153. Parthasarathy S, Ruggiero SM, Gelot A, Soardi FC, Ribeiro BFR, et al. A recurrent de novo splice site variant involving DNM1 exon 10a causes developmental and epileptic encephalopathy through a dominant-negative mechanism. *Am J Hum Genet*. Dec 1 2022;109(12):2253-2269. doi:10.1016/j.ajhg.2022.11.002

154. Joshi S, Braithwaite AW, Robinson PJ, Chircop M. Dynamin inhibitors induce caspase-mediated apoptosis following cytokinesis failure in human cancer cells and this is blocked by Bcl-2 overexpression. *Mol Cancer*. Jun 28 2011;10:78. doi:10.1186/1476-4598-10-78

155. Thompson HM, Skop AR, Euteneuer U, Meyer BJ, McNiven MA. The large GTPase dynamin associates with the spindle midzone and is required for cytokinesis. *Curr Biol*. Dec 23 2002;12(24):2111-7. doi:10.1016/s0960-9822(02)01390-8

156. Moon HM, Hippenmeyer S, Luo L, Wynshaw-Boris A. LIS1 determines cleavage plane positioning by regulating actomyosin-mediated cell membrane contractility. *Elife*. Mar 11 2020;9doi:10.7554/eLife.51512

157. Drerup CM, Wiora HM, Morris JA. Characterization of the overlapping expression patterns of the zebrafish LIS1 orthologs. *Gene Expr Patterns*. Jan 2010;10(1):75-85. doi:10.1016/j.gep.2009.10.001

158. Sun C, Xu M, Xing Z, Wu Z, Li Y, et al. Expression and function on embryonic development of lissencephaly-1 genes in zebrafish. *Acta Biochim Biophys Sin (Shanghai)*. Aug 2009;41(8):677-88. doi:10.1093/abbs/gmp056

159. Ye S, Fowler TW, Pavlos NJ, Ng PY, Liang K, et al. LIS1 regulates osteoclast formation and function through its interactions with dynein/dynactin and Plekhm1. *PLoS One*. 2011;6(11):e27285. doi:10.1371/journal.pone.0027285

160. Rakotomamonjy J, Rylaarsdam L, Fares-Taie L, McDermott S, Davies D, et al. PCDH12 loss results in premature neuronal differentiation and impeded migration in a cortical organoid model. *Cell Rep*. Jul 20 2023;42(8):112845. doi:10.1016/j.celrep.2023.112845

161. Rampon C, Prandini MH, Bouillot S, Pointu H, Tillet E, et al. Protocadherin 12 (VE-cadherin 2) is expressed in endothelial, trophoblast, and mesangial cells. *Exp Cell Res*. Jan 1 2005;302(1):48-60. doi:10.1016/j.yexcr.2004.08.024

162. Aiken J, Moore JK, Bates EA. TUBA1A mutations identified in lissencephaly patients dominantly disrupt neuronal migration and impair dynein activity. *Hum Mol Genet*. Apr 15 2019;28(8):1227-1243. doi:10.1093/hmg/ddy416

163. Belvindrah R, Natarajan K, Shabajee P, Bruel-Jungerman E, Bernard J, et al. Mutation of the alpha-tubulin Tuba1a leads to straighter microtubules and perturbs neuronal migration. *J Cell Biol*. Aug 7 2017;216(8):2443-2461. doi:10.1083/jcb.201607074

164. Keays DA, Cleak J, Huang GJ, Edwards A, Braun A, et al. The role of Tuba1a in adult hippocampal neurogenesis and the formation of the dentate gyrus. *Dev Neurosci*. 2010;32(4):268-77. doi:10.1159/000319663

165. Bamba Y, Shofuda T, Kato M, Pooh RK, Tateishi Y, et al. In vitro characterization of neurite extension using induced pluripotent stem cells derived from lissencephaly patients with TUBA1A missense mutations. *Mol Brain*. Jul 19 2016;9(1):70. doi:10.1186/s13041-016-0246-y

166. Hoff KJ, Aiken JE, Gutierrez MA, Franco SJ, Moore JK. TUBA1A tubulinopathy mutants disrupt neuron morphogenesis and override XMAP215/Stu2 regulation of microtubule dynamics. *Elife*. May 5 2022;11doi:10.7554/eLife.76189

167. Ramachandran R, Reifler A, Parent JM, Goldman D. Conditional gene expression and lineage tracing of tuba1a expressing cells during zebrafish development and retina regeneration. *J Comp Neurol*. Oct 15 2010;518(20):4196-212. doi:10.1002/cne.22448

168. Jin Y, Zhang S, Liu L. Circular RNA circ_C16orf62 Suppresses Cell Growth in Gastric Cancer by miR-421/Tubulin beta-2A Chain (TUBB2A) Axis. *Med Sci Monit*. Oct 2 2020;26:e924343. doi:10.12659/MSM.924343

169. Sferra A, Fattori F, Rizza T, Flex E, Bellacchio E, et al. Defective kinesin binding of TUBB2A causes progressive spastic ataxia syndrome resembling sacsinopathy. *Hum Mol Genet*. Jun 1 2018;27(11):1892-1904. doi:10.1093/hmg/ddy096

170. Leandro-Garcia LJ, Leskela S, Landa I, Montero-Conde C, Lopez-Jimenez E, et al. Tumoral and tissue-specific expression of the major human beta-tubulin isotypes. *Cytoskeleton (Hoboken)*. Apr 2010;67(4):214-23. doi:10.1002/cm.20436

171. Shin D, Park J, Han D, Moon JH, Ryu HS, et al. Identification of TUBB2A by quantitative proteomic analysis as a novel biomarker for the prediction of distant metastatic breast cancer. *Clin Proteomics*. 2020;17:16. doi:10.1186/s12014-020-09280-z

172. Breuss M, Morandell J, Nimpf S, Gstrein T, Lauwers M, et al. The Expression of Tubb2b Undergoes a Developmental Transition in Murine Cortical Neurons. *J Comp Neurol*. Oct 15 2015;523(15):2161-86. doi:10.1002/cne.23836

173. Stottmann RW, Donlin M, Hafner A, Bernard A, Sinclair DA, et al. A mutation in Tubb2b, a human polymicrogyria gene, leads to lethality and abnormal cortical development in the mouse. *Hum Mol Genet*. Oct 15 2013;22(20):4053-63. doi:10.1093/hmg/ddt255

174. Denarier E, Brousse C, Sissoko A, Andrieux A, Boscheron C. A neurodevelopmental TUBB2B beta-tubulin mutation impairs Bim1 (yeast EB1)-dependent spindle positioning. *Biol Open*. Jan 29 2019;8(1)doi:10.1242/bio.038620

175. Saillour Y, Broix L, Bruel-Jungerman E, Lebrun N, Muraca G, et al. Beta tubulin isoforms are not interchangeable for rescuing impaired radial migration due to Tubb3 knockdown. *Hum Mol Genet*. Mar 15 2014;23(6):1516-26. doi:10.1093/hmg/ddt538

176. Latremoliere A, Cheng L, DeLisle M, Wu C, Chew S, et al. Neuronal-Specific TUBB3 Is Not Required for Normal Neuronal Function but Is Essential for Timely Axon Regeneration. *Cell Rep*. Aug 14 2018;24(7):1865-1879 e9. doi:10.1016/j.celrep.2018.07.029

177. Sobierajska K, Wieczorek K, Ciszewski WM, Sacewicz-Hofman I, Wawro ME, et al. beta-III tubulin modulates the behavior of Snail overexpressed during the epithelial-to-

mesenchymal transition in colon cancer cells. *Biochim Biophys Acta*. Sep 2016;1863(9):2221-33. doi:10.1016/j.bbamcr.2016.05.008

178. Liu Z, Li S, Dong J, Miao Y. TUBB3 Promotes Growth and Invasion of Gallbladder Cancer Cells by Akt/mTOR Signal Pathway. *J Environ Pathol Toxicol Oncol*. 2021;40(2):23-33. doi:10.1615/JEnvironPatholToxicolOncol.2021036821

179. Narvi E, Jaakkola K, Winsel S, Oetken-Lindholm C, Halonen P, et al. Altered TUBB3 expression contributes to the epothilone response of mitotic cells. *Br J Cancer*. Jan 15 2013;108(1):82-90. doi:10.1038/bjc.2012.553

180. Ivanova EL, Gilet JG, Sulimenko V, Duchon A, Rudolf G, et al. TUBG1 missense variants underlying cortical malformations disrupt neuronal locomotion and microtubule dynamics but not neurogenesis. *Nat Commun*. May 13 2019;10(1):2129. doi:10.1038/s41467-019-10081-8

181. Yuba-Kubo A, Kubo A, Hata M, Tsukita S. Gene knockout analysis of two gamma-tubulin isoforms in mice. *Dev Biol*. Jun 15 2005;282(2):361-73. doi:10.1016/j.ydbio.2005.03.031

182. Sanchez-Huertas C, Freixo F, Viais R, Lacasa C, Soriano E, et al. Non-centrosomal nucleation mediated by augmin organizes microtubules in post-mitotic neurons and controls axonal microtubule polarity. *Nat Commun*. Jul 13 2016;7:12187. doi:10.1038/ncomms12187

7 Chapter 6: Final conclusion and summary

Our study provides evidence for the involvement of DENND5A in two well-known processes implicated in primary microcephaly: centrosome positioning during cell division and premature NPC cell cycle exit and differentiation[1]. We propose a disease model, presented in **Figure 6.1**, in which DENND5A-related DEE is driven by a significant reduction in symmetric cell divisions during early development due to the misorientation of cells away from the proliferative apical domain of the ventricular zone. This results in an imbalance of signaling molecules from the stem and progenitor cell niche to each daughter cell and unequal inheritance of apical determinants such as MUPP1 and PALS1, biasing one daughter cell toward a more fate-committed state[2]. Ultimately, the period of neurogenesis is shortened which leads to microcephaly and/or observable abnormalities in gray and white matter structures. The reduced volume of neurons likely leads to compensatory ventriculomegaly, and improperly positioned prematurely-born neurons that do not undergo apoptosis may form aberrant synaptic contacts resulting in seizures that can further adversely affect development.[3]

The work done in this thesis demonstrates several significant contributions to knowledge in the fields of neurology and cell biology: 1) we provided the most detailed clinical description to date of individuals with biallelic DENND5A variants, including the first-ever description of compound heterozygous individuals and how their neuroanatomical phenotypes are generally milder than homozygous individuals, but does not necessarily correlate to a milder DEE; 2) we clarified that certain missense variants, currently classified as likely benign or variants of uncertain significance, are rather likely pathogenic; 3) we identified other variants, currently classified as variants of uncertain significance, are likely benign; 4) we identified a previously-unknown

protein-protein interaction between DENND5A and components of the heavily studied Crb complex; 5) we discovered that DENND5A must undergo a conformational change to bind both the Crb complex proteins and its Rab substrate; 6) we discovered that neural progenitor cells lacking *DENND5A* have an inherent and strong propensity to immediately differentiate into neurons; 7) we established that *DENND5A* is required for neural stem cells to divide symmetrically against an apical surface; and 8) the cell division and differentiation phenotypes explain the pathological mechanism behind microcephaly and ventriculomegaly *ex vacuo* in *DENND5A*-related DEE.

We anticipate that the implications of this research will be far-reaching and of interest to a multidisciplinary audience. Physicians will benefit from the phenotypic descriptions provided in our clinical study to refer carriers to genetic counseling and to communicate realistic expectations to families with children harboring biallelic *DENND5A* variants. Finally, cell biologists studying polarity or stem cell biology will no longer overlook DENND5A as a major regulator of stemness and self-renewal.

7.1 Figures

Figure 6.1

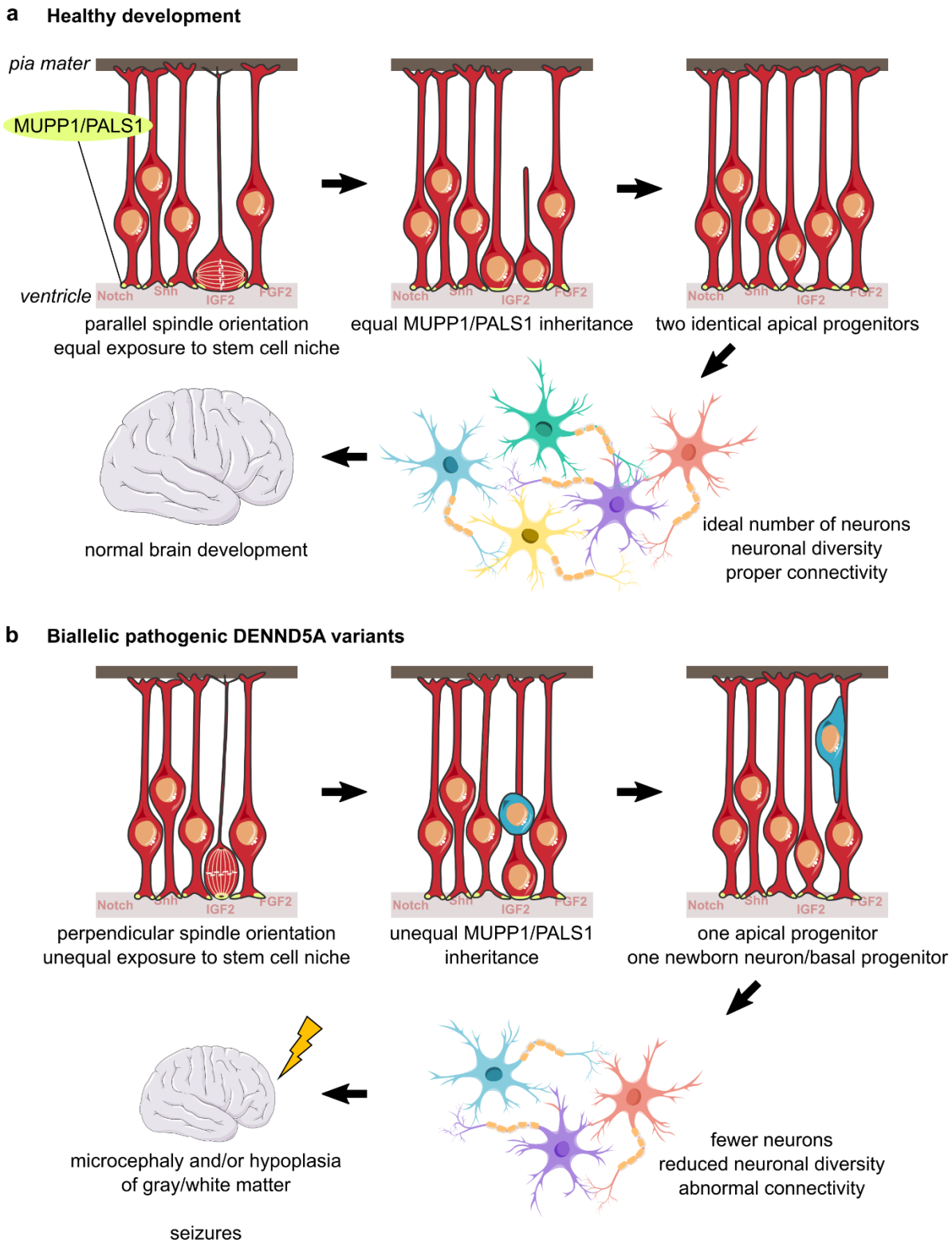

Figure 6.1: *DENND5A*-related DEE disease model. a, Under healthy developmental circumstances, apical progenitors are able to obtain a spindle orientation parallel to the apical ventricular surface. This allows both daughter cells to receive equal exposure to the stem and progenitor cell niche as well as inherit equal proportions of apical determinants, such as MUPP1 and PALS1, producing two identical apical progenitors after mitosis. The expansion of the progenitor pool early in brain development allows for an ideal production of neurons from diverse lineages and contributes to healthy brain development. **b,** In the presence of biallelic pathogenic *DENND5A* variants, apical progenitors increasingly divide with a spindle angle perpendicular to the ventricular surface. This scenario only allows for one daughter cell to receive signaling molecules from the stem and progenitor cell niche and to inherit apical determinants, and the more basal daughter cell becomes either a basal progenitor or an immature neuron. Increased asymmetric cell division of apical neural progenitors during early development reduces the number of progenitors available for neurogenesis, resulting in a decreased overall number and diversity of neurons that contributes to microcephaly. This may contribute to abnormal neuronal connectivity, resulting in seizures that further adversely affect development, leading to DEE.

7.2 References

1. Jean F, Stuart A, Tarailo-Graovac M. Dissecting the Genetic and Etiological Causes of Primary Microcephaly. *Front Neurol*. Oct 14 2020;11:570830. doi:10.3389/fneur.2020.570830

2. Knoblich JA. Mechanisms of asymmetric stem cell division. *Cell*. Feb 22 2008;132(4):583-97. doi:10.1016/j.cell.2008.02.007

3. Banks E, Francis V, Lin S-J, et al. Loss of symmetric cell division of apical neural progenitors drives *DENND5A*-related developmental and epileptic encephalopathy. *medRxiv*. 2023-01-01 00:00:00 2023;doi:https://doi.org/10.1101/2022.08.23.22278845